Dissertation

Zur Erlangung eines Doktorgrades der Naturwissenschaften

The Spatial Organization of MAPK Activity

vorgelegt von

Lisa Sophia Karajannis

bei der Fakultät Chemie der TU Dortmund

11.09.2014

1. Gutachter: Prof. Dr. Philippe I. H. Bastiaens

2. Gutachter: Prof. Dr. Roland Winter

Eidesstattliche Erklärung

Hiermit erkläre ich an Eides Statt, dass ich die vorliegende Dissertation selbstständig und ohne unzulässige fremde Hilfe erarbeitet habe Ich habe keine anderen als die hier angegebenen Quellen und Hilfmittel benutzt, sowie wörtliche und sinngemäße Zitate durch Angabe der Quellen kenntlich gemacht. Diese Arbeit ist weder in Teilen noch als Ganzes für die Erlangung eines Doktorgrades eingereicht worden.

Contents

List of Figures

List of Abbreviations

AMCA Aminomethylcoumarin Acetate

ATP Adenosine triphosphate

ATP adenosine triphosphate

CD common docking

CFL coherent feedforward loop

EGFR Epidermal growth factor receptor

EphA3 ephrin receptor tyrosine kinase 3

ErbB erythoblastosis oncogene B

ERK extracellular-signal-regulated kinase

FAM Carboxyfluorescein

FLIM fluorescence lifetime imaging microscopy

FRET Förster resonance energy transfer

FRET Förster Resonance Energy Transfer

Fus3 fusion-3

GF growth factor

GFP green fluorescent protein

GPCR G-protein coupled receptor

HER human epidermal growth factor receptor

Hog1 high osmolarity/glycerol-1

HRG Heregulin

IEG immediate early gene

IQGAP1 IQ motif-containing GTPase activating protein 1

IRDye InfraRedDye

JNK Jun N-terminal kinase

KSR1 kinase suppressor of ras-1

Kss1 kinase suppressor of Sst2-1

MALDI-TOF Matrix Assisted Light Desorption Ionisation - Time Of Flight

MAPK mitogen-activated protein kinase

MAPK mitogen-activated protein kinase

MAPKK MAP kinase kinase

MAPKKK MAP kinase kinase kinase

NES nucleus-export-sequence

NTS nuclear translocation signal

PAK p21-activated protein kinase

PM plasma membrane

PTB phospho-Tyrosine-binding

RBD Ras binding domain

RSK p90-ribosomal-S6-kinase

RTK receptor tyrosine kinase

Ser Serine

SH2 Src-homology-2

Slt2 suppressor of LYT2

TCSPC time-correlated single photon counting

Thr Threonine

Tyr Tyrosine

WT wild type

Summary

Mitogen activated protein kinase (MAPK) cascades are evolutionarily conserved signaling modules in eukaryotes, starting from unicellular *Saccharomyces cerevisiae* to humans. These modules respond to a variety of extracellular stimuli and convert them into defined cellular responses, such as proliferation, differentiation or apoptosis. Different phenotypic responses depend on the diverse dynamical spatio-temporal activity profiles of MAPKs, which are inherent in the hierarchical architecture of MAPK signaling cascades. Specificity of the spatio-temporal activity profiles is thus effected by the integration of the MAPK module into networks of regulatory proteins such as scaffolds, which then effect specific responses. While the temporal regulation and function of MAPK activity has been widely studied, quantitative information about the spatial organization of MAPK activity in mammalian cells has been inaccessible due a lack of suitable imaging approaches. However, imaging of MAPK activity is crucial for understanding how their signaling can be specified for the global function in transcriptional regulation in the nucleus and specific local functions in the cytoplasm. The spatial partitioning of the MAPK activation cycle into phosphorylation at the plasma membrane and dephosphorylation in the cytoplasm was postulated to generate spatial activity gradients, which emanate from the PM [Brown & Kholodenko, 1999].

A versatile and quantitative approach for the mapping of MAPK activity was established in this work to pursue the spatial profiling of MAPK activity. In particular, the universality of the phosphoprotein-binding compound Phos-Tag was combined with Förster resonance energy transfer-fluorescence lifetime imaging microscopy (FRET-FLIM) to obtain a quantitative and specific read-out of the MAPK activity state, referred to as PTag-FLIM [Kinoshita et al., 2006]. Furthermore, PTag-FLIM is the first universal approach to quantitatively image the phosphorylation of every fluorescently-tagged protein.

This novel method was used to confirm the known activity gradient of the MAPK Fus3 in yeast cells forming a projection tip [Maeder et al., 2007]. Moreover, a newly identified negative feedback from Fus3 on upstream MAPKKK Ste11 was shown to decrease the decay length of the Fus3 activity gradient [Hecker et al., 2014]. A constitutively active Ste11 mutant in which the negative feedback was impaired resulted in an increase in the amplitude and decay length of the Fus3 activity gradient. These results provide the first experimental insight into how the network architecture influences MAPK activity gradients.

The application of the PTag FLIM approach on human cell lines HeLa and MCF-7 demonstrated that the active MAPKK Mek1 and MAPK ERK2 indeed emanate in gradients from the plasma membrane. Nuclear ERK2 was also found to be distributed in an activity gradient, emanating from the nuclear membrane into the interior of the nucleus. The confinement of ERK activity to the nuclear envelope correlates with known roles of ERK2 in heterochromatin remodeling, transcriptional activation and cell cycle progression.

In the breast cancer cell line MCF-7 cells, stimulation with EGF causes transient ERK2 activity leading to proliferation, while HRG induces sustained ERK2 activity in the cytoplasm which causes differentiation [Nagashima et al., 2007]. In this thesis EGF and HRG growth factors were shown to induce comparable gradients of Mek1 activity, whereas HRG stimulation demonstrably induced steeper ERK2 activity gradients in comparison to the EGF stimulation. The correlation between persistent cytoplasmic activity of ERK2 and increased steepness of the ERK2 activity gradient in the cytoplasm upon HRG stimulation suggest that ERK2 is maintained in the cytoplasm by the cofinement of ERK2 activity in steep gradients. The differential spatio-temporal activity profiles of Mek1 and ERK2 by EGF and HRG obtained here support

the hypothesis that the scaffold KSR1 is integrated in the HRG-induced MAPK network. Ectopic expression of KSR1 indeed distributed Mek1 activity, but confined active ERK2 to the plasma membrane. The cumulative evidence indicates that regulatory proteins may differentiate MAPK functions in distinct cellular locations by promoting steep MAPK activity gradients.

Zusammenfassung

Mitogen-aktivierte Proteinkinase (MAPK) Kaskaden sind eukaryotische Signaltransduktionsmodule, welche von der einzelligen Saccharomyces cerevisiae bis zum Mensch evolutionär konserviert sind. Diese Module werden durch verschiedenste extrazelluläre Stimuli aktiviert, welche sie in definierte Zellantworten, wie Proliferation, Differenzierung und Apoptose umsetzen. Diese unterschiedlichen phänotypischen Zellantworten werden durch vielfältige dynamische Aktivitätsprofile der MAPK in Zeit und Raum ermöglicht, welche auf dem hierarchischen Aufbau von MAPK Signalwegen basieren. Die Spezifizierung des Zeit-Raum-Profils von MAPK Aktivität, und somit die Zellantwort, erfolgt durch die Integration des MAPK Moduls in ein Netzwerk regulatorischer Proteine, wie z.B. Gerüstproteine (englisch "scaffold"). Während die zeitliche Regulation und Funktion von MAPK Aktivität gut untersucht sind, konnte die räumliche Organisation der MAPK Aktivität aufgrund fehlender Bildgebungsverfahren nicht betrachtet werden. Die Untersuchung der räumlichen Organisation von MAPK Aktivität ist jedoch unabdingbar um zu verstehen, wie die globale Funktion der MAPK in der Aktivierung der Transkription im Zellkern und spezifische lokale Funktionen im Zytoplasma differenziert werden können. Anhand von Computermodellen wurde gezeigt, dass die räumliche Trennung des Aktivierungszyklus der MAPK in Phosphorylierung an der Plasmamembran und Dephosphorylierung im Zytoplasma zu Aktivitätsgradienten führt [Brown & Kholodenko, 1999]. Um herauszufinden, ob diese Aktivitätsgradienten tatsächlich auftreten und wie diese gegebenenfalls die Differenzierung der MAPK Funktionen im zellulären Raum ermöglichen, wurde in der vorliegenden Arbeit eine vielseitig einsetzbare und quantitative Methode zur Bildgebung der MAPK Aktivität entwickelt. Diese Methode basiert auf der Detektion der Phosphorylierung von MAPKs als Reporter ihrer Aktivität und kombiniert dafür das Reagenz Phos-Tag, welches universell an phosphorylierte Proteine bindet, mit Forster Resonanzenergietransfer/Fluoreszenzlebenszeit (FRET/FLIM) Messungen, im folgenden bezeichnet als PTag-FLIM. Als Nebenprodukt ermöglicht PTag-FLIM als erste Methode spezifisch die Phosphorylierung jedes Fluorophore-fusionierten Proteins zu verbildlichen.

Mit PTag FLIM konnte der bekannte Aktivitätsgradient der MAPK Fus3 in der Konjugationsspitze von Hefen bestätigt werden [Maeder et al., 2007]. Darüberhinaus wurde gezeigt, dass eine kürzlich identifizierte negative Rückkopplung von Fus3 auf die höherliegende MAPKKK Ste11 zu einer Fokussierung des Fus3 Aktivitätsgradienten führt [Hecker et al., 2014]. Eine Mutante von Ste11, welche die negative Rückkopplung verhindert und konstitutiv aktiv ist, führte zu einem Anstieg der Amplitude sowie einer Verlängerung des Gradienten.

Außerdem wurde mit PTag-FLIM gezeigt, dass die aktiven MAPKK Mek1 und MAPK ERK2 in den humanen Zelllinien Hela und MCF-7 tatsächlich in Gradienten ausgehend von der Plasmamembran verlaufen. Überraschenderweise wurde auch ein nuklearer Gradient von aktivem ERK2 beobachtet, welcher von der Zellkernmembran ins Zentrum des Kerns verlief. Die räumliche Begrenzung der ERK2 Aktivität im Zellkern korreliert mit bekannten Funktionen von ERK2 an der Kernhülle (englisch "nuclear envelope"), wie die Umstrukturierung von Heterochromatin, die Aktivierung der Transkription sowie die Fortführung des Zellzyklus.

In der Brustkrebszelllinie MCF-7 wurde gezeigt, dass die Wachstumsfaktoren EGF und HRG vergleichbare Aktivitätsgradienten von Mek1 verursachen, während der ERK2 Aktivitätsgradient steiler nach HRG als nach EGF Stimulation war. Diese Beobachtung korreliert mit der bekannten anhaltenden Aktivität von ERK2 im Zytoplasma nach HRG Stimulation und deutet daraufhin, dass der steilere ERK2 Aktivitätsgradient nötig ist, um die ERK2 Aktivität im Zytoplasma zu halten. Die kumulierten Ergebnisse führen zu der Hypothese, dass

das Gerüstprotein KSR1 in das HRG-induzierte MAPK Netzwerk intergriert wird. Tatsächlich begünstigte die ektopische Expression von KSR1 zu einer Ausbreitung der Mek1 Aktivität und einer Begrenzung der ERK2 Aktivität an die Plasmamembran.

1 Introduction

About one third of the human proteome is predicted to become reversibly modified by phosphorylation on Serine (Ser), Threonine (Thr) or Tyrosine (Tyr) residues with a respective ratio of 1800:200:1 [KREBS & FISCHER, 1955, Cohen, 2002]. This covalent modification can potentially induce a conformational change in the protein due to the double-negative charge at physiological pH and the capacity of forming electrostatic interactions and hydrogen-bonds [Johnson & Lewis, 2001]. Phosphorylation can therefore alter the catalytic activity or change the accessibility of interaction sites, which in turn can affect the protein localization and stability or mark the protein for further modification. Kinases, making up 2% of the human genome, transfer the phosphate anion from adenosine triphosphate (ATP) to its substrate, while phosphatases catalyze protein dephosphorylation [Burnett & Kennedy, 1954, Manning et al., 2002, Lander et al., 2001].

Protein phosphorylation plays an essential cellular role in the cellular signal transduction. Central to many signal transduction pathways are kinase cascades, which provide a large spectrum of spatio-temporal signaling modes. Major phosphorylation cascades are the highly conserved mitogen activated protein kinases (MAPKs), which convert information from the extracellular space into fundamental cell responses, like proliferation, differentiation, and apoptosis [Chen et al., 2001]. Germline mutations causing the dysregulation of MAPK activity drive developmental disorders, while acquired MAPK dysregulation is frequently found in cancer [Schubbert et al., 2007, Roberts & Der, 2007]. The first identified and best examined MAPK pathway is the Ras-Raf/Mek/ERK cascade which is deregulated in up to 30% of human cancer types [Roberts & Der, 2007].

MAPK activity has been widely studied by measuring its phosphorylation in large cell populations using chromatography-based approaches, like gel-electrophoresis followed by Western blotting or mass spectrometry. These have revealed detailed temporal response profiles of MAPKs [Olsen et al., 2006, Olsen et al., 2010]. However, the precise spatial organization of MAPK activity remained subject to computations, which predict that the spatial partitioning of activation at the plasma membrane from deactivation in the cytosol would generate a gradient of MAPK activity [Brown & Kholodenko, 1999]. This activity gradient is supposed to emanate from the plasma membrane (PM) and be restricted to membrane-proximal regions. Based on that, further theories have been proposed how the signal can nevertheless be propagated to intracellular locations, like the nucleus [Kholodenko, 2006]. However, the verification of these theories in mammalian cells has been experimentally inaccessable due to low dynamic range or substrate-based measures of MAPK activity.

To pursue the spatial profiling of MAPK activity, we developed a cytochemical approach based on Phos-Tag and Förster resonance energy transfer-fluorescence lifetime imaging microscopy (FRET-FLIM), which allows to quantitatively visualize the phosphorylation of fluorophore-tagged MAPKs as read-out for their activity with subcellular resolution. The reagent Phos-Tag, which is coupled to a dye via Streptavidin as acceptor in FRET, binds universally to phosphomonoesters and therefore to all phosphorylated amino acids. The technique presented in this thesis expands the hitherto universal pTyr imaging approach to all, and therefore the majority, of phosphorylated proteins [Bastiaens & Squire, 1999, Grecco et al., 2010].

1.1 Signaling components of the ERK cascade

MAPK pathways are evolutionaryly conserved signaling modules in eukaryotes, from humans down to unicellular *Saccharomyces cerevisiae* (hereafter named "yeast"). These pathways transmit signals from cell-surface receptors, which are activated by extracellular stimuli, e.g. growth factors (GF), hormones, cytokines or high osmolarity and starvation. The MAPKs are organized in cascades, consisting of three to four serially phosphorylated, and thereby activated, protein kinases. The proteins are formally named after their position in the cascade with the terminal MAPK being phosphorylated by MAP kinase kinase (MAPKK), and so forth [Chen & Thorner, 2007]. The terminal MAPK links the signal transmission with the conversion into essential cellular responses, like proliferation, differentiation or apoptosis [Wolf & Seger, 2002, Chen & Thorner, 2007]. Additionally to the extracellular-signal-regulated kinase (ERK) cascade, there are three further well characterized MAPK modules in mammalian cell lines, which are (named after their terminal MAPK) Jun N-terminal kinase (JNK), p38 and ERK5, with about 20 MAPK molecules in total [Chen et al., 2001, Roberts & Der, 2007].

Surprisingly, in some cases the same cascade can induce different cell fates, depending on the stimulus. In PC-12 cells for instance, the ERK cascade can trigger differentiation upon NGF stimulation or proliferation after EGF treatment [Nguyen et al., 1993, Traverse et al., 1994]. The respective cellular responses arise from the GF-specific signaling network architecture, which encodes time, localization and amplitude of MAPK activity [Santos et al., 2007].

Signal transduction via the ERK cascade is usually associated with receptor tyrosine kinase (RTK) activation (figure 1.1). However, the stimulation of G-protein coupled receptors (GPCRs) can also trigger ERK activation, either by transactivation of RTKs or signal integration via adaptor proteins like β-arrestin [Chen et al., 2001, Waters et al., 2004]. In the case of most RTKs, ligand binding induces receptor homo-/heterodimerization and autophosphorylation of intracellular tyrosine residues. Receptor activation leads to recruitment of adaptor proteins like Grb2 and the Ras-guanine nucleotide exchange factor (GEF) son-of-sevenless (SOS), which changes the Ras nucleotide state from GDP to GTP [Simon et al., 1993, Nada et al., 1993, Lowenstein et al., 1992]. GTP-bound Ras transduces the signal to the MAPK cascade by interacting with the MAPKKK Raf.

1.1.1 The MAPKKK Raf

Raf was first identified as viral oncogene (v-Raf) which has in comparison to cellular, non-transforming Raf (c-Raf) a capped N-terminus and is constitutively active [Rapp et al., 1983, Patschinsky & Bister, 1988, Heidecker et al., 1990]. In human cell lines two further isoforms, A-Raf and B-Raf, were found. Raf activation and dimerization has been studied extensively in the last decade, as B-Raf mutations account for 43% of melanomas and new potent B-Raf inhibitors paradoxically induced ERK1/2 activation [Poulikakos et al., 2010, Heidorn et al., 2010, Lavoie et al., 2013, Hatzivassiliou et al., 2010].

While inactive, a region in the N-terminal kinase domain of B-Raf is constitutively phosphorylated, flanked by two acidic residues. In contrast, the corresponding c-Raf motif is hydrophobic and intramolecularly occludes the kinase domain. This closed state is clamped by a 14-3-3 dimer binding to a C-terminal and an internal pSer, maintaining c-Raf cytosolic [Light et al., 2002]. Upon growth factor stimulation the activity of the phosphatases PP1 and PP2A is induced, which dephosphorylate the internal pSer site. Hence, 14-3-3 is only bound to the C-terminal pSer site [Abraham et al., 2000, Rodriguez-Viciana et al., 2006]. The free Raf N-terminus can specifically bind the GTP bound Ras via its Ras binding domain (RBD) and additionally interact with Ras independently of its guanine-nucleotide state through a cysteine-rich domain (CRD) [Herrmann et al., 1995]. The collective Ras-Raf interactions recruit Raf to the plasma membrane, leading to conformational changes in Raf, which in turn induce homo- and hetero-dimerization of Raf proteins [Luo et al., 1996, Weber et al., 2001, Garnett et al.,

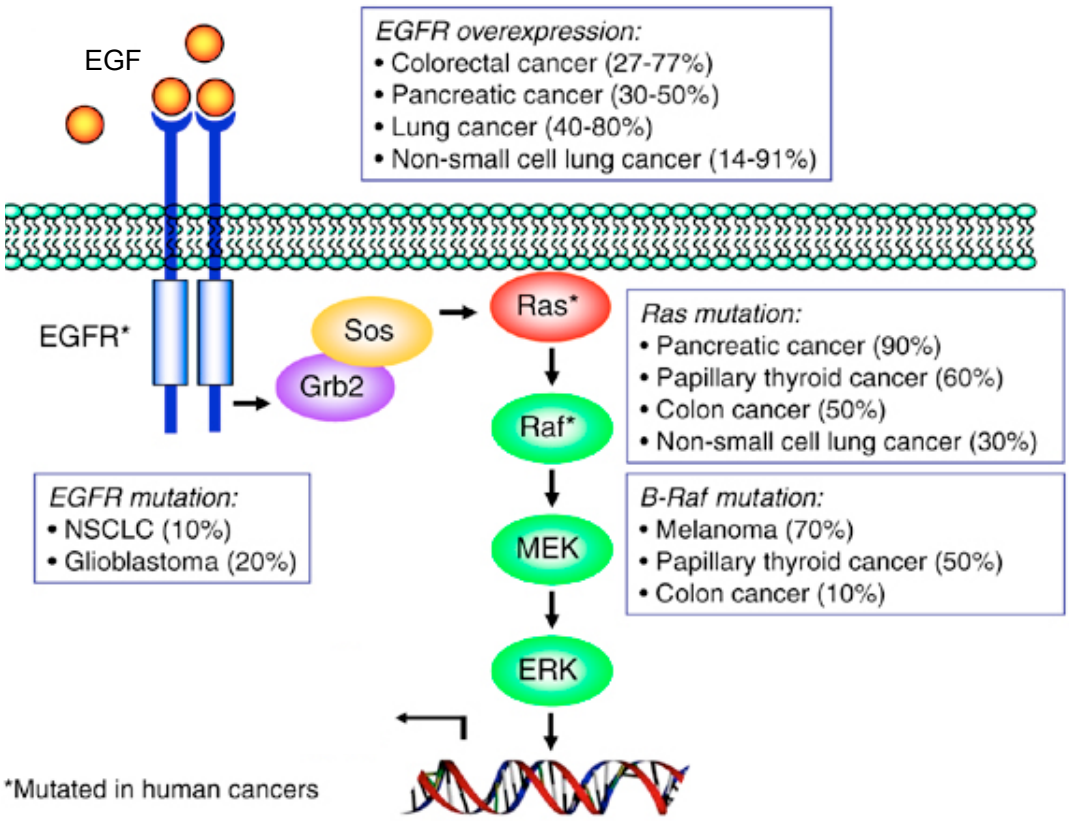

Figure 1.1: **Signal transduction via the ERK cascade and associated human cancers.** An extracellular ligand (EGF) binds to a cell surface receptor (EGFR) and induces its activation. This information is transduced via Ras to Raf and in a phosphorylation cascade from Raf to Mek and from Mek to ERK. Active ERK induces a transcriptional program in the nucleus. Boxes indicate the human cancers associated with the oncogenes EGFR, Ras and Raf (adapted from [Roberts & Der, 2007]).

2005, Rajakulendran et al., 2009]. 14-3-3 dimers support dimerization by bridging the two monomers. In hetero-dimers of c- and B-Raf, the polar N-terminus of B-Raf induces in c-Raf allosterically a "hydrophobic" spine, with a "DFG-in" conformation guiding the c-Raf activation loop in an active conformation, which is then intramolecularly autophosphorylated [Kornev et al., 2008, Hu et al., 2011, Hu et al., 2013]. Thereby, c-Raf achieves full kinase activity and becomes independent of B-Raf stabilization and phosphorylates the MAPKK Mek1/2 [Hu et al., 2013]. In a feedback, Mek1/2 in turn phosphorylates the designated N-terminal motif on c-Raf, which was also reported to be phosphorylated by Src, PAK and PKC family kinases [Hu et al., 2013, Zang et al., 2008]. This N-terminally phosphorylated c-Raf is able to transactivate other Rafs in the next cycle of dimerization. B-Raf therefore acts as a catalyst of c-Raf activation, which explains why B-Raf is much less abundant in the cell than c-Raf. This suggests a pivotal role for a scaffold function of B-Raf in the onset of GF signaling, supported by the fact that B-Raf is the only oncogene of the Raf family.

Raf activation requires asymmetric Raf dimers with one molecule acting as allosteric activator and the other as receiver. Unveilling the Raf activation this mechanism explains how potent B-Raf inhibitors can paradoxically activate the MAPK pathway: These inhibitors are ATP-analogues, which bind selectively to B-Raf-Val600Glu/Lys mutants and inhibit their kinase activity. However, the binding of the inhibitor induces a stable, closed conformation of the kinase domain which serves as a steady dimerization interface for another Raf molecule, for example c-Raf [Lavoie et al., 2013]. The inhibited Raf can therefore still serve as part of the activation mechnism for other wild-type Raf proteins.

1.1.2 The MAPKK Mek1/2

The Mek1/2 proteins become activated by phosphorylation on Ser218 and Ser222 in their activation segment through Raf [Howe et al., 1992, Dent et al., 1992, Kyriakis et al., 1992, Zheng & Guan, 1994]. The interaction with Raf is mediated by a MAI-motif in Mek1/2, which is also involved in binding to kinase suppressor of ras-1 KSR1 [McKay et al., 2009]. Mek1 binds preferentially to KSR1, while the association with B-Raf is weak and interaction with c-Raf below the detection limit [McKay et al., 2009]. The Ser/Thr-kinase PAK1, involved in cytoskeletal reorganization, phosphorylates Mek1 on Ser298 which induces a sustained duration of Mek1 activity [Coles & Shaw, 2002, Slack-Davis et al., 2003]. Mek1 is negatively regulated by a feedback phosphorylation from ERK on residue Thr292, which prevents the phosphorylation by PAK1, while Mek2 is independent from this feedback as the corresponding site is mutated to a proline [Eblen et al., 2004]. However, Mek1 and Mek2 form constitutive heterodimers and the negative feedback from ERK induces the dephosphorylation of both MAPKKs [Catalanotti et al., 2009]. Inhibition of the feedback or deletion of Mek1 causes prolonged Mek2 phosphorylation and ERK activity. This regulation might also be involved in the embryogenic lethality of Mek1 deficient mice, which cannot be compensated for by Mek2. The negative regulation of Mek1 by phosphorylation of Thr292 was also reported from the cell cycle factor Cdcd2 *in vitro* [Rossomando et al., 1994]. Additionally, Mek1 is negatively regulated by phosphorylation on Ser212, since a phosphomimetic amino acid substitution completely abolished Mek activation [Gopalbhai et al., 2003]. Mek1/2 proteins are actively exported out of the nucleus due to a "nucleus-export-sequence" (NES) and hence mainly cytosolic [Fukuda et al., 1996, Adachi et al., 2000].

1.1.3 The MAPK ERK

In resting cells, Mek1/2 and other proteins like PEA-15 maintain ERK in the cytoplasm by binding to the C-terminal common docking () domain [Tanoue et al., 2000, Fukuda et al., 1997]. Ectopic overexpression of ERK in cells therefore requires the coexpression of Mek to retain ERK in the cytoplasm [Adachi et al., 2000]. Upon pathway stimulation, Mek1/2 phos-

phorylate ERK on Thr183 and Tyr185 on a conserved Thr-Xxx-Tyr motif (Thr-Glu-Tyr for ERK proteins) in the activation segment [Payne et al., 1991, Robbins et al., 1993]. Activation of ERK leads to the dissociation of the Mek-ERK dimer and simultaneously to the association of ERK homodimers [Canagarajah et al., 1997, Fukuda et al., 1997, Tanoue et al., 2000]. Mek-ERK dimers and ERK homodimers are mutually exclusive, as both interactions involve the CD domain in ERK [Fukuda et al., 1997, Tanoue et al., 2000]. A conformational change in the dually phosphorylated protein renders ERK1/2 fully active and gives access to the DEF domain, to which many interaction partners and targets with the complemeting Phe-Xxx-Phe-Pro motif bind [Tanoue et al., 2000, Lee et al., 2004, Reményi et al., 2006].

Active ERK1/2 transiently accumulates in the nucleus and induces transcription. The detailed mechanism of the translocation has been a controverse point. One group has identified a nuclear translocation signal (NTS) encompassing a nine amino-acid-long sequence with two phosphorylation sites Ser-Pro-Ser in ERK, Mek and other signaling proteins [Chuderland et al., 2008]. This NTS is thought to become phosphorylated subsequent to the Thr-Glu-Thr motif by Casein Kinase2 (CK2) and autophosphorylation of ERK. The phosphorylated NTS then supports the nuclear translocation by the association with importin-7 [Chuderland et al., 2008, Plotnikov et al., 2011]. However, the existence of a NTS motif in ERK is not recognized by others [Caunt & McArdle, 2010, Lidke et al., 2010]. The only consensus is that the enzymatic activity of ERK is not required for the stimulus-induced nuclear accumulation, which was shown using the inactive mutant ERK-Lys52Arg. Other theories are based on the conformational change in ERK upon activation which changes the accessibility of ERK motifs, for instance to the DEF domain, and potentially enables dimerization. These changes in the ERK conformation might influence either the affinity for substrates or the import and/or export kinetics through the nuclear membrane. The nuclear accumulation of ERK indeed positively correlates with the phosphorylation on the activation segment [Caunt & McArdle, 2010]. However, the single cell variation in the dose-response of ERK phosphorylation is high with a range of 30-fold, while the ratio of nuclear to cytoplasmic localization of ERK ranges only 3-fold [Caunt & McArdle, 2010]. While this study's authors attribute this discrepancy to an uncoupling of phosphorylation and translocation, it can also be explained by the fact that not the fold-change in single cells but only the absolute phosphorylation of ERK in fixed cell was measured [Caunt & McArdle, 2010]. The influence of interactions on the nuclear accumulation of ERK was investigated using either DEF or CD domain mutants [Yazicioglu et al., 2007, Caunt & McArdle, 2010]. These publications show contradictory results: one study found significant changes only for CD domain mutants while the other only for DEF site mutants [Caunt & McArdle, 2010, Yazicioglu et al., 2007]. An explanation for the stimulus-induced accumulation of ERK would however depent on a DEF site-based mechanism, because this motif becomes accessible only upon ERK activation. *De novo* protein synthesis of, for instance, nuclear substrates was demonstrated not to be involved in ERK nuclear acccumulation. The mobility of ERK in the cytoplasm and the nucleus is invariably high before and after stimulation, which was determined by fluorescence correlation spectroscopy (FCS) [Lidke et al., 2010]. Therefore, either the interactions in the nucleus are transient or the complexes of ERK and its binding partners are mobile. One way that ERK nuclear import and export is mediated, is by nucleoporins to which ERK can bind in either activation state [Matsubayashi et al., 2001]. The import of active ERK is enhanced in an energy-dependent fashion, while the export of inactive ERK is facilitated by the binding to MEK which is exported via its NES. Older studies claimed that ERK dimers are actively transported into the nucleus, but this could not be confirmed in a study using dimerization deficient ERK mutants and fluorescence recovery after photobleaching (FRAP) [Adachi et al., 1999, Khokhlatchev et al., 1998, Lidke et al., 2010]. In this recent study the activation of ERK by phosphorylation was again shown to influence the transport kinetics. In summary, it is probably the combination of altered affinities and transport kinetics upon stimulation, that induce the translocation and retention of ERK in the nucleus.

The ERK translocation into the nucleus is a prerequisite for the induction of the transcriptional response and proliferation [Brunet et al., 1999, Torii et al., 2004]. A major part of the ERK induced transcriptional response are genes under the control of the serum response element (SRE). In order to activate it, ERK phosphorylates the p90-ribosomal-S6-kinase (RSK) and the ternary complex factors (TCFs) Elk-1, Net-1 and Sap [Yoon & Seger, 2006, Buchwalter et al., 2004, Anjum & Blenis, 2008]. RSK phosphorylates the serum response factor (SRF) which binds together with one of the TCFs to the SRE in the promoter of immediate early genes (IEG), like Fos, Myc, Fra-1 and Egr-1 [Buchwalter et al., 2004, Anjum & Blenis, 2008, Murphy et al., 2002]. Among these IEGs are transcription and cell cycle factors which in turn activate delayed early genes (DEGs) so that the response is further specified [Avraham & Yarden, 2011]. In order to investigate the correlation of ERK activity and proliferation, Albeck and colleagues did steady-state live-cell experiments with a substrate-based ERK activtiy sensor EKAR-EV [Albeck et al., 2013]. This sensor comprises an ERK substrate phosphosite and a phosphosite recognition motif, which are sandwiched between two fluorophores. This sensor detects the activtiy of ERK indirectly by a change in FRET upon phosphorylation of the construct [Komatsu et al., 2011]. This sensor showed stochastic ERK activitiy pulses which increase in frequency and duration with increasing EGF concentration [Albeck et al., 2013]. This group determined that the entry into S phase and therefore the progress in cell cycle is dependent on the integrated ERK activity [Albeck et al., 2013]. Another group confirmed the occurence of ERK pulses with the same sensor, but observed a correlation between pulse frequency and proliferation rate [Aoki et al., 2013]. In this study it is further demonstrated that ERK activity decreases with increasing cell density [Aoki et al., 2013]. Using chemical inhibition or dominant negative mutants, they found that EGFR, Ras, Rac and the cytoskeleton are required for the ERK pulses, but activity pulses of Ras and Rac could not be measured [Aoki et al., 2013]. The application of Raf inhibitors strongly prolonged the ERK activity pulses, while the inhibition of Mek decreased the number of pulses [Aoki et al., 2013]. Raf and Mek are therefore involved in the pulse generation and regulation [Aoki et al., 2013]. In combination with a light-inducible Raf it was further demonstrated that ERK activation is propagated from cell to cell. The lateral propagation is thought to depend on ERK-induced ADAM17 which cleaves surface-bound EGF. The free EGF then activates EGFR in neighbouring cells.

Additionally to the transcriptional regulation in the nucleus, ERK has essential functions in the cytoplasm and organelles as well, like cytoskeletol rearrangements, endosomal traffic or mitochondrial transcription [Yoon & Seger, 2006, Casar et al., 2009, Galli et al., 2009, Torii et al., 2004]. In support of this notion, about half of the 160 ERK substrates are non-nuclear [Yoon & Seger, 2006]. Using the ERK activity sensor EKAR-EV, [Albeck et al., 2013] demonstrated that cytoplasmic and nuclear ERK activity pulses are concurrent and equally strong. Concerning the cytoplasmic function of ERK, dimerization is again subject to controverse debate. One group showed that ERK dimers are bound by scaffolds and that these complexes are essential for the phosphorylation of cytoplasmic substrates [Casar et al., 2008]. Further, the prevention of ERK dimerization using ERK mutants prohibited proliferation [Casar et al., 2008]. However, another group which investigated the ERK function in the mitochondria found dimers in the mitochondria and the nucleus, but not in the cytoplasm [Galli et al., 2009]. *In vivo* observation of ERK dimers in the cytoplasm also failed in studies using various other techniques [Burack & Shaw, 2005, Wilsbacher et al., 2006, Lidke et al., 2010].

ERK inactivation is catalyzed by phosphatases of the MAPK phosphatase (MKP) family which has 10 members [Owens & Keyse, 2007, Britson et al., 2009, Caunt & Keyse, 2013]. Some of these dual-specificity phosphatases (DUSPs) are either specific for ERK (DUSPs 5, 6, 7 and 9) or for p38/JNK, while others are non-specific. MKPs can be localized to the nucleus, the cytoplasm and or throughout the cell. Phosphatases have a strong impact on ERK signalling as some are induced by ERK which generates a negative feedback.

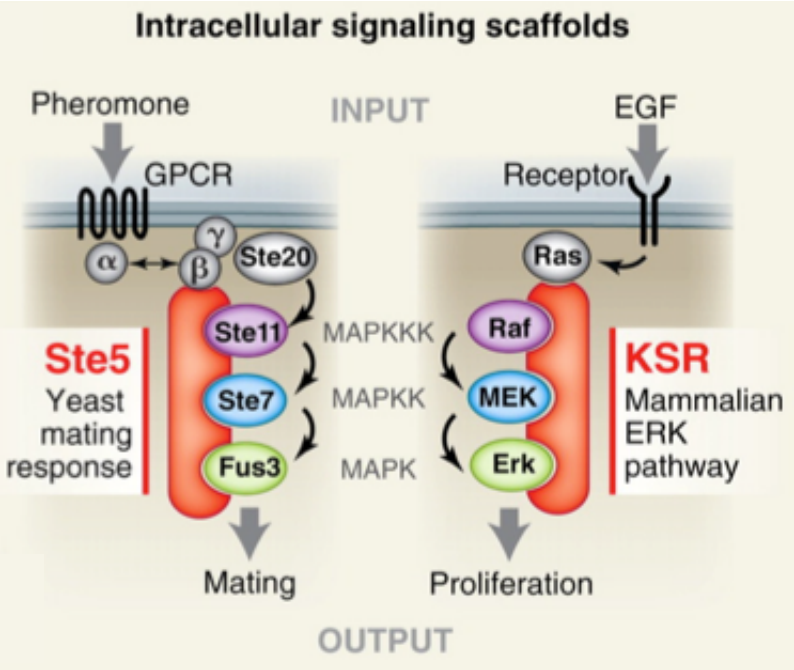

Figure 1.2: **Scaffolds colocalize signaling proteins in a cell.** Scaffolds, e.g. Ste5 in yeast or KSR for the ERK cascade, tether the MAPKs to the activated receptor at the PM and assemble the three-tiered MAPK cascade in a complex. The involvement of scaffolds facilitates signal transduction by colocalization of the signaling molecules in the 3-dimensional cellular space (adopted from [Good et al., 2011]).

1.1.4 Scaffolds and Regulatory Interactors of MAPK proteins

The first MAPK scaffold Sterile5 (Ste5) has been identified in yeast [Printen & Sprague, 1994, Hartwell, 1980]. Ste5 has binding sites for each protein of the yeast pheromone MAPK cascade (figure 1.2). Derived from the first investigations on Ste5, scaffolds were originally defined as passive "meeting places" which have binding sites for at least two proteins, e.g. enzyme and substrate, but no catalytic activity [Elion, 1995]. The assembly of specific proteins in a fixed geometric arrangement on the scaffold locally increases the concentration of the substrate and therefore enhances reaction rates [Bardwell et al., 2001]. In this process, the stoichiometry between scaffold and its binding partners is critical: Too low of scaffold abundance hampers signaling fidelity, while an excess of scaffolds to binding proteins would isolate enzyme and substrate on different scaffold molecules and thereby abrogate the signal transduction (see also 1.3.3.1) [Chapman & Asthagiri, 2009, Witzel et al., 2012]. Scaffolds can further localize signaling molecules to distinct cell compartments like activated receptors at the PM or organelles (figure 1.2). The clustering of a subset of proteins on a scaffold can either insulate a pathway from others or positively regulate pathway cross-talk. Additionally to these passive roles, scaffolds were later found to be allosteric regulators of the activation of interacting partners (Ste5) or to exhibit catalytic activity (KSR1/2) [Good et al., 2009].

Among the regulatory interactors are scaffolds (KSR, arrestin, Sef, IQGAP), modulators (RKIP and PEA15) and adaptors (MP1), whereby the transitions between classes are gradual.

1.1.4.1 KSR1/2

Kinase suppressor of Ras (KSR) was first identified in Drosophila and *C. elegans* as suppressor of active Ras with two orthologues in mammals, KSR1 and KSR2 [Therrien et al., 1995, Kornfeld et al., 1995, Sundaram & Han, 1995, Dougherty et al., 2009]. KSR proteins have five

domains, CA1 to CA5. CA1 contains a CC-SAM motif required for RTK-induced membrane localization, CA2 is proline-rich, CA3 binds to phospholipids in membranes, at least one motif for binding to the activity-dependent DEF domain in ERK1/2 is found in CA4 and CA5 constitutes a kinase domain which has mutations in the key residues regarded as essential in kinase activity [Therrien et al., 1995, Zhou et al., 2002, Kornfeld et al., 1995, Brennan et al., 2011, Koveal et al., 2012].

In quiescent cells, KSR is phosphorylated by C-TAK on Ser297 and Ser392, which are bound by 14-3-3 proteins, keeping KSR1 with constitutively bound Mek in the cytosol [Xing et al., 1997, Denouel-Galy et al., 1998, Cacace et al., 1999, Müller et al., 2001]. Upon RTK activation, PP2A dephosphorylates KSR1 at the 14-3-3 binding sites, enabling KSR to translocate to the plasma membrane [Ory et al., 2003]. Here, KSR proteins form heterodimers with Raf proteins which are sufficient to allosterically activate Raf [Rajakulendran et al., 2009]. A KSR mutant was developed with inhibited ATP binding capacity, which is stabilized in its active conformation enabling the separate investigation of scaffolding function and kinase activity [Hu et al., 2011]. While this mutant constitutively bound to Raf and Mek, it did not show kinase activity, compared to wild-type KSR1, which phosphorylated Mek1 *in vitro* when immuno-precipitated from induced Raf-KSR dimers [Hu et al., 2011]. A structural study revealed that Mek1 and the KSR2 kinase domain interact by facing each other's catalytic site in a mirror-imaged formation that mutually constrains the activation loop in an inactive position [Brennan et al., 2011]. Upon pathway activation KSR2 forms a heterodimer with B-Raf, inducing an allosteric chain reaction unfolding an active conformation of KSR2 and subsequently of MEK [Brennan et al., 2011]. The accessible Mek activation segment can then become phosphorylated by a second Raf molecule in trans [Brennan et al., 2011]. Homology modeling of the equivalent KSR kinase domain-Mek1 interaction revealed that the amino acids involved in Raf and Mek binding are conserved and therefore the binding mode between Mek and KSR1 or KSR2 is supposedly highly similar [Sibilski et al., 2013]. The ternary interplay of KSR1-Raf-Mek1 is furthermore regulated by phosphorylation of KSR1-Tyr728, which is in KSR2 mutated to a histidine. The mutant KSR1-Y728F exhibits stronger Raf, but weaker Mek1 interaction and produces stronger Mek1 phosphorylation supporting the model of KSR1-Raf dimer as catalytic platform [Sibilski et al., 2013]. KSR1 is like Raf a target of negative feedback phosphorylation by active ERK [Razidlo et al., 2004, McKay et al., 2009, Canal et al., 2011]. ERK binds to KSR at its DEF domain and phosphorylates B-Raf and KSR1 leading to the dissociation of the heterodimer BRaf-KSR and the release from the membrane [McKay et al., 2009]. Mutation of the KSR1 phosphosite leads to a change in the MAPK response from transient to sustained, as signaling from Raf-KSR1 dimers cannot be attenuated [Razidlo et al., 2004, Canal et al., 2011]. A further positive feedback between MAPK signaling and KSR1 action was found recently [Cullis et al., 2014]. The activation of MAPK signaling was shown to induce the expression of the Rho GEF GEF-H1, which is in quiescent cells bound to microtubuli. Surprisingly, this protein associates transiently with KSR1 upon growth factor stimulation and stimulates the dephophorylation of KSR1 on S392 by PP2A in a mechanism independently of its GEF activity. The dephosphorylation causes the membrane association of KSR1 and GEF-H1 as wells the induction of MAPK signaling. It was further shown that the KSR1 and GEF-H1 are required for Ras/BRaf dependent cell transformation.

1.1.4.2 $\beta-$arrestin 2

$\beta-$arrestin 2 is responsible for desensitization and internalization of GPCRs, but also links GPCR signaling to RTK activation. While GPCR activation generally causes transient ERK1/2 activity leading to ERK1/2 translocation into the nucleus, the involvement of $\beta-$arrestin 2 targets Raf/Mek/ERK signaling in early endosomes, resulting in sustained, cytoplasmic activity of ERK1/2 [Perez-Aso et al., 2013, DeFea et al., 2000, Ahn et al., 2004]. $\beta-$arrestin 2 further regulates signaling of JNK and Src-PI3K-AKT pathways [Luttrell et al., 1999, Luttrell et al.,

2001].

1.1.4.3 IQGAP 1

The IQ motif-containing GTPase activating protein 1 (IQGAP) binds to more then 90 proteins and is involved in cytoskeletal processes like regulation of cell-cell adhesion, polarity, and migration [Johnson et al., 2009, White et al., 2012]. It modulates EGFR activation and positively regulates ErbB2 expression, phosphorylation and signaling in breast cancer cells [McNulty et al., 2011, White et al., 2011]. IQGAP's interactions include Raf, Mek and ERK, and it was shown to regulate the latter two proteins in their activity [Roy et al., 2004, Roy et al., 2005]. Although IQGAP1 is non-essential, a recent study reports that ERK activity-dependent tumorigenesis can be attenuated by titrating the IQGAP1 - ERK2 interaction with a peptide which binds to the WW domain of IQGAP [Li et al., 2000, Jameson et al., 2013]. The ERK activity dependent proliferation of breast, colorectal or skin tumor cells conferred by either EGFR overexpression, KRas or BRaf mutation, was impaired by the WW binding peptide, without being toxic to wild-type cells [Jameson et al., 2013]. Application of the WW peptide furthermore terminated growth of established tumors and PLX4032 resistant B-Raf-Val600Glu cells [Jameson et al., 2013]. Despite numerous IQGAP interactions, ERK is the only protein reported to bind the IQGAP WW domain [Roy et al., 2004]. Therefore, as IQGAP is not required for normal development, but essential in ERK mediated tumorigenesis it seems to be a promising anti-carcinogenic target.

1.1.4.4 Sef

Sef is a transmembrane protein, originally found as inhibitor of fibroblast growth factor (FGF)-induced Ras/ERK signaling in embryogenesis of zebrafish. It has orthologues in different vertebrates including humans, exerting a negative regulatory role in RTK activation [Fürthauer et al., 2002, Tsang et al., 2002, Yang et al., 2003, Xiong et al., 2003]. Sef inhibits ERK nuclear translocation by binding to active Mek and ERK as homodimers, restraining them to the Golgi, ER and plasma membrane without altering ERK activity [Torii et al., 2004, Casar et al., 2009].

1.1.4.5 RKIP

The Raf kinase inhibitor protein (RKIP) is able to bind c-Raf and B-Raf, Mek and ERK. The binding sites for Raf and Mek partially overlap so that binding is mutually exclusive and hence, RKIP physically separates the two kinases [Yeung et al., 1999]. Additionally, RKIP is a competitive inhibitor for Raf, suppressing the phosphorylation of Mek and therefore the signal transduction [Yeung et al., 2000], [Park et al., 2005]. RKIP-Raf dissociation is initiated by PKC phosphorylation on RKIP Ser153, inducing RKIP dimerization [Lorenz et al., 2003], [Corbit et al., 2003], [Deiss et al., 2012]. The RKIP dimer inhibits G protein receptor kinase 2 (GRK2) which in turn enables the activation of a GPCR and couples RTK to GPCR activation [Deiss et al., 2012], [Corbit et al., 2003], [Park et al., 2005].

In PC-12 cells RKIP is the distinctive factor resulting in differentiation or proliferation via the ERK cascade upon NGF or EGF treatment (for more information see chapter 1.3.2) [Santos et al., 2007].

1.1.4.6 PEA-15

Phosphoprotein enriched in astrocytes (PEA-15) is a small regulatory protein localized to the cytoplasm, where it anchors ERK1/2. Hence, with increasing PEA-15 abundance nuclear entry of ERK1/2 can be prevented [Formstecher et al., 2001, Whitehurst et al., 2004, Glading et al., 2007, Gaumont-Leclerc et al., 2004]. However, cases of PEA-15 supporting tumor growth have also been reported [Sulzmaier et al., 2012, Eckert et al., 2008]. A recent crystallographic

study revealed that PEA-15 bound to phosphorylated ERK2 sets the activation loop of the active ERK allosterically in an inactive conformation [Mace et al., 2013]. PEA-15 therefore sequesters and retains active ERK2 [Mace et al., 2013]. The exact mechanism of ERK2 release from the complex is still unsolved but involves PEA-15 phosphorylation [Mace et al., 2013]. An accumulation of ppERK1/2 in cells overexpressing PEA-15 hints towards a protection from phosphatases [Eckert et al., 2008]. A continuous retardation of active ERK1/2 can potentially lead to sustained cytoplasmic ERK1/2 activity.

1.1.4.7 MP1

MEK partner 1 (MP1) specifically binds to Mek1/2, supporting Erk1/2 activation and MAPK signaling *in vivo* [Schaeffer et al., 1998, Teis et al., 2002]. MP1 is part of a trimeric protein complex with p14 and the lipid raft adaptor protein p18 in which p14 bridges between Mek1 and p18, which anchors the p14-MP1 complex to late endosomes [Teis et al., 2002, Nada et al., 2009]. p14 and p18 are each essential during early mouse embryogenesis. Additionally, mouse embryonic fibroblasts (MEFs) lacking p14 or p18 show distorted endosome and lysosome distribution, as well as endosome sorting defects, accompanied by decreased Mek1/2 and ERK1/2 activity [Teis et al., 2006, Teis et al., 2002, Nada et al., 2009]. MP1 associates with PAK to enhance PAK-dependent Mek1 activation, connecting MAPK signaling with cell migration and spreading via Rho [Pullikuth et al., 2005]. The Mp1-p14-p18 complex has further been shown to be essential in the amino acid dependent mTORC1 activation at lysosomes [Sancak et al., 2010].

1.2 *Saccharomyces cerevisiae* MAPK pathways

In *S. cerevisiae* (budding yeast), four MAPK pathways are well known [Gustin et al., 1998, Chen & Thorner, 2007]. In contrast to mammalian cell lines, yeast has an easily modifiable genome, enabling the study of MAPK signaling without altering expression levels [Janke et al., 2004]. Using engineered interactions the transition to synthetic biology has been accomplished [Bashor et al., 2008, Peisajovich et al., 2010].

The yeast MAPK cascades are induced by starvation, osmotic shock, pheromone stimulation or cell wall stress. Under each condition specific cell surface receptors transmit the information to the activation of a certain terminal MAPK protein; these are Kss1 (kinase suppressor of Sst2), Hog1 (high osmolarity/glycerol), Fus3 (fusion) and Slt2 (suppressor of LYT2). However, in three of the four pathways the signal from receptor to MAPK is transduced via shared components. Pheromone and starvation pathways share the MAPKK Ste7 (sterile), the MAPKKK Ste11 and PAK Ste20. The two latter kinases function additionally in a third pathway, the osmotic shock cascade (figure 1.3). To ensure the correct cellular response despite the use of the shared intermediary signaling components, scaffolds connect the signal from the receptor to the activation of the appropriate MAPK. In the case of pheromone stimulation or high osmolarity, these are the scaffolds Ste5 and Pbs2. They are required additionally to an active Ste7 or Ste11 to activate the MAPKs Fus3 or Hog1. If solely an intrinsically active Ste7 or Ste11 mutant is expressed, Kss1 from the starvation response becomes activated as a default response.

During mating of haploid yeast, the different pathways need to cooperate in order to maintain the cell's homoeostasis: The mating-specific cell response is generated via the yeast pheromone pathway. One aspect of the mating response is polarized growth of the otherwise round yeast cell. The polarized morphology is called "shmoo". Hereby, the cell wall stress pathway is required to support the cell wall remodeling during polarized growth. Further, it was recently shown that subsequent to polarized growth, the intracellular osmolarity is balanced by the Hog1 pathway [Baltanás et al., 2013].

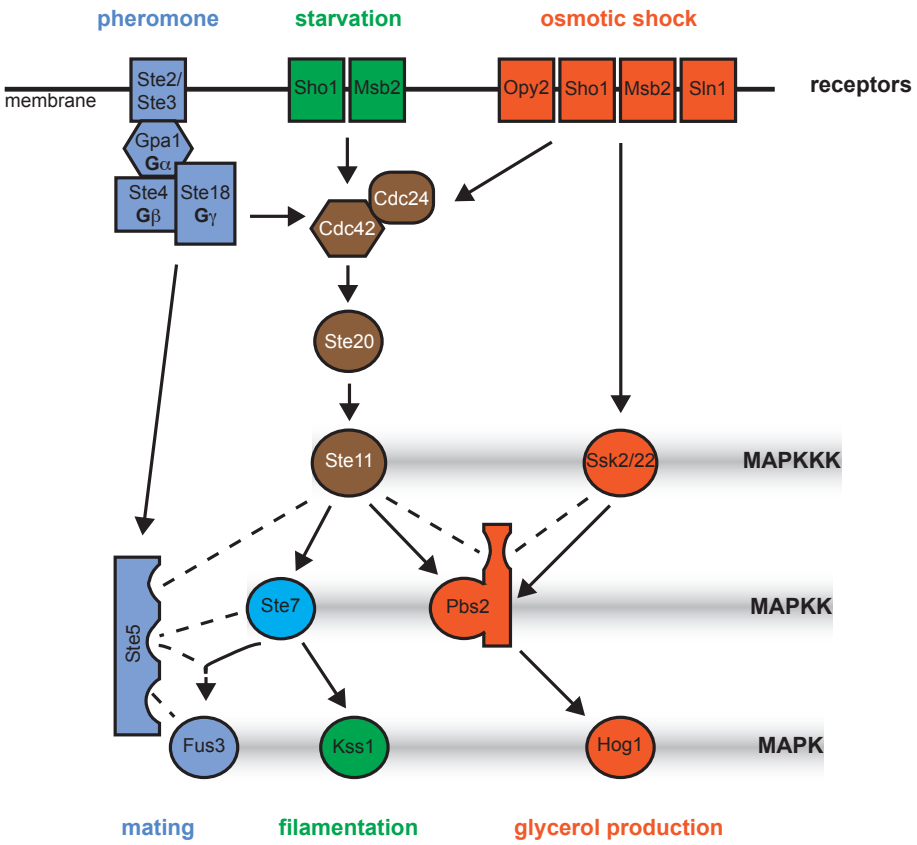

Figure 1.3: **Scaffolds specify signals from shared components in yeast MAPK pathways.** Three of the four yeast MAPK pathways share the small GTPase Cdc42, the PAK Ste20 and and MAPKKK Ste11 (brown). The pheromone (blue) and starvation (green) pathways further share the MAPKK Ste7 (turquoise). To achieve signal specificity, the pheromone and high osmolarity pathways utilize scaffolds (Ste5 and Pbs2), which connect a pathways specific upstream component, e.g. the receptor, to the specific MAPK Fus3 or Hog1.

1.2.1 Signaling components of the pheromone MAPK cascade

Yeast exists in two sex types, Mat**a** and Matα. They secrete short peptides, either C-terminally farnesylated 12-amino-acid or unmodified 13-amino-acid long, which are named pheromone or **a**- and α- factor, respectively. The pheromone binds to a Mat type-specific GPCR Ste2 or Ste3, inducing the dissociation of the G protein α-subunit from $\beta\gamma$-subunit [Klein et al., 2000]. The free G$\beta\gamma$ is able to bind a p21-activated protein kinase (PAK) Ste20 and a scaffold protein Ste5, which has binding sites for each of the pheromone pathway MAPKs [Choi et al., 1994, Inouye et al., 1997, Feng et al., 1998]. Processes involving the small GTPase Cdc42 activate Ste20, initiating the activation of the MAPK cascade [Wiget et al., 2004, Winters & Pryciak, 2005]. The MAPKKK Ste11 is phosphorylated by Ste20 on three activation loop sites S302, S306 and T307 [van Drogen et al., 2001]. Active Ste11 in turn phosphorylates MAPKK Ste7 on the two activating sites S359 and T363 [Zheng & Guan, 1994]. Ste7 has six further phosphorylation sites of unknown function [Maleri et al., 2004]. Ste7 phosphorylates the MAPKs Fus3 and Kss1 on Thr180 and Tyr182 (Fus3 nomenclature) of the conserved Thr-Glu-Tyr motif in the activation loop. Kss1 can assume up to 10% of the function of Fus3 [Elion et al., 1991, Cook et al., 1997, Farley et al., 1999].

Signaling of Fus3 leads to a cell cycle arrest to align the potential mating partners, a specific transcriptional program and polarized growth in direction of the highest pheromone concentration [Chang & Herskowitz, 1990, McCaffrey et al., 1987]. The cell cycle arrest in G1 phase is conferred by Fus3 phosphorylating Far1, which in turn inhibits the cyclin dependent kinase 1 (CDK1). In other stages of the cell cycle CDK1 inhibits the cell cycle arrest by phosphorylating Ste5, which impairs the Ste5 membrane association [Strickfaden et al., 2007]. Other targets of Fus3 are the transcription factors Ste12 and Dig1/2, whose phosphorylation results in the expression of Fus1 among others. Fus1 expression is commonly used as reporter for pheromone pathway activation. Finally, haploid cells of opposite mating types fuse and build a diploid yeast cell.

1.2.2 Regulatory mechanisms of the pheromone MAPK cascade

The regulatory mechanisms of the pheromone pathway are required to ensure pathway insulation, orientation in the extracellular pheromone concentration field and the robustness of the mating response. Pathway insulation is necessary to translate the activation of the pheromone receptor into the mating response instead of one of the other MAPK responses. Fus3 is intrinsically a poor substrate for its MAPKK Ste7, which prevents Fus3 activation upon starvation signaling [Good et al., 2009]. To achieve activation of Fus3, a complex of Fus3, Ste7 and a domain of Ste5 is required. Ste5 allosterically "unlocks" the activation loop of Fus3, which increases the activity of Ste7 towards Fus3 5000-fold [Good et al., 2009]. To prohibit cross-activation from the pheromone into the filamentous growth pathway, Fus3 phosphorylates the filamentous-specific transcription factor Tec1, causing its ubiquitin-dependent degradation [Chou et al., 2004, Bao et al., 2004]. The requirement for Ste5 as catalyst for full Fus3 activation ensures additionally to pathway insulation a localized activation of Fus3 at the site of pheromone receptor activation. In pheromone-stimulated cells which form a shmoo, a gradient of active Fus3 emanates from the shmoo tip towards the nucleus (figure 1.4) [Maeder et al., 2007]. This Fus3 activity gradient was speculated to ensure the correct shmoo morphology and position of the nucleus (for more information see chapter 1.3.3.3) [Maeder et al., 2007]. The gradient might further serve as an intracellular morphogen to link receptor activation with polarized cell growth. The orientation of the projection tip in the direction of the highest pheromone concentration enables the cell to fuse with the closest potential mating partner and thereby preserve energy. Economic viability also defines a minimum pheromone concentration upon which yeast cells start the mating program. The pheromone concentration sensed by a cell can be interpreted as the distance to the secreting mating partner. Below a certain pheromone

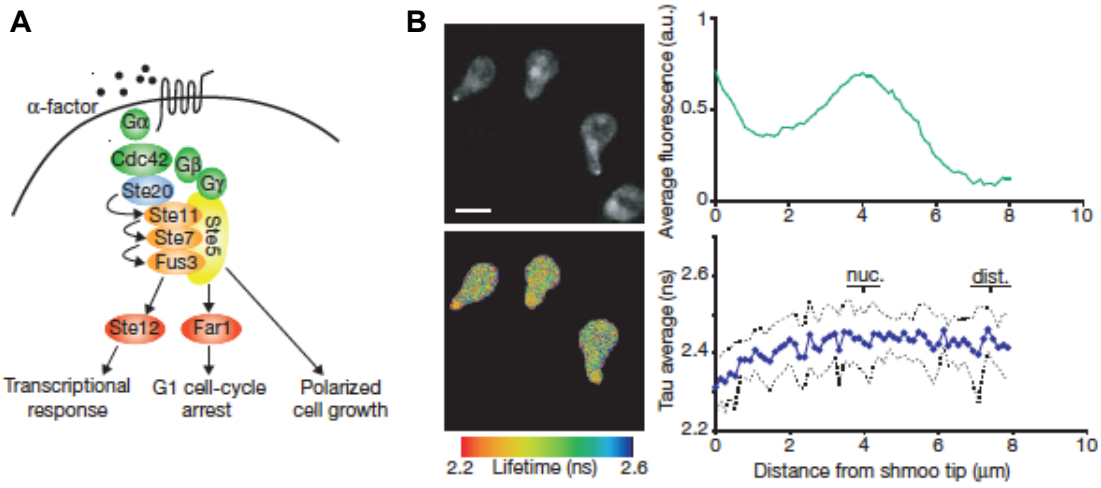

Figure 1.4: **Yeast pheromone pathway and MAPK Fus3 phosphorylation gradient.** (A) Schematic representation of the yeast pheromone MAPK module. (B) FLIM of phosphorylated Fus3 in stimulated yeast. Yeast expressing Fus3-GFP was fixed and stained with Cy3 labeled anti-ppFus3 antibody. Images show intensity and lifetime distribution with false-color look-up-table (left side) with corresponding distribution from shmoo tip to end (adapted from [Maeder et al., 2007]).

concentration threshold, the mating partner is too far away and growth in this direction would consume too much energy. However, if the pheromone concentration is sufficiently high, the mating response is initiated in a switch-like manner [Malleshaiah et al., 2010]: In vegetatively growing yeast, Ste5 allosterically supports the autophosphorylation of Fus3 on Tyr182, which increases Fus3 activity by factor 25 (doubly phosphorylated Fus3 shows an 120-fold increase in activity) [Bhattacharyya et al., 2006]. Partially activated Fus3 in turn phosphorylates Ste5 on four Thr and Ser sites, thereby strengthening the interaction between Fus3 and Ste5 [Bhattacharyya et al., 2006, Malleshaiah et al., 2010]. Upon pheromone stimulation with sufficiently high concentration, Ste5 is dephosphorylated by the phosphatase Ptc1, leading to the switch-like dissociation of Fus3 from Ste5 [Malleshaiah et al., 2010]. The switch-like mating decision is potentially essential for the robustness of the mating response despite cell-to-cell variability in protein stoichiometry [Malleshaiah et al., 2010, Paliwal et al., 2007].

1.3 Regulation of the ERK network

While MAPK pathways in yeast share single signaling components, some mammalian cells employ the complete Raf/Mek/ERK cascade for differential cell responses. This chapter will explain how signaling specificity can still be achieved by dynamic regulation of the ERK response.

The utilization of the ERK cascade for the GF-specific induction of the differential cell fates differentiation and proliferation in the same cell line has been described in the following examples: NGF vs. EGF in PC12 cells, HRG and FGF vs. EGF in MCF-7 and PDGF vs. EGF in fibroblasts [Nguyen et al., 1993, Nagashima et al., 2007, Wosikowski et al., 1993, Razidlo et al., 2004, Thottassery et al., 2004]. The differential cellular outcome is determined by the ligand-specific environment of signaling; each GF binds to a different receptor which additionally recruits other regulatory interactors to the MAPK cascade, like GTPases or scaffolds (see 1.3.1). This receptor specific protein network constitutes a unique set of interactions and spatio-temporal activity profiles (see 1.3.2). The incoming signal is processed through the complex network and focussed in the ERK activity. However, ERK is not the endpoint or a passive

receiver in the signal processing, it participates by phosphorylating upstream network proteins in a feedback or inducing transcriptional feedbacks. simultaneously, ERK, like all MAPKs, links the signal procession with the execution into a cell response. Differential regulation of ERK response properties results in the activation of distinct substrates and effects differential between cell fates.

1.3.1 Ligand-specific context of signaling

The ERK cascade is integrated in a ligand-specific protein network. Each ligand binds to a different receptor which in turn recruits and activates a different set of regulatory interactors. The network composition is further determined by the cellular state and the spatio-temporal activity profile of the receptor, as each receptor has differential recycling and degradation kinetics. The internalization of the active receptor in endosomes can generate intracellular signaling platforms. At these endosomes certain regulatory interactors are available, for instance β-arrestin in early and MP1 at late endosomes. So in this context, the ERK cascade interacts with different proteins than at the PM. Additionally, ERK activated at endosomes can penetrate more deeply into the cytosol and reach for instance the nucleus, although phosphatases in the cytosol restrain the spreading of phosphorylated ERK (see chapter 1.3.3.3). Targeted trafficking of endosomes to organelles delivers active molecules to accomplish local functions, like migration at focal adhesions.

Additionally to the diverse functions of the regulatory interactors described in chapter 1.1.4, also differential activation dynamics of GTPases can regulate the activation of the MAPK cascade. The ERK-induced transcription can change the stochiometry of network proteins after 20-60 minutes of stimulation. Particularly phosphatase transcription is induced by ERK. Phosphatases deactivate the kinases in the cytosol which constitutes a negative feedback [Bhalla et al., 2002].

1.3.2 Network topology

Dynamic MAPK signaling arises from the differential composition of the surrounding network and the underlying individual interactions. The entirety of positive and negative interactions (e.g. activation and deactivation) in a network is defined as the network topology. Additionally to the linear sequence of signal transduction, a pathway output (e.g. active MAPK) can modify its own input (e.g. MAPKKK), which is referred to as feedback (positive or negative). Another network motif is the feedforward loop, here a network component influences a target, which is at least two levels downstream. Therefore, the target is modified by its direct upstream and additionally by the two-level upstream (indirect) component.

In MAPK pathways, the signal is channeled through the terminal MAPK. Therefore, the specific protein network and its topology find expression in the activity of the terminal MAPK. However, the MAPK exerts feedback by phosphorylating upstream proteins and is therefore involved in its own regulation.

1.3.3 Dynamic responses of signaling networks

The differential response of ERK, although always always part of the same three-step cascade, has been explained with differential protein network compositions and their individual topology. These influence amplitude, duration and localization of ERK activity. However, every spatio-temporal activity profile relies on a specific dose-response relation. Therefore, the behavior of a network component can be either investigated as spatio-temporal dependence induced by a constant stimulus, or as dose-dependence at steady-state. A reversible, covalent modification process, like protein phosphorylation, exhibits a variety of dose-response

behaviours. In this chapter the kinetics of protein phosphorylation and different network architectures are described and how they shape the spatio-temporal ERK activity profile.

1.3.3.1 Dose-response relations of MAPK phosphorylation

The presented mechanisms of stimulus-phosphorylation relations apply for every reversible and covalent modification cycle. The prevalence of phosphorylation over other modifications in many cellular functions can be attributed to its stability under physiological conditions, which requires for enzymatic regulation [Westheimer, 1987, Kamerlin et al., 2013].

In general, the dose-response behaviour of a certain protein with multiple phosphorylation sites depends on the following conditions: the concentrations of the converter enzymes (kinase and phosphatase) relative to the substrate, the affinities of the converter enzymes for each phosphorylation state of the substrate and the kinetics of the catalytic steps [Salazar & Höfer, 2009].

The kinetics of phosphorylation can roughly be divided into cooperative or Michaelis-Menten type. If the first phosphorylation of a protein with at least two phosphorylation sites increases the probability for further modification, a cooperative mechanism takes place. The first phosphorylation therefore accelerates the second one. A cooperative mechanism is represented by a sigmoidal relation of dose and response, referred to as ultrasensitivity [Goldbeter & Koshland, 1981]. The response is amplified relatively to the input, if the stimulus concentration is above a certain threshold. Such a behaviour supports the maintenance of the proportional activity from one cascade level to the next, if the substrate is in excess relative to its enzyme, which applies to Mek and Raf (measured concentration of Mek 1.4 μM to 0.013 μM for Raf [Fujioka et al., 2006]). The suppression of signals below the threshold filters out spurious signals.

There are three major mechanisms which cause ultrasensitivity: inhibitor ultrasensitivity, multi-step ultrasensitivity (like cooperativity) or zero-order ultrasensitivity [Goldbeter & Koshland, 1981, Huang & Ferrell, 1996, Ferrell Jr, 1996]. For MAPKs, the zero-order mechanism is specifically important. Here, the converter enzymes which catalyze the (de-)phosphorylation operate near saturation. Therefore, a small increase in stimulation, equivalent with an increase in the concentration of active kinase, will cause a steep response because the constant phosphatase level remains saturated.

The dual phosphorylation required to activate a MAPK was considered a multi-step mechanism enabling ultrasensitivity for a long time [Goldbeter & Koshland, 1981, Huang & Ferrell, 1996, Ferrell Jr, 1996]. More recent studies find that multisite phosphorylation alone constitutes a sufficient threshold, upon which active molecules begin to accumulate, but not a switch [Gunawardena, 2005]. However, in combination with cooperativity, switch-like responses can still be generated by biphosphorylation processes. Thereby, the rate of the first phosphorylation of a MAPKK is determined by the linearly increasing concentration of the activating kinase MAPKKK* (* indicates MAPKKK is active). The substrate concentration, the unphosphorylated protein MAPKK, stays constant because it is in excess. The second phosphorylation of MAPKK-P is a second-order reaction, because the concentrations of activating kinase MAPKKK* and the substrate, MAPKK-P, both increase linearly. This applies only for a distributive phosphorylation process [Goldbeter & Koshland, 1981, Huang & Ferrell, 1996, Ferrell Jr, 1996]. In a distributive process only one site is modified per binding event, while in a processive catalysis both phospho-sites are modified upon a single interaction. However, in the crowded environment of the cytoplasm both cases, distributive and processive phosphorylation will take place [Humphreys et al., 2013].

In a cascade with multiple levels, like the three-step MAPK cascade, the response was demonstrated to become more sensitive with every cycle of phosphorylation and dephosphorylation (figure 1.5) [Huang & Ferrell, 1996].

Scaffolds are thought to favour a processive reaction because binding and rebinding of kinase and substrate to the scaffold are assumed to be unlikely [Burack & Shaw, 2000, Takahashi &

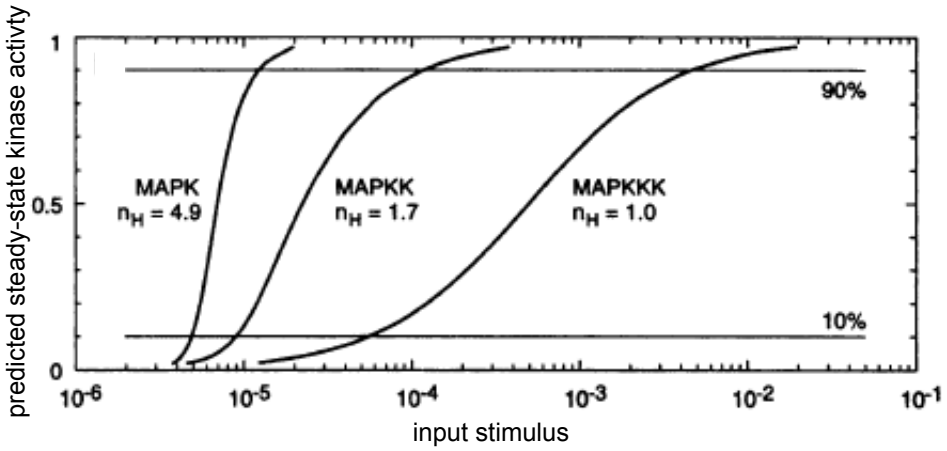

Figure 1.5: **Sensitivity amplification in a cascade.** Semi-logarithmic dose-response plot for each level of a three-tiered cascade with distributive phosphorylation steps. The dose-response of the MAPKKK follows Michaelis-Menten-kinetics, expressed by a Hill-coefficient of $n_H = 1$. Ultrasensitivity increases with each cascade level. Adapted from [Huang & Ferrell, 1996].

Pryciak, 2008]. Consequently, scaffolds promote a graded dose-response behaviour, which is more sensitive at low doses. Simulations demonstrate further that scaffolds can increase the rate of MAPK activation and increase the steady-state concentration of active MAPK [Levchenko et al., 2000]. In order to amplify the activation of a bound MAPK, the scaffold concentration within a certain range, relative to its binding partners [Bray & Lay, 1997, Chan et al., 2012]. At too high concentrations, enzyme and substrate will be physically separated on different scaffolds so that signaling will be attenuated, an effect termed "pro-zone" or "combinatorial inhibition" [Bray & Lay, 1997, Levchenko et al., 2000]. Too low concentrations are not sufficient to effectively support the signal transduction. However, scaffolds are conversely also involved in a mechanism which can produce an ultrasensitive dose-response in conjunction with multisite phosphorylation. This model discusses the sequestration and protection of the active substrate from (de-)phosphorylation [Serber & Ferrell, 2007, Liu et al., 2010, Dushek et al., 2011]. The protecting environment can be a protein, a membrane or an organelle. Here, the ultrasensitivity arises from the (supra-)molecular structure serving as a sink for the (un-)phosphorylated protein. For example, unlike the phosphorylated Ste5, the unphosphorylated Ste5 has an increased affinity to the PM, which results in reduced availability for both forward and backward reaction. Once the unphosphorylated Ste5 leaves the membrane, the first phosphorylation decreases the possibility of Ste5 rebinding to the PM and therefore promotes further phosphorylation and maintenance in the cytosol. So, under utilization of the membrane as sink for unphosphorylated Ste5, the multisite phosphorylation generates a switch-like dose-response of Ste5 phosphorylation and membrane dissociation [Serber & Ferrell, 2007]. That way, scaffolds can either promote a graded or an ultrasensitive response. The respective outcome is again dependent on affinities, kinetics and the relative concentrations of the relevant proteins (see above) [Locasale et al., 2007, Liu et al., 2010, Levchenko et al., 2000].

The combination of a non-linear dose-response, like ultrasensitivity, and either a positive or a double-negative feedback can generate bistability (see figure 1.6) [Ferrell & Xiong, 2001]. A bistable system can flip between two steady-states, but not remain in an intermediate state [Ferrell, 2002]. The ultrasensitive behaviour keeps the system in an "off" state below a certain concentration of stimulus, while upon crossing the threshold the positive feedback immediately amplifies the sigmoidal response and the system is directly in the "on" state [Ferrell &

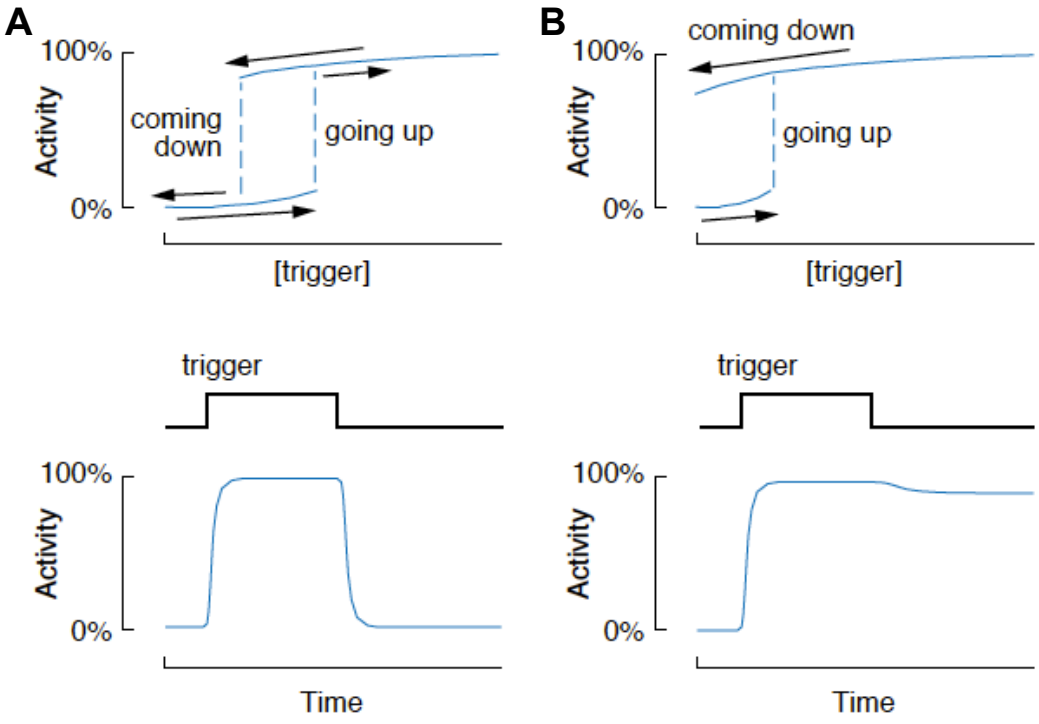

Figure 1.6: **Bistability and hysteresis.** (A) A reversible, bistable system is "on" as long as the stimulus is present. The switching threshold between "on" and "off" states depends on the initial point. (B) An irreversible, bistable system stays "on", also if the stimulus is withdrawn. Adapted from [Ferrell, 2002].

Xiong, 2001]. A property of bistable responses is hysteresis. Either the switching point shifts, depending on the initial stimulus concentration, or, the system becomes stuck in the "on" state, once it is flipped and is hence irreversible [Ferrell & Xiong, 2001]. Multi-site phosphorylation alone can cause bistability without a feedback, if the converter enzymes fulfill certain kinetic characteristics [Markevich et al., 2006, Ortega et al., 2006, Thomson & Gunawardena, 2009]. These conditions can be supported by the involvement of scaffolds [Chan et al., 2012].

1.3.3.2 Network responses – in time domain

Most recent results from ERK activity sensors in live cells demonstrate that network responses, cumulated in the ERK activity, might be – unsurprisingly – more complex than assumed [Albeck et al., 2013, Aoki et al., 2013]. These publications showed that ERK activity pulses occur stochastically during a cell cycle in dependence on the cell density [Albeck et al., 2013, Aoki et al., 2013]. Cell division seems to be proportional to the frequency of activity pulses [Aoki et al., 2013]. Here, the basic network responses adaptation, oscillation and bistability and their downstream interpretation are described.

In an adaptive response, the ERK activity increases upon a fold-change in the stimulus concentration, but is thus downregulated, despite a constant stimulation of the receptor (figure 1.7 B). Adaptation to the stimulus is typically caused by a negative feedback. Repeated increase of the stimulus concentration causes further transient periods of ERK activity in the range of one to ten minutes. This transient MAPK activity results in the initiation of protein synthesis of immediate early genes (IEGs).

An ultrasensitive, negative feedback with a time delay can lead to sustained oscillations (figure 1.7 C). The time delay can be accomplished by the suppression of a component which is at least two steps upstream, e.g Raf in the case of ERK. The ultrasensitivity in the feedback is nec-

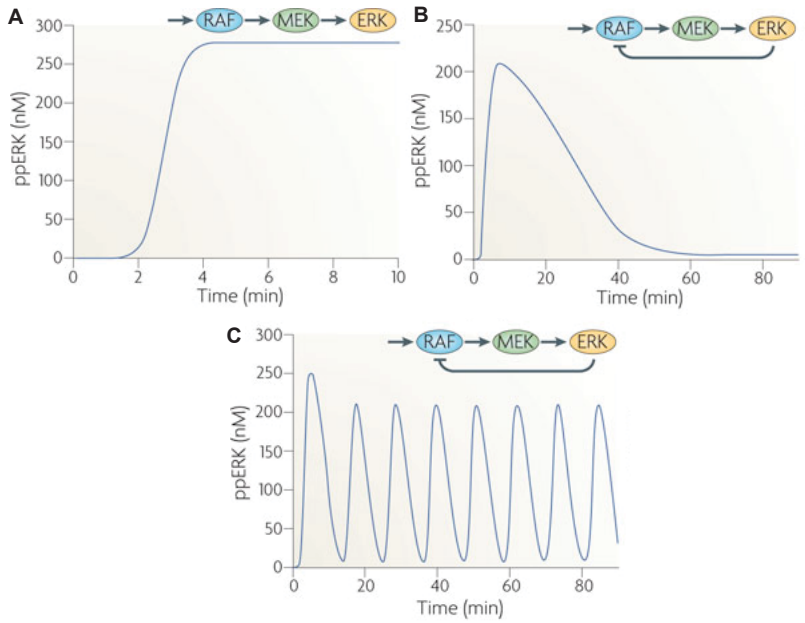

Figure 1.7: **Temporal dynamics of ERK activity in different network motifs.** (A) Response of ERK in a solely linear cascade. (B) ERK activity is transient, if a negative feedback is present. (C) ERK activity can oscillate if the negative feedback is delayed. Adapted from [Kholodenko et al., 2010].

essary to prevent a dampening of the amplitudes [Asthagiri & Lauffenburger, 2001, Brightman & Fell, 2000, Kholodenko, 2000, Avraham & Yarden, 2011].

An irreversible response is for instance important in the cell cycle or in the decision to differentiate [Huang & Ferrell, 1996]. Prolonged duration of MAPK activity additionally effects the post-translational phosphorylation of the protein after 30-60 minutes, constituting a "logic AND gate" or a coherent feedforward loop (CFL) for proteins which are intrinsically unstable [Murphy et al., 2002, Mangan et al., 2003, Nakakuki et al., 2010]. This kind of network motif follows the mechanism of multi-step ultrasensitivity as well.

1.3.3.3 Network responses – in spatial domain

Additionally to the temporal regulation of ERK activity, the spatial control allows for further variations of the ERK response, although time and space profiles are not independent from each other. In this paragraph the influence of dose-response relations and network motifs on the spatial activity distribution are described.

The binding of an extracellular ligand to a receptor induces the recruitment and activation of signaling proteins to the PM. Furthermore, the relocation from the three-dimensional cytosol on the two-dimensional membrane increases the concentration of these proteins and potentially their reaction rate. A spatial partitioning of activation and deactivation takes place, because the deactivating phosphatases cannot bind to the PM and reside in the cytoplasm. The PM is therefore the source of active signaling molecules, while the cytosolic phosphatases constrain the signal propagation in the axial direction. So, how do active molecules attain intracellular locations, especially the nucleus? Computational modeling of the activity distribution of a soluble substrate which is activated and deactivated in separated areas results in a gradient [Brown & Kholodenko, 1999, Bastiaens et al., 2006]. The distance λ, to which the gradient decays to $\frac{1}{e}$ of its initial intensity is thereby dependent on the dephosphorylation rate k_{Dephos} with $k_{Dephos} = c(phosphatase) \cdot k_M(phosphatase)$ and the diffusion D of the active molecule:

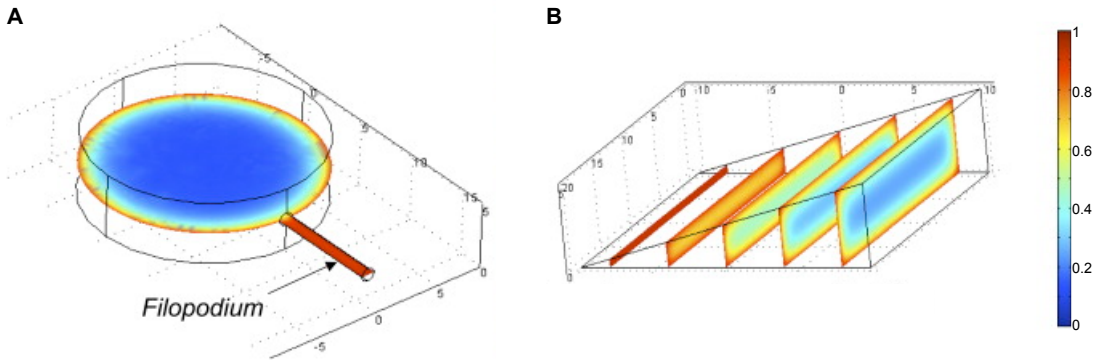

Figure 1.8: **Relation of cell shape and gradient length determines local phosphorylated fraction.** Concentration profile (look-up table on the right) of the phosphorylated form of the substrate are shown for parameters: $\lambda = 1\mu m$, $k_{kin} = 50s^{-1}$. A) Planar slice through a cylindrical cell (radius = $8\mu m$, height = $5\mu m$) with a filopodium (radius = $0.5\mu m$, length = $8\mu m$). Owing to the different radii of cylindrical cell and filopodium, the phosphorylated fraction in the filopodium is high, while the concetration of phosphorylated substrate in the cytoplasm is low. B) The phosphorylated fraction increases at a site of polarization because the distance between membranes is small relative to the gradient length. Shown are 5 planar slices of a cell with width = 20 μm, length = 20 μm, height = μm. Adapted from [Meyers et al., 2006].

$$\lambda(\mu m) = \sqrt{\frac{D(\mu m^2 s^{-1})}{k_{Dephos}(s^{-1})}}$$

The concentration of the phosphorylated form of a protein at the PM, which is the amplitude of the phospho-gradient, mainly depends on the reaction rate of the activating kinase [Brown & Kholodenko, 1999].

In order to determine the resulting global concentration of the phosphorylated protein, the gradient length has to be set in relation to the three-dimensional cell shape [Meyers et al., 2006]. The surface-to-volume ratio and local membrane proximity determine the global and local phosphorylated fraction. Cell protrusions and flat cell edges exhibit higher phosphorylated fractions than regions around the cell's center because gradient length and membrane distances are on the same scale (see figure 1.8) [Meyers et al., 2006].

From these considerations the following consequences for the activity distribution of the MAPK elements can be derived. Raf must bind to Ras-GTP at the membrane for activation. Its spatial activity profile is a steep gradient which defines then the area of Mek activation. The Mek activity profile is therefore extended in axial direction and the area of ERK activation is accordingly even broader. Modeling the activity distribution of each cascade level with Michaelis-Menten-kinetics reveals gradients for each active component which become extended and shallower down the cascade (figure 1.9 A) [Kholodenko, 2006]. The derived decay length of active ERK is sufficiently extended to enable active ERK to enter the nucleus and therefore overcome the range of the phosphatases.

However, under ultrasensitive conditions, the substrate gradient's extent does not substantially exceed the gradient length of its converting enzyme (figure 1.9 C and B) [Markevich et al., 2006, Melen et al., 2005, Semenov et al., 2013]. The detailed influence of the (de-)phosphorylation mechanism (processive or distributive) and positive or negative feedback from ERK to Ras on the spatial propagation of ERK activity is shown in figure 1.10. Negative feedback from ERK to Ras reduces the amplitude and extent of the ERK activity gradient [Sun et al., 2014].

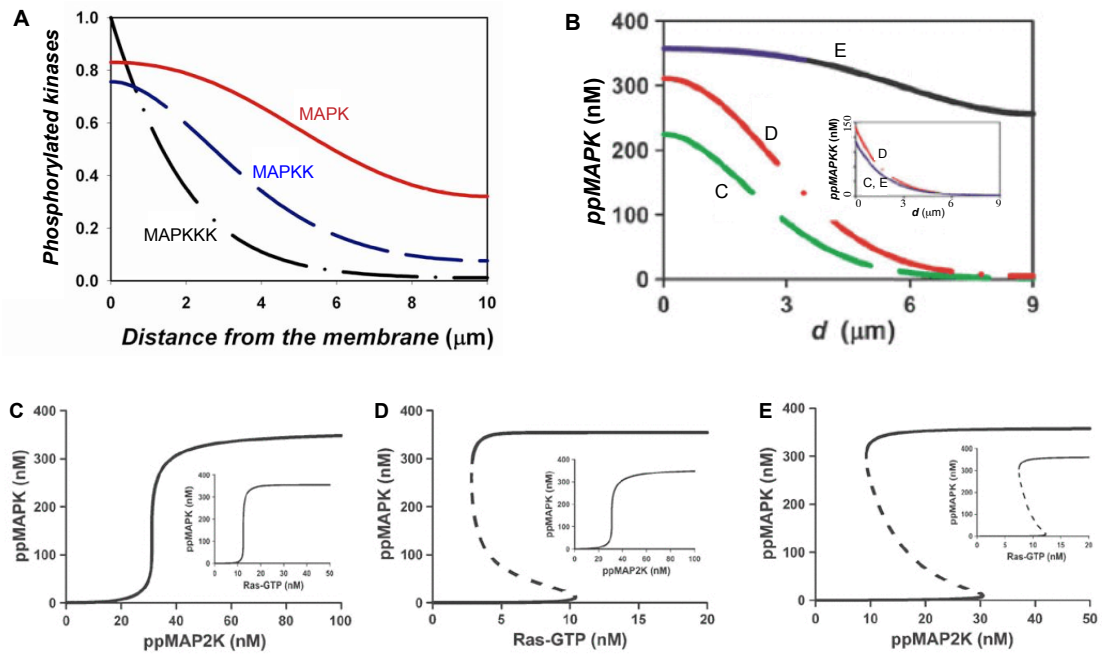

Figure 1.9: **Influence of the cascade's dose-response on the spatial distribution of ppMAPK.** (A) Phosphogradients of serially activated enzymes become shallower with each level if the enzymatic steps follow Michaelis-Menten kinetics. (B) Spatial distributions of ppMAPK in steady-state corresponding to the dose-responses from (C-E). Inset: Corresponding distributions of ppMAPKK. (C-E) Different dose-responses shown each for Ras - ppMAPK and the subordinated input-output ppMAPKK - ppMAPK. (C) Amplified ultrasensitivity in the cascade. (D) Ultrasensitivity from ppMAPKK to ppMAPK and bistability in the Ras - ppMAPK relationship generated by a positive feedback from ppMAPK to Ras. (E) Bistability in the ppMAPKK - ppMAPK dose-response. Adapted from [Markevich et al., 2006, Kholodenko, 2006].

In any network motif, a slight degree of processivity in the dephosphorylation steps abolishes the spreading of active ERK so that processive dephosphorylation seems unlikely [Sun et al., 2014]. The processivity of the kinase however changes the ERK distribution explicitly only in combination with a negative feedback.

In steady-state, a bistable dose-response between cytosolic proteins Mek and ERK nearly homogenizes the distribution of active ERK throughout the cytoplasm, although Mek activity is still restrained to the PM-proximal region (figure 1.9 E and B) [Markevich et al., 2006]. Observation of the time-resolved activity distribution between stimulation and steady-state reveals a wave of phosphorylation which travels through the cytosol. This wave rapidly propagates the signal from the PM to intracellular locations which is especially important to cover large distances where diffusion would be too slow.

Bi- or multistability during signal transduction at the membrane generates spatial inhomogenity. Depending on the local stimulus concentration, e.g. the receptor occupancy, the response can result in any stable steady-state, for instance "on" or "off" in bistability. These disparities at the membrane are involved in pattern formation and polarization, for example in differentiation.

The location of differential signaling can be controlled by the stimulus-induced recruitment of scaffolds, like Ste5 and KSR, to connect a spatial landmark at the PM to the activation of MAPKs. This accumulation may optimize scaffold concentration in locally restricted membrane patches and prevent scaffold-enhanced signaling in the cytoplasm, if the cytoplasmic scaffold concentration is unfavourable [Levchenko et al., 2000]. As discussed above, scaffolds can influence the sensitivity and signal procession in multiple ways. The scaffolded signaling domains may therefore either contribute to the propagation of MAPK activity towards the nucleus or direct the MAPK to local functions. MAPK activity can be guided towards the locally available targets either by global restriction or confined activation, respectively, for instance by signaling endosomes [Ge et al., 2003]. Signaling endosomes relocate MAPK activation from the PM into the intracellular space [Ginty & Segal, 2002]. The described spatial propagations of MAPK activity occur in the same manner from signaling endosomes, but the distances in axial direction are shorter so that active MAPK can penetrate further in direction of the cell's center.

In the case of yeast, the scaffold Ste5 is a prerequisite to yield fully phosphorylated Fus3. As the scaffold accumulates at the prospective mating tip by binding to the active receptor, it connects a spatial landmark to the localized activation of Fus3. Fus3 therefore builds a primary, steep gradient. However, the extent of its gradient is sufficient for the dimensions of a yeast cell, at least in the beginning of the tip growth, to reach the nucleus and start the transcriptional program (diameter of yeast is about 5-10 μm, HeLa cell about 50 μm).

1.3.4 Case studies of dynamic signaling via the ERK cascade

The best-investigated case of differential signaling via the ERK cascade is the NGF-induced differentiation and EGF-induced proliferation in PC-12 (rat pheochromocytoma) cells. Upon EGF stimulation ERK1/2 show transient activity, while NGF induces sustained ERK1/2 activity. Different mechanisms have been found for this dynamic behaviour. First, the activation of different GTPases Ras or Rap1 were identified as decisive factors [York et al., 1998, Sasagawa et al., 2005]. Also the differential internalization and degradation dynamics of EGFR and the NGF receptor were thought to be responsible [Schoeberl et al., 2002]. Later however, it was found by modular response analysis (MRA) that ERK exhibits upon EGF stimulation a negative and upon NGF stimulation a positive feedback on Raf, thereby attenuating or promoting its own activity [Santos et al., 2007]. Additionally to the different network topologies, it was shown that the positive feedback is mediated via PKC which is integrated in the NGF-dependent MAPK network. PKC phosphorylates RKIP, thereby impairing a negative feedback from RKIP on Mek activation [Yeung et al., 1999, Corbit et al., 2003]. A positive feedback

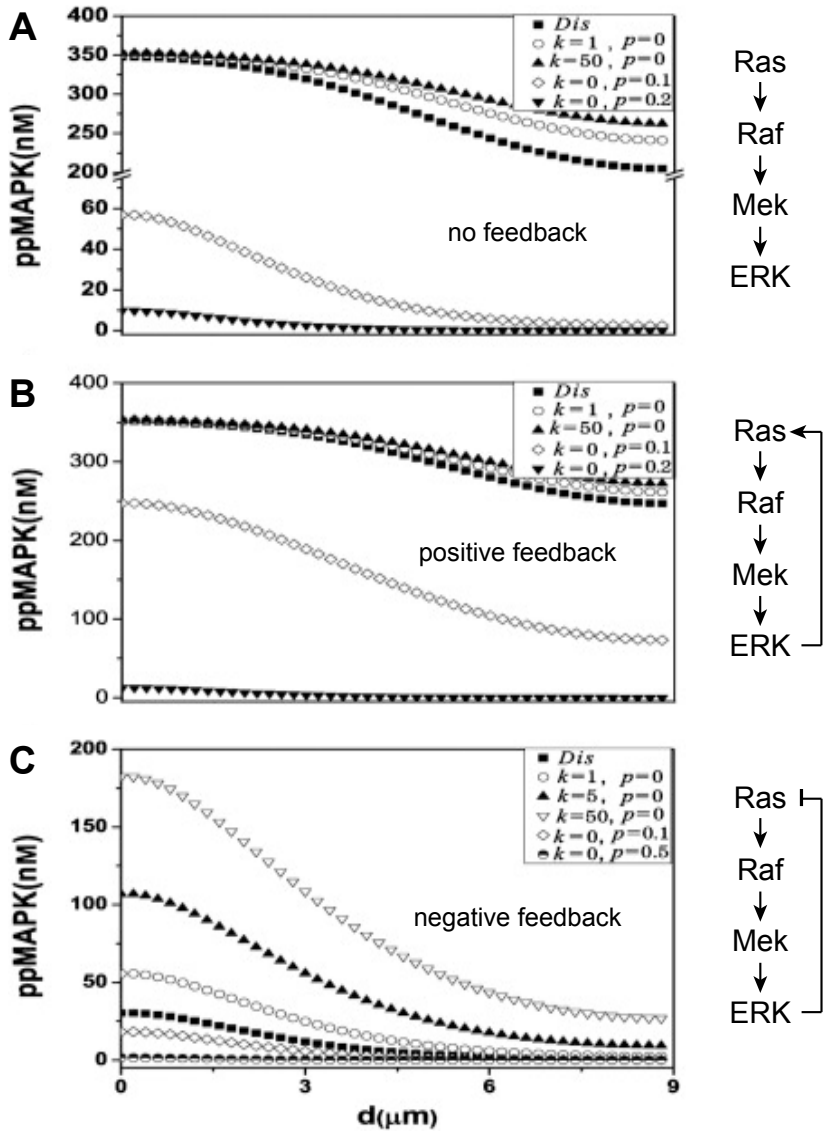

Figure 1.10: **Predicted influence of different network topologies on MAPK activity gradients.** Computational modeling demonstrating gradients of doubly-phosphorylated MAPK in a three-step cascade generated by (A) a linear cascade or (B) with positive feedback from ERK to Ras or (C) with negative feedback from ERK to Ras. Distributions of ppMAPK are calculated for distributive (*Dis*) enzymatic steps or different degrees of processivity for phosphorylation (k) and dephosphorylation (p) steps. Adapted from [Sun et al., 2014].

from ERK on Raf is recovered, leading to sustained ERK activity [Balan et al., 2006]. Having identified PKC as distinctive factor, it was possible to rewire the cellular outcome by activation or inhibition of PKC additionally to GF stimulation [Santos et al., 2007]. Later it was shown that ERK could phosphorylate RKIP directly on a different site than PKC, also inhibiting the suppression of Raf by RKIP [Shin et al., 2009]. Therefore, the recruitment of PKC might not be necessary to switch between positive and negative feedback.

MCF-7 (Michigan Cancer Foundation-7) is a human breast adenocarcinoma cell line exhibiting estrogen-dependent tumorigenicity [Clarke et al., 1990]. MCF-7 cells express all four members of the epidermal growth factor receptor (EGFR) (or human epidermal growth factor receptor (HER) or erythoblastosis oncogene B (ErbB)) family, [Goldenberg et al., 1989, Tavassoli et al., 1989, Fiddes et al., 1995]. This protein family comprises receptor tyrosine kinases (RTKs), which become activated by binding of a ligand [Cohen et al., 1980] to the receptor's extracellular domain, leading to homo- and heterodimerization between members of the EGFR family, followed by mutual crossphosphorylation [Cohen, 1983, Yarden & Schlessinger, 1987, Cochet et al., 1988, Wada et al., 1990, Graus-Porta et al., 1997]. Partial exceptions are on the one hand the orphan receptor ErbB2, for which no ligand was found and which is solely activated by heterodimerization, and secondly ErbB3, which has no enzymatic activity [Sliwkowski et al., 1994, Roskoski Jr., 2014]. The ligands for the EGFR family include EGF and the three isoforms of heregulin (HRG) which are coded by the gene neuregulin. The three HRG isoforms have an EGF-like domain in common, which is sufficient to induce receptor activation [Meyer et al., 1997]. While EGF binds to EGFR, HRG is a ligand of ErbB3 and ErbB4, leading to the heterodimerization with ErbB2 but also EGFR [Carraway et al., 1994, Fiddes et al., 1995, Graus-Porta et al., 1997]. While EGFR is downregulated upon ligand binding via the Ubiquitin kinase Cbl, ERB-B2 and -B3 are preferentially recycled upon ligand binding [Waterman et al., 1998, Lenferink et al., 1998, Levkowitz et al., 1998]. Furthermore, ERB-B2 and -B3 activate additionally to the ERK pathway also the phosphatidylinositide 3-kinase (PI3K) - Akt pathway and phospholipase-Cγ (PLCγ) [Peles et al., 1992, Peles et al., 1991].

In MCF-7 cells, stimulation with EGF causes proliferation, while HRG induces differentiation [Dong et al., 1992, Wosikowski et al., 1993, Nagashima et al., 2007]. However, in both cases the signal is channeled through the Raf/Mek/ERK cascade. Analoguesly to the case of PC-12 cells, a difference in the spatio-temporal ERK activity regulation was determined: The cytoplasmic ERK activity is transient upon EGF stimulation but sustained after HRG induction [Thottassery et al., 2004, Nagashima et al., 2007, Nakakuki et al., 2010]. The nuclear ERK activity is transient for both stimuli [Nakakuki et al., 2010]. Only sustained ERK activity leads to phosphorylation and stabilization of the IEG cFos, triggering differentiation in contrast to proliferation upon transient ERK activity. However, cFos mRNA is always temporarily abundant, independent of the ERK1/2 activity duration. Nakakuki et al. revealed that an unknown ERK activity-dependent, transcriptionally-activated repressor is responsible for the transient cFos mRNA transcription [Nakakuki et al., 2010]. The distinctive mechanisms of how the EGF vs. HRG stimulation guide the ERK activity into different cell fates is unknown. The costimulation of MCF-7 cells with EGF and PKC activator PMA led to sustained activtiy of ERK [Nakakuki et al., 2010]. However, PKC may activate MAPK signaling also directly by activating Raf instead of inhibiting the negative feedback from RKIP on Mek1 activation [Kolch et al., 1993]. In oder to demonstrate that PKC determines the ERK activity duration also in EGF vs. HRG, it would be necessary to show that the inhibition of PKC in the presence of HRG induces a transient ERK activity and proliferation.

1.4 Fluorescence Microscopy

Light microscopy is a tool for directly visualizing the morphology of cells. Conventional light microscopy generates a magnified image of the object near the microscope objective's focal

plane. Structures like the cell membrane or the nucleus can be resolved from their (liquid) surrounding by a differential transmission or reflection (i.e. contrast) of the illuminating white light. Dissolved molecules cannot be localized due to a lack of contrast against its environment and most notably the limitation of light microscopy (about 200 nm). Fluorescence microscopy techniques overcome both of these issues by labelling the protein of interest with a fluorescent molecule. Fluorescence is the characteristic absorption of photons of a certain energy to excite an electronic transition in an atom or molecule and subsequent re-emission (spontaneous emission) of a new photon which has either equal or lower energy than the absorbed one. The emitted photon is then detected and localizes the labelled protein as a bright spot in the image against dark background.

Protein fluorophores, like green fluorescent protein (GFP), provide the interface between the physical demands for a fluorophore and the biological compatibility. A protein of interest can be fused on the genetic level with a protein fluorophore, which allows to study the characteristics of molecules inside living cells in a way that is minimally invasive [Shimomura et al., 1962, Chalfie et al., 1994]. Variants of GFP from jellyfish and anthozoas have been isolated and developed to span the entire range of the visible spectrum with optimized fluorescence properties, e.g. enhanced brightness and photostability [Verkhusha & Lukyanov, 2004, Shaner et al., 2007]. Different approaches exploit the diverse chemical and physical qualities of the fluorophores: fluorophore maturation time (time until chromophore is built after protein translation) and spectral changes of the fluorophore until its degradation are used to study the turnover of a protein of interest simultaneously to its localization [Terskikh et al., 2000, Subach et al., 2009, Tsuboi et al., 2010, Khmelinskii et al., 2012]. The measurement of light depolarization allows for quantitative analysis of oligomerization of proteins or the rigidity of the local protein-fluorophores environment.

1.4.1 Förster Resonance Energy Transfer (FRET)

The phenomenon of Förster resonance energy transfer (FRET), on which all microscopy experiments in the present work are based, is the non-radiative transfer of energy from an excited chromophore (donor) to a chromophore in the ground state (acceptor) which may occur under certain spectroscopic and spatial conditions [Förster, 1948]. In principle, two fluorophores are able to resonantly exchange energy if their transition dipoles oscillate with the same frequency in each others nearfield. The rate of energy transfer k_T is thereby dependent on the donor's fluorescence lifetime τ_D, which is defined by the excited state decay profile, the Förster radius R_0, which is unique for every donor-acceptor pair and combines spectroscopic and dipole orientation parameters, and the distance r.

$$k_T = \frac{1}{\tau_D}\left(\frac{R_0}{r}\right)^6$$

with

$$R_0 = 9.78 \cdot 10^3 (\kappa^2 \cdot n^{-4} \cdot J(\lambda) \cdot Q_D)^{1/6}$$

Here, κ is the relative dipole-dipole orientation factor, n the index of refraction, the spectral overlap $J(\lambda)$ and the quantum yield of the donor Q_D. For efficient energy transfer the dipoles are aligned in parallel, while a perpendicular relative orientation impedes energy transfer; for freely rotating molecules an average orientation of $\kappa = 2/3$ is used for calculations of R_0. For fluorophores, the possible energy transitions are encoded in the absorption and emission spectra. The overlap integral between donor emission and acceptor excitation spectra therefore represents the probability of matching energy, or frequency, of the transition dipoles [Clegg, 2006]. The fluorescence of a molecule is characterized by the quantum yield Q, which is the ratio between emission and absorption of photons, and the fluorescence lifetime τ, i.e. the time

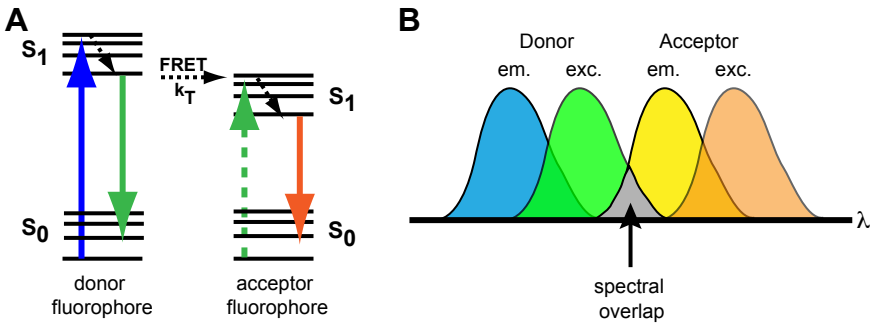

Figure 1.11: **Spectral overlap of donor emission and acceptor excitation is essential for FRET.** (A) Jablonski diagramm showing the energy transitions in FRET. A donor fluorophore is excited from the ground state S_0 to a vibrational level of the first excited energy state S_1 by absorption of a photon (blue arrow) declining into the ground state of the first electronic state. If the emission wavelength (green arrow) matches the excitation wavelength of the acceptor, FRET can occur, leading to induced emission of the acceptor (orange arrow). (B) Schematic representation of overlapping donor and acceptor spectra, depicting the energy resonance.

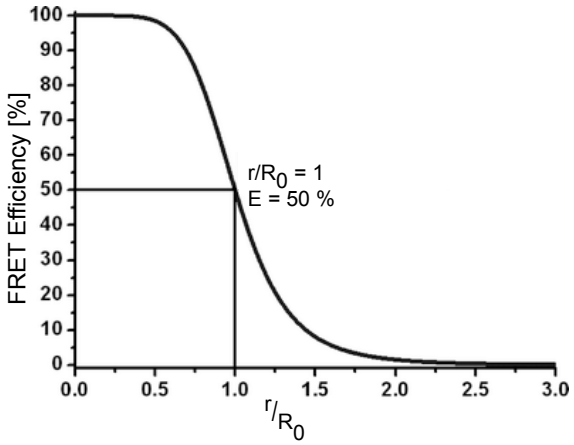

Figure 1.12: **Distance dependence of FRET efficiency.**

in the excited state. Common values of R_0 for protein fluorophores are in the range of about 5 nm and limit the radius for efficient transfer to less than 10 nm. Considering that a GFP molecule has a Stokes radius of 2.82 nm, the detection of FRET allows for measurement of protein interaction below the resolution limit of light microscopy [Terry et al., 1995].

The efficiency of FRET is defined in analogy to the quantum yield as the fraction of transferred to absorbed photons by the donor fluorophore

$$E = \frac{k_T}{\tau^{-1} + k_T}$$

replacing k_T reveals

$$E = \frac{R_0^6}{R_0^6 + r^6}$$

showing that the Förster radius R_0 defines 50% effiency for the case $r = R_0$.

1.4.2 Fluorescence lifetime imaging microscopy (FLIM)

FRET reduces the donor fluorescence intensity and its excited state lifetime τ_D, and further induces the emission of acceptor fluorescence. Therefore, FRET can be measured by different approaches, based on changes either of donor and acceptor fluorescence intensity or of the excited state lifetime τ_D.

For the intensity-based technique "ratiometric imaging", the donor intensity decrease and acceptor intensity increase upon excitation of the donor fluorophore are measured. This method can be applied in case donor and acceptor are in a one-to-one ratio, for instance in a sensor construct. It is a fast approach and therefore well suited for live-cell imaging. Accordingly, "sensitized emission" can be applied, which also measures the FRET dependent donor intensity decrease and acceptor intensity increase. Here, corrections for the bleed-through from the donor in the acceptor channel, and the direct excitation of the acceptor from the donor channel are conducted, which make this method very sensitive to noise. For "acceptor photobleaching", the difference of donor intensity before and after acceptor photobleaching is measured. The intensity-based techniques for FRET detection are sensitive for bleedtrough or "bleed-excitation" between donor and acceptor channels and therefore have to be corrected. Furthermore, sample drift, different photostability of donor and acceptor fluorophore and in live cells the fluctuating local fluorophore concentration can falsify FRET measurements.

The measurement of the change in the excited state decay profile as read-out for FRET is more reliable, because the lifetime is an intrinsic property of the fluorophore, independent of the fluorophore's concentration. Environmental conditions like temperature and pH influence the excited state lifetime, but these are constant over the course of the experiment. The excited state lifetime of a donor fluorophore τ_D can be reduced by radiative and non-radiative (collisional quenching) processes (k_r and k_{nr}) and additionally by resonance energy transfer with k_{FRET} in presence of the acceptor, yielding the lifetime τ_{DA}.

$$\tau_D = \frac{1}{k_r + k_{nr}} > \tau_{DA} = \frac{1}{k_r + k_{nr} + k_{FRET}}$$

The excitation of a fluorophore sample with an infinitesimally short light pulse causes the emission within a certain time period, following a single exponential decay.

$$I(t) = I_0 \cdot e^{-t/\tau}$$

If some molecules undergo FRET with an acceptor fluorophore, this fraction of molecules will have a faster intensity decay. If donor and acceptor interact in one fixed geometric arrangement, the resulting decay is bi-exponential, comprising τ_D and τ_{DA}. However, in most cases donor and acceptor can interact in multiple spatial configurations, which is expressed in a multi-exponential decay, which sums the decays for all lifetimes τ_i, weighted by their fluorescence amplitude f_i at timepoint $t = 0$.

$$I(t) = \sum_{i=1}^{n} f_i \cdot e^{-t/\tau_i}$$

The fractional contribution of each decay is defined by α_i with

$$\alpha_i = \frac{f_i \tau_i}{\sum f_j \tau_j}$$

1.4.3 Measurement and Analysis of FLIM data

Excited state decay profiles can be either measured in the "time-domain" or in the "frequency-domain". In time-domain measurements, ultra-short laser pulses are applied, while in the

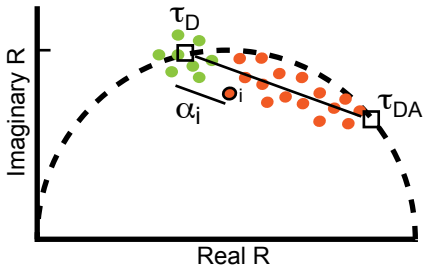

Figure 1.13: **Global analysis of biexponential lifetime data.** Plot of real and imaginary parts of the Fourrier coefficients (R) illustrates that all possible mono-exponential decays lie on a semi-circle, like donor-only lifetime τ_D and FRET lifetime τ_{DA} corresponding decays (green and orange circles). Pixels corresponding to biexponential decays with mixtures of τ_D and τ_{DA} are scattered along the secant between τ_D and τ_{DA}. The secant's intercept of each pixel represents the contribution α_i (adapted from [Grecco et al., 2010]).

frequency- domain approach continuous, intensity-modulated light is used to excite the fluorophore. Both methods are based on a known, fixed property of the excitation light, which is either the frequency of the pulses or the frequency of modulation. They are used as reference to calculate the excited state decay profile from the emission light. Frequency-domain measures the phase-shift and demodulation of the emission light. In time-domain measurements, the time period between emission of a single photon and the laser pulse is recorded (time-correlated single photon counting (TCSPC)) yielding a histogram of the number of photons versus time. To evaluate the corresponding excited state lifetime the histogram is fit with appropriate decay models.

A further approach named "global analysis" for bi-exponential decay data calculates the fraction α_i of donor molecules bound to acceptor molecules in each pixel, in addition to the excited state lifetime. The theory of global analysis requires that the investigated FRET pair exhibits only two invariant lifetimes τ_D and τ_{DA} leading to maximally a bi-exponential decay. From this, the contribution α_i can be calculated, which represents the respective fraction of lifetimes in each pixel and therefore the fraction of donor in complex with the acceptor. The sum of the fractions $\alpha_D + \alpha_{DA}$ in each pixel is normalized to one and all pixels are analyzed simultaneously with invariant lifetimes conferring the result global character [Verveer et al., 2000, Grecco et al., 2009]. Plotting the Fourier coefficients (R) of the fluorescence emission in the complex plane reveals that all possible mono-exponential decays lie on a semicircle including the two observed decays for τ_D and τ_{DA} 1.13. The secant cutting the two points represents all possible fractions of donor molecules in interaction with the acceptor. The relative location of a pixel on this line reveals the fraction of molecules in complex with the acceptor, represented by α, from which an image was reconstructed.

In reality, the excited state lifetimes are in most cases not invariant in presence of the acceptor due to multiple possible binding geometries between donor and acceptor. An antibody for instance has two binding sites and can therefore adopt two possible binding configurations, each exerting a different distance between donor and acceptor fluorophores. If multiple antibody epitopes are accessible, e.g. different phosphorylation sites, the fluorescence decay is further split. However, if the investigated system ideally adopts two states, for instance phosphorylated or unphosphorylated, the approximation of invariant lifetimes is valid.

1.4.4 Imaging MAPK activity

As discussed in chapter 1.3.3.3, MAPK activity is predicted to be distributed in intracellular activity gradients. To map the activity distribution of different MAPKs, like Mek, ERK and Fus3, a universal kinase assay is required, which provides high dynamic range and a specific and quantitative read-out for the kinase of interest.

A described kinase assay ultilizes γ -phosphate-modified ATP which allows to track the phosphorylation of a labeled kinase substrate by measuring the induced change in the FRET signal [Green & Pflum, 2007, Green & Pflum, 2009]. However, this approach was only used in cell extracts. This indirect approach has various disadvantages. The tracking of the substrate requires that the substrate be specific for the kinase of interest and not phosphorylated by other kinases. Additionally, the substrate has different diffusion and transport kinetics than the kinase, so that the spatial distribution of the phosphorylated substrate likely differs from the distribution of the active MAPK. Furthermore, the ATP-conjugate concentration would have to be in the range of mM, comparable to the endogenous ATP, which is difficult to implement experimentally.

Enzyme-substrate (ES) imaging measures the interaction between labeled enzyme and labeled substrate by the change in FRET [Yudushkin et al., 2007]. Here, it is required that only the active kinase binds to the substrate. However, Mek1 and Fus3 bind their substrate independently of their activity state over docking sites. ES imaging would therefore not be suited for these MAPKs. Additionally, the ratio between enzyme and substrate concentration has to be constant in all cellular compartments in order to derive quantitative spatial differences of kinase activity. Furthermore, to generate a significant FRET change and preferably exploit the full dynamic range, the substrate concentration needs to saturate the enzyme. However, the substrate concentration is required to be as low as 100 μM - 1 mM, which is barely feasible [Klüßendorf, 2011]. Beyond that, this approach requires specific substrates for every kinase and is therefore not universally applicable.

Common to all MAPKs is their activation by phosphorylation. The residues which become phosphorylated are however different: While MAPKs are modified on Thr and Tyr, MAPKKs are phosphorylated only on Ser and MAPKKKs on Ser and Thr. A suitable technique would have to detect all of these different phosphorylated amino acids. However, there are no antibodies or binding domains which bind universally to phosphate-monoesters, or the different phosphorylated amino acids with equal affinity. Commonly, generic antibodies or binding domains are only available for pTyr. Here, the Src-homology-2 (SH2) domain, expressed as fluorophore-fusion, has been utilized as a generic phospho-Tyr (pTyr) sensor for a fluorescently-tagged protein of interest in a FRET-based approach. Accordingly, phospho-Tyrosine-binding (PTB) domains were used as generic pTyr sensors or as part of a specific activity sensor for the epidermal growth factor receptor (EGFR) [Sato et al., 1999, Sato et al., 2002, Offterdinger et al., 2004]. pSer and pThr have a variety of binding domains which include are FHA, MH2, WW and 14-3-3. However, these are all dependent on the sequence surrounding the phosphosite, precluding their usage as a generic tool [Heldin et al., 1997, Lu et al., 1999, Hammet et al., 2003]. The same applies for antibodies, which can be selective for pTyr but not for pSer/pThr residues. The affinity of pSer/pThr antibodies depends on the sequence surrounding the phosphosite [Grønborg et al., 2002].

The only commercially available chemical reagents, which bind to phosphorylated amino acids in general are the gel stain ProQ Diamond and Phos-Tag [Martin et al., 2003, Kinoshita et al., 2004]. Phos-Tag is a polydentate ligand which chelates two dinuclear metal ions, Zn^{2+} or Mn^{2+} [Kinoshita et al., 2004]. It is the only known substance which universally binds phosphate-monoesters with high selectivity in aqueous solution at neutral pH (the phenyl phosphate dianion is bound with a K_d of 25 nM).

Therefore, phosphorylated proteins are detected by Phos-Tag irrespectively of the amino acid that is modified. Phos-Tag was originally used as phosphate capture molecule for matrix-

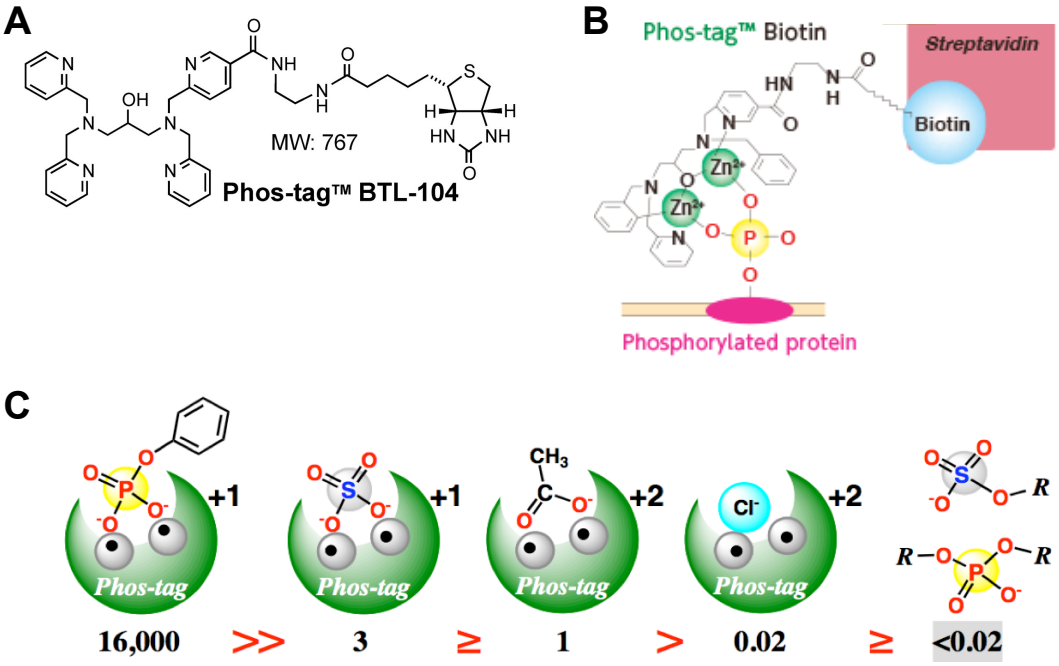

Figure 1.14: **Binding mode and selectivity of the Phos-Tag dizinc(II) complex for phosphate-monoesters.** A) Structural formula of the Phos-Tag ligand as Biotin compound. (MW: mass weight). B) The binding mode of the Phos-Tag dizinc(II) complex (1,3-bis[bis(pyridin-2-ylmethyl)amino]propan-2-olato dizinc(II)) to an immobilized phosphorylated protein. C) Selectivity of the Phos-Tag dizinc complex for phosphate-monoesters.

assisted light desorption ionisation-time of flight (MALDI-TOF) and later developed as agarose-, acrylamide- and biotin conjugates for the use in gel electrophoresis and Western blots [Takeda et al., 2003, Kinoshita et al., 2004, Kinoshita et al., 2006]. In a FRET experiment, the phosphorylation of AMCA-labeled peptides was measured *in vitro* using covalently FAM-linked Phos-Tag [Takiyama et al., 2009]. The labeling of Phos-Tag with an acceptor fluorophore would facilitate the detection of a phosphorylated, donor-labeled protein of interest in a cytochemical FRET approach. This technique necessitates the fixation and permeabilization of cells, so that only selected time points can be observed. The application of such a generic protein phosphorylation-detecting reagent to monitor the activity state of a protein would suffer from being sensitive also to non-activating phosphorylations. However, if the kinase of interest is labeled with a fluorophore and its phosphorylation is tracked via a cytochemical approach with a fluorophore-labeled phospho-binder, this can serve as a universal kinase imaging assay.

2 Rationale and aims of the thesis

MAPK activity regulates transcription in the nucleus, but also has specific local roles in the cytoplasm, such as cytoskeleton remodeling. Computational models have predicted that the active MAPKs are patterned in gradients that emerge from the plasma membrane, which in turn define the activity range of the MAPKs. The specificity of the spatial MAPK activity range could be conferred by differential regulation of the MAPK module by various regulatory proteins, which would then focus or distribute the MAPK activity. The major objective of this work was to elucidate if MAPK activity gradients occur and if so, how they regulate the local vs. the global MAPK functions. To accomplish this task it was therefore required to develop a universal method to image MAPK activity in mammalian, as well as yeast cells. This method should combine the generic phosphoprotein-binding compound Phos-Tag with FRET-FLIM to enable a quantitative and specific read-out of the MAPK activity state, referred to as PTag-FLIM.

Using the PTag-FLIM approach, the following questions were addressed:

Regarding the yeast pheromone pathway:

- Recently, a negative feedback from Fus3 to Ste11 was identified. How does this specific network architecture affect the Fus3 activity gradient? This was in particular studied in yeast mutant cells upon impairing the negative feedback phosphorylation from Fus3 to Ste11.
- How is the inherent hierarchical structure of the mating MAPK-module reflected in the spatial distribution of the MAPK-module components?

Regarding the ERK cascade in mammalian cells:

- Do the MAPK ERK2 and MAPKK Mek1 exhibit activity gradients? If so, how are they related to each other?
- How is the differential ERK2 activity duration in the cytoplasm induced by EGF and HRG related to the Mek1 and ERK2 activity gradients? Which conclusions can be drawn regarding the network architecture?
- Is the MAPK scaffold KSR1 an important factor to maintain these gradients?

3 PTag-FLIM to map phosphorylation in cells

3.1 Principle of PTag-FLIM

MAPKs are activated by phosphorylation on different amino acids, comprising Ser, Thr and Tyr. In order to detect the different phosphorylated residues of MAPKs as read-out for their activity, the phosphate-monoester binding compound Phos-Tag was chosen. Due to the universality of Phos-Tag, it will bind to every available phosphate-monoester in the cell (for further information on Phos-Tag see chapter 1.4.4). Phosphate-monoesters are terminal phosphates which occur for instance in proteins, DNA, RNA or nucleotides. In order to specifically detect the phosphorylation of the kinase of interest, the Phos-Tag was complexed to an acceptor dye for FRET-FLIM of the kinase which is genetically fused to a donor fluorophore. Using FRET-FLIM, the molecular proximity between the phosphorylated kinase and the Phos-Tag-Dye complex is measured (for information on FRET-FLIM see chapter 1.4). This approach facilitates specific and quantitative imaging the phosphorylation of the kinase of interest.

The functional PTag-Dye complex was built by conjugation of a Phos-Tag-Biotin compound to an acceptor fluorophore labeled with Streptavidin (STV). The Biotin-STV bond is one of the strongest non-covalent interactions known. The complex between Phos-Tag-Biotin and labeled STV was stable in aqueous solution. In particular, STV was labeled with a ratio of 5-7 molecules Cy3.5 per STV as acceptor fluorophore for mCitrine-tagged kinases in FRET-FLIM. Compared to an antibody, which has typically a size of about 150-200 kilo-Dalton, STV is rather small (55 kilo-Dalton) rather small and therefore has better accessibility to phosphosites. In order to exploit the full dynamic range of PTag-FLIM and label the phosphorylated kinase with high occupancy, the cellular phosphosites have to be saturated by excess PTag-Dye. However, FLIM is a donor-based and intensity-independent FRET approach and therefore not affected by the excess of acceptor fluorophores.

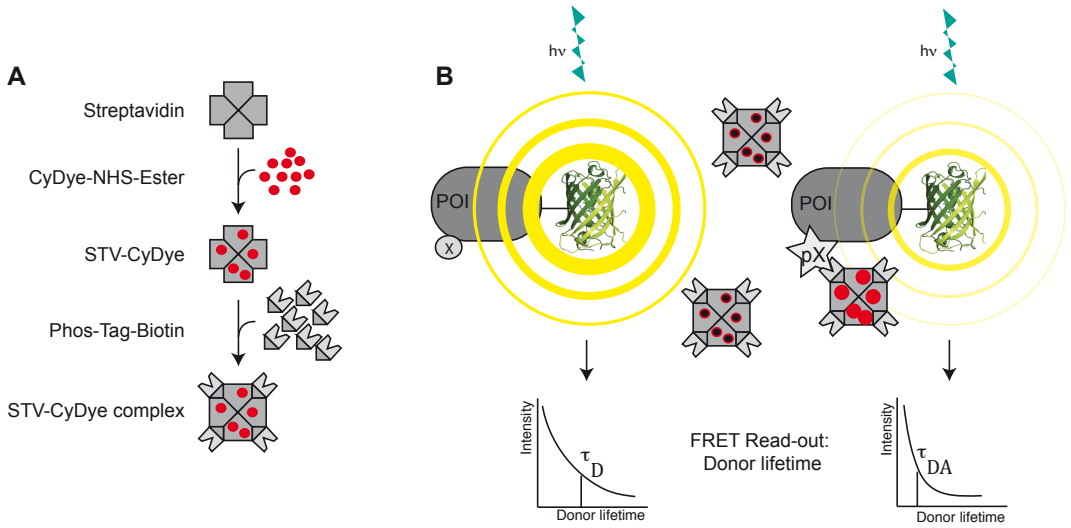

Figure 3.1: **PTag-FLIM Overview.** (A) Streptavidin (STV) is labeled on free amino groups using a N-Hydroxysuccinimide (NHS) ester conjugate of a CyDye. To obtain the PTag-Dye complex, STV-Dye is incubated with Phos-Tag-Biotin. (B) Left side: The protein of interest (POI) is genetically tagged to a fluorescent protein (donor fluorophore), for instance mCitrine, which is excited by laser pulses of the appropriate wave length ($h\nu$). The emission of the donor fluorophore is represented by the yellow circles which indicate for FRET important properties: the emission wavelength (yellow), the donor intensity and the radius R_0 for which FRET is detectable. In the absence of the FRET acceptor PTag-Dye or if the POI is unphosphorylated (X), no FRET occurs, which is measured by FLIM revealing a long donor lifetime τ_D in the decay profile at the bottom. If the POI is phosphorylated (pX) in the presence of the FRET acceptor, the FRET acceptor binds to the phosphorylated residue. If donor and acceptor fluorophore are sufficiently close, FRET occurs and reduces the donor lifetime to τ_{DA}.

3.2 *In vitro* validation of PTag-FLIM

In order to demonstrate that PTag-Cy3.5 quantitatively reports protein phosphorylation by FRET-FLIM, an *in vitro* experiment with phosphorylated and non-phosphorylated versions of a mCitrine-tagged protein was performed. Purified ephrin receptor tyrosine kinase 3 (EphA3), which has several phosphorylation sites (www.phosphonet.ca), was incubated with ATP for full phosphorylation. mCitrine-EphA3 (U) and its phosphorylated version (P) were mixed in ratios of 4:0, 3:1, 2:2, 1:3 and 0:4. Aliquots of the protein mixtures were subjected to native PAGE as independent assay to ascertain the fraction of phosphorylated EphA3 derived from the FLIM experiment in figure 3.2. In native PAGE the protein charge is not shielded by SDS, so that proteins are separated by size and polarity.

The gel in figure 3.2 and the quantification in C show the relative fraction of unphosphorylated to phosphorylated protein (U:P) in every protein mix. The sample of EphA3, that was incubated with ATP (U:P = 0:4) contains more than a fifth of unphosphorylated protein. Still, the fractions of phospho-EphA3 range between nearly zero and 0.75, which should provide a sufficient range of phosphorylated fraction to validate PTag FLIM. In figure 3.2B the distributions of the excited state lifetime τ corresponding to the EphA3 mixtures above are shown. The higher the phosphorylated fraction, the more PTag-Cy3.5 should bind and reduce the excited state lifetime τ. As expected, with increasing phosphorylated fraction, τ decreases. The fractions of phosphorylated EphA3 derived from PTag-FLIM and native PAGE can be fit to a linear function with a slope of 1.0 and a correlation coefficient of R^2= 0.996, indicating that the fractions derived from native PAGE and PTag-FLIM are consistent. Therefore, the complex of Phos-Tag-Biotin bridged via STV to Cy3.5 can be used in FRET-FLIM as quantitative read-out for protein phosphorylation.

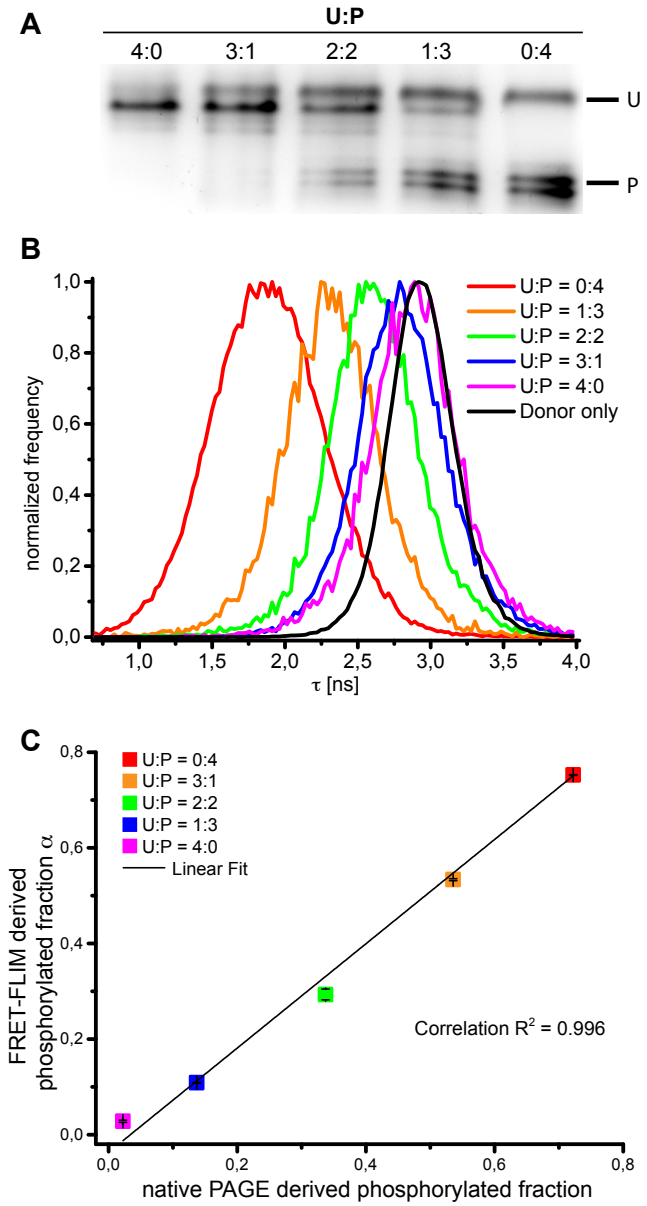

Figure 3.2: **Validation of PTag-Cy3.5 complex as acceptor for mCitrine-tagged proteins *in vitro*.** Phosphorylated (P) and unphosphorylated (A) mCitrine-EphA3 kinase were mixed in ratios of 4:0, 3:1, 2:2, 1:3 and 0:4 and measured by native PAGE (A) or FRET-FLIM (B). In (A) proteins were separated in a 10% native gel and stained by Coomassie Blue. (B) For FLIM, protein mixtures were incubated with beads and washed with blocking buffer to prevent unspecific binding of the PTag-Cy3.5 complex to the beads. (C) The fraction of phosphorylated EphA3 as measured by FRET-FLIM was determined by global analysis. Correlation coefficient $R^2 = 0.996$, linear equation $y = 1.09067x \pm 0.01869x - 0.03688 \pm 0.00952$.

3.3 Mapping EGFR - Tyr phosphorylation by PTag-FLIM

In order to quantitatively image a phosphorylated protein in cells by PTag-FLIM, cells were fixed after stimulation. The protocol of cell fixation, permeabilization and staining was adapted from immuno-cytochemical applications for the use with PTag-Cy3.5: Steps applying phos-

phate buffers were exchanged for Tris buffers to prevent PTag-Cy3.5 saturation by binding to excess phosphate in the solution (for further information see chapter 8.6.4).

To test the application of PTag-FLIM in cells, with EGFR a target of known spatio-temporal activation profile was chosen, which enables the comparison of the PTag-FLIM profile with the known one [Wouters & Bastiaens, 1999]. Upon EGF stimulation, EGFR becomes phosphorylated on 6 Tyr sites.

In starved and fixed cells (figure 3.3, 0 min EGF), PTag-Cy3.5 localized mainly to the nucleus and to a lesser extend to the cytoplasm. After EGF treatment, the overall fluorescence intensity increased, which indicates an elevated level of phosphorylation and hence signaling in the cell. Additionally, a strong localization of PTag-Cy3.5 to the PM could be observed, which can be attributed to EGFR phosphorylation after EGF binding and downstream phosphorylation processes.

The phosphorylation of EGFR-mCitrine upon EGF treatment is reported by the decrease in the excited state lifetime τ which originates from FRET due to binding of PTag-Cy3.5 to phosphorylated EGFR-mCitrine. Based on the observed time points of EGF treatment, EGFR-mCitrine phosphorylation reached a maximal phosphorylation level at ten minutes and then declined to a steady-state level at 30 minutes after EGF stimulation. After five and ten minutes of EGF stimulation, phosphorylated EGFR-mCitrine was mostly localized to the PM and declined gradually towards the cell's center. At the 30 minutes time point, phosphorylated EGFR could be observed in endosomes.

The derived spatio-temporal profile of EGFR activation after EGF treatment measured by PTag-FLIM is consistent with previous data using a pTyr antibody [Wouters & Bastiaens, 1999]. The consistence of both profiles despite the use of different phospho-acceptors can be attributed to the fact that EGFR activation is predominantly Tyr phosphorylation.

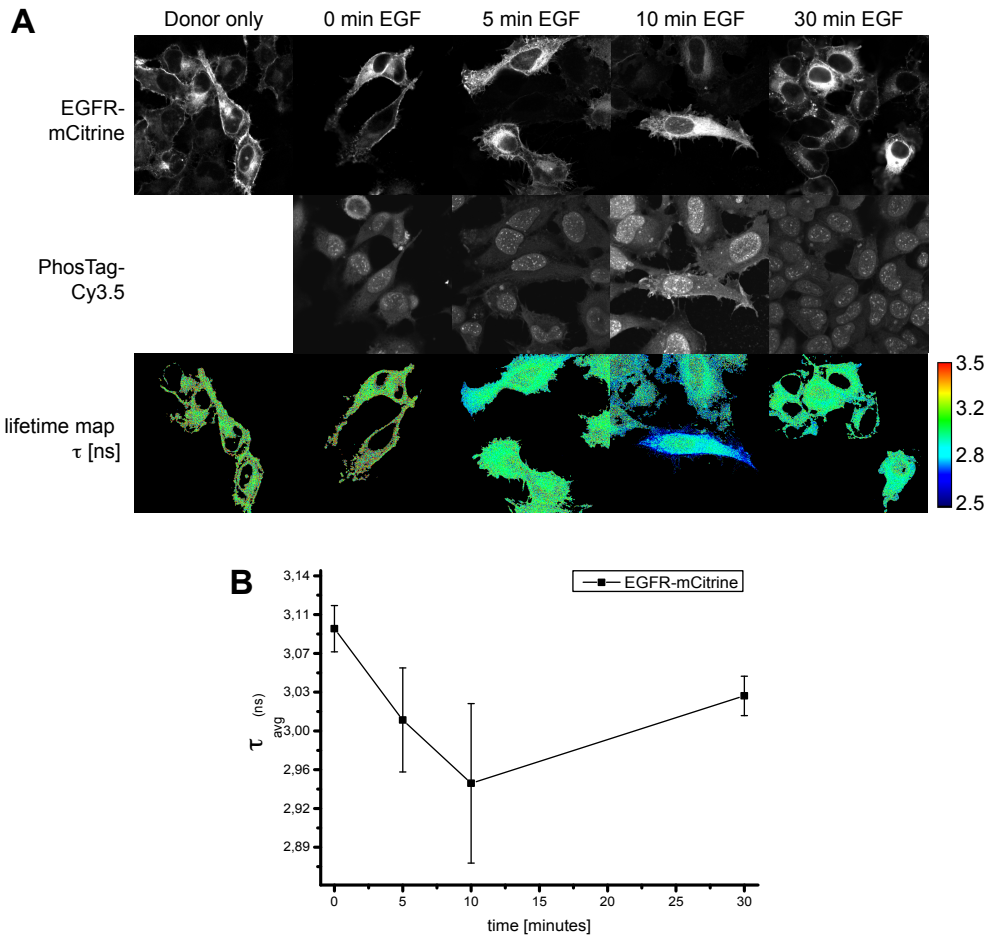

Figure 3.3: **PTag-Cy3.5 is a suitable phosphoacceptor for a mCitrine-fused Tyr-phosphorylated protein.** (A) HeLa cells expressing EGFR-mCitrine were starved for 24 hours, stimulated with 100 ng/ml EGF for the indicated time points, fixed, permeabilized and stained with PTag-Cy3.5. Fluorescence intensity distributions of EGFR-mCitrine and PTag-Cy3.5 are shown in the top rows, the distribution of the fluorescence lifetime τ with false-colour look-up table is pictured in the bottom row. (B) Average lifetimes from several images are plotted against the specified time points of EGF stimulation with n = 5 for each time point.

3.4 Mapping Mek1 - Ser/Thr phosphorylation by PTag-FLIM

In order to show that PTag-Cy3.5 also detects pSer and pThr, the phosphorylation of MAPKK Mek1, which has only Ser/Thr phosphorylation sites, was examined. Mek1 becomes activated by phosphorylation of Ser218 and Ser222, but harbors also the deactivating phosphosites Thr286 and Thr292 (chapter 1.1.2). It is known that the stimulation of cells with EGF induces the transient phosphorylation on the activating sites of Mek1. On the contrary, the phosphorylation of the deactivating threonines is sustained [Eblen et al., 2004]. Therefore, the investigation of the EGF induced temporal Mek1 phosphorylation profile can deliver information about the phosphosites, which contribute to a decrease in the excited state lifetime of mCitrine-Mek1 in PTag-FLIM. This contribution depends on the extent of phosphorylation of each site and the geometrical parameters of each donor - acceptor pair. In particular, these geometrical parameters are the steric accessibility of the phosphosite for the PTag-Cy3.5 complex, as well as the distance and average orientation between donor and acceptor fluorophore for each phosphosite. A transient phosphorylation profile would hint towards a major contribution of the activating

phosphosites, while a sustained profile would suggest that other sites are also phosphorylated to a significant extent.

The spatial distribution of phosphorylated mCitrine-Mek1 was investigated in HeLa cells, which were treated with EGF, fixated, permeabilized and stained with PTag-Cy3.5. As shown in figure 3.4, mCitrine-Mek1 was localized to the cytoplasm, excluding the nucleus due to a NES and was recruited to membrane ruffles after 5-10 minutes of EGF stimulation [Fukuda et al., 1996]. After thirty minutes of stimulation, Mek1 was again homogeneously distributed over the cell.

The time profile of mCitrine-Mek1 phosphorylation reported by PTag-FLIM followed a transient trend with a maximal phosphorylation at 5-10 minutes. Therefore, PTag-FLIM of Mek1 can be interpreted as a read-out for Mek1 activity.

At any time, mCitrine-Mek1 was stronger phosphorylated at PM-proximal regions than close the the nucleus. To quantify the spatial distribution of Mek1 phosphorylation, α profiles were recorded in a rectangle from the PM to the nucleus of 5-10 cells per time point. These were normalized in length and the average profiles over several cells calculated. Interestingly, gradients of Mek1 activity could be observed at 0-10 minutes of stimulation that emanated from the plasma membrane (3.4 C). The gradient dissipated at the thirty minute time point. While the gradient's profile shape did not change significantly between 0 and 5-10 minutes, the overall amplitude from PM to nucleus was elevated at 5-10 minutes of EGF stimulation which extends Mek activity in the direction of the nucleus.

Using PTag-FLIM, for the first time an intracellular activity gradient of a MAPKK could be demonstrated, indicating that the predicted spatial distribution of MAPK activity in gradients occurs [Brown & Kholodenko, 1999].

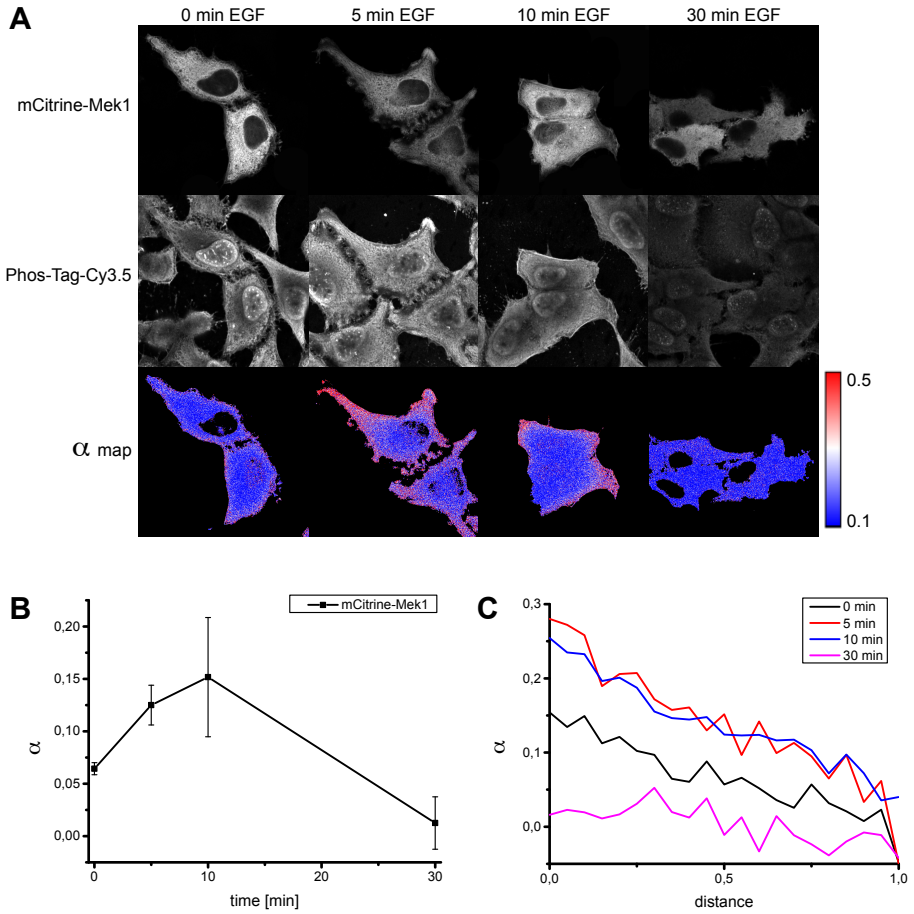

Figure 3.4: **pMek1 gradient emanates from the PM.** FLIM-FRET measurements using PTag-Cy3.5 in fixed HeLa cells expressing mCitrine-Mek1. (A) Top: Fluorescence intensity distributions of mCitrine-Mek1. Middle: Fluorescence intensity distribution of PTag-Cy3.5. Bottom: Spatial distribution of the fraction of interacting molecules α as determined by global analysis of FLIM data. False-color look-up table indicates the fraction α of phosphorylated protein. (B) Average α values of several images (N = 3-6) with s.d. plotted against the specified time points of EGF stimulation. (C) Quantification of the Mek1 gradient at different time points of EGF treatment. α profiles were obtained within rectangulars that spanned from the PM to the nucleus of 5-10 cells per time point. These were normalized and the average profiles calculated.

3.5 Mapping ERK2 - Thr/Tyr phosphorylation by PTag-FLIM

ERK1/2 is activated by phosphorylation on Thr183 and Tyr185 in its activation loop. Human ERK2 has further Ser/Thr phosphorylation sites, but these are not reported to be modified upon EGF stimulation [Zhang et al., 2005, Daub et al., 2008, Lorenz et al., 2009].

While the cytoplasmic mCitrine-ERK2 was subtly prephosphorylated, the increase of nuclear mCitrine-ERK2 phosphorylation coincided with ERK2 nuclear translocation at five minutes of EGF stimulation (figure 3.5). The time profile of ERK2 phosphorylation after EGF stimulation derived from PTag-FLIM in figure 3.5 B exhibits the known transient behavior.

To determine if the decrease in the excited state lifetime of mCitrine-ERK2 is due to binding of PTag-Cy3.5 to the activating phosphorylation sites instead of binding to other ERK2 phosphosites, a control was generated by mutating the two activating phosphorylation sites Thr183 and Tyr185 in Citrine-ERK2 to non-phosphorylatable amino acid Ala. As shown in figure 3.5, the mutant mCitrine-ERK2-T183A,Y185A was barely phosphorylated upon five minutes EGF treatment and the fraction of phosphorylation is below the phosphorylation of mCitrine-ERK2 in starved cells. The residual phosphorylation must be attributed to other phosphorylation sites of ERK2. Therefore, the main contribution to the phosphorylation measurement under the investigated conditions deliver the activating sites Thr183 and Tyr185. Furthermore, PTag-Cy3.5 binds selectively to the phosphorylated protein under the conditions of this cytochemical approach.

The ERK2 activating protein Mek1 showed an activity gradient (figure 3.4), which defines a spatial probability distribution for ERK2 activation. Therefore, ERK2 activity should exhibit a secondary gradient which is accordingly extended in direction of the nucleus. Indeed, mCitrine-ERK2 phosphorylation declines from the PM and spreads almost to the nucleus, so that it is broader than the ppMek1 gradient. The presented experiments in figures 3.4 and 3.5 confirm for the first time the predicted cytoplasmic restriction in gradients of MAPK activity in mammalian cells.

Additionally, a phosphorylation gradient of ERK2 emanating from the nuclear membrane into the nucleoplasma could be observed, which implies a spatial regulation of ERK2 activity also in the nucleus. A nuclear gradient has not been expected, because ERK2 activating proteins do not reside at the nuclear membrane.

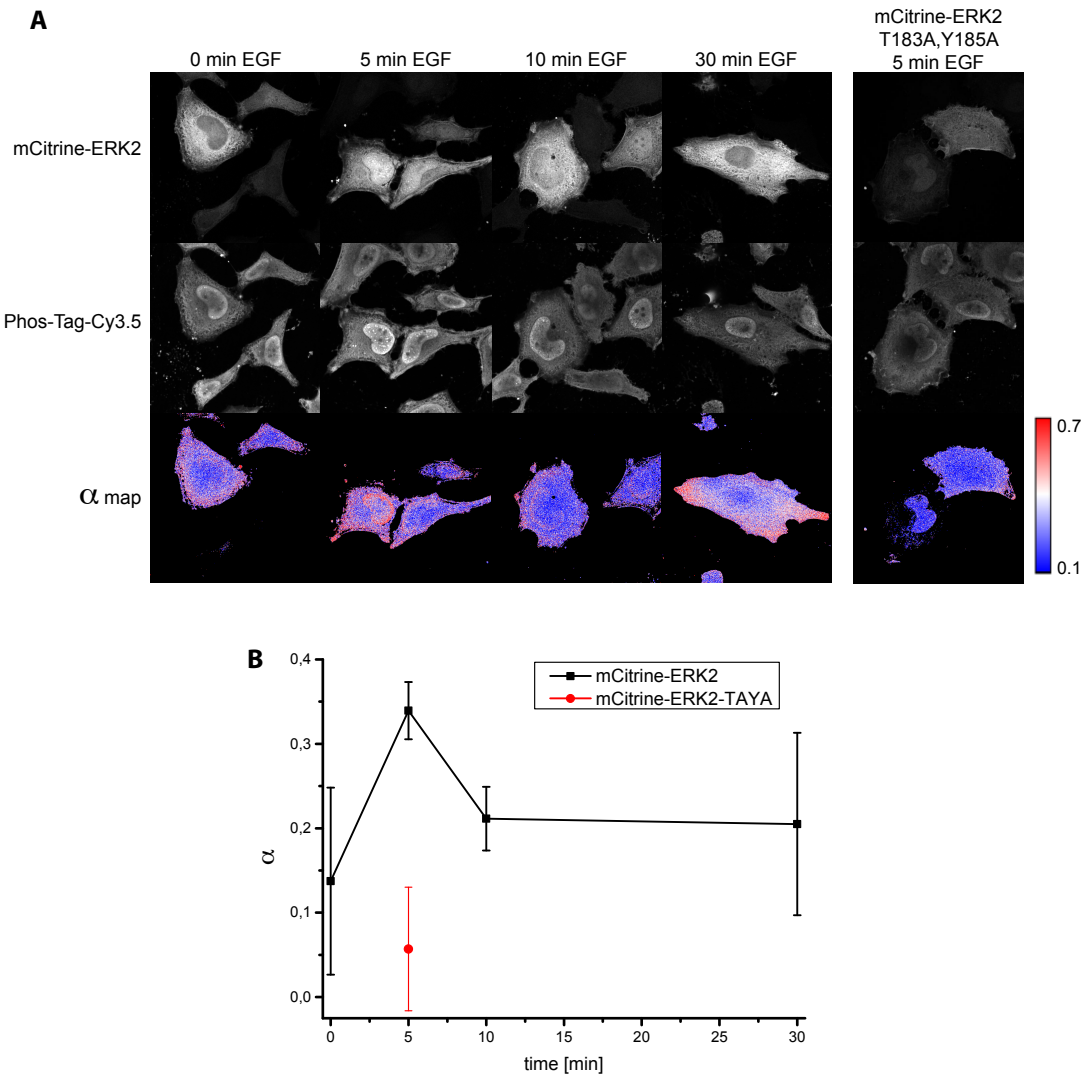

Figure 3.5: **Mapping mCitrine-ERK2 phosphorylation reveals a gradient of ppERK emanating from the PM.** (A) FLIM-FRET measurements in fixed HeLa cells expressing mCitrine-ERK2 or mCitrine-ERK2-T183A,Y185A stimulated with 100 ng/ml EGF for the indicated time points. For each sample, the fluorescence intensity of mCitrine-ERK2 (donor), the fluorescence intensity of PTag-Cy3.5 (acceptor) and the spatial distribution of the fraction of interacting molecules α as determined by global analysis of FLIM data are shown. False-color look-up table indicates the fraction of phosphorylated protein. (B) Average α values from several images (N = 3-6) with s.d. plotted against the specified time points of EGF stimulation.

3.6 Dark acceptor QC1

While in intensity-based FRET, the measurement needs to be corrected for bleed-through or bleed-excitation, in FLIM exclusively the donor's fluorescence is recorded. Hence, at least either the donor fluorophore excitation or detection must be separated from spectra of additional fluorophores in the sample. Accordingly, FLIM of two or even three donor fluorophores is accomplishable, if separate excitation or detection, respectively, allows to discriminate their fluorescence. Naturally, it is also necessary that the fluorophores or their tags do come in

close proximity and thereby affect each others excited state lifetime due to energy transfer. In multi-donor FRET, the excitation spectrum of the acceptor fluorophore needs to span the emission spectra of all donor fluorophores without its emission leaking into one of the donor's emission. To reduce the number of spectra, it is advantageous to use an acceptor which is itself non-fluorescent, referred to as "dark". The absorption of IRDye QC-1 spans nearly the complete visible range, while itself is dark. Therefore, this small dye was tested as acceptor fluorophore in PTag-FLIM with three different donor fluorophores. STV was labeled with QC-1 following the protocol in chapter 8.5.3 with a ratio of 10 dyes per STV.

In figure 3.6 a FRET-FLIM measurement between EGFR-mCitrine or EGFR-mTFP is depicted, which demonstrated that QC-1 is a potent acceptor for donor fluorophores in the range of 480-520 nm (mTFP) or 510-550 nm (mCitrine). In unstimulated cells, the complex of PTag-QC-1 did not reduce the lifetime of EGFR-mCitrine, showing that PTag-QC-1 bound specifically to the phosphorylated protein.

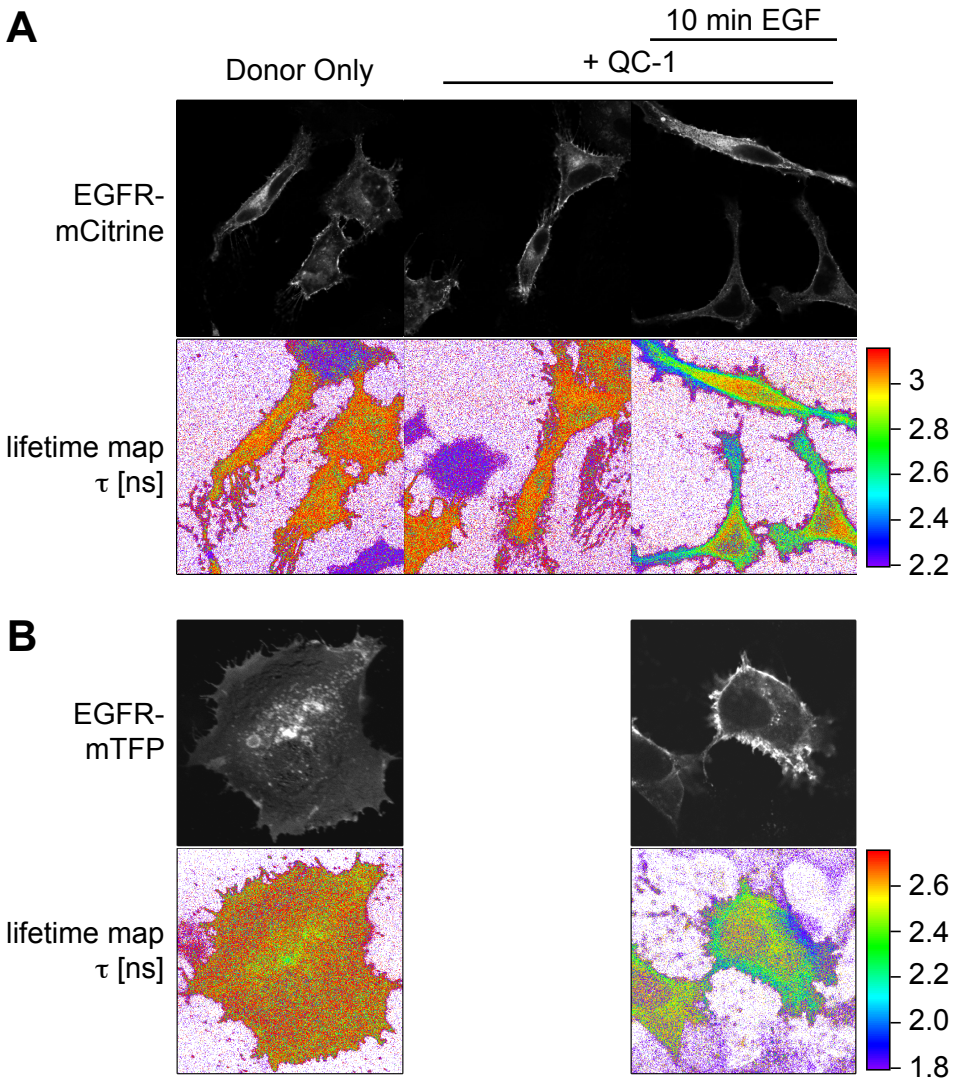

Figure 3.6: **QC1 as acceptor for mCitrine and mTFP in a FRET-FLIM experiment.** HeLa cells were transfected with EGFR-mCitrine (A) or EGFR-mTFP (B), starved, stimulated with 100 ng/ml EGF and fixed. For each sample the fluorescence intensity of EGFR-mCitrine or EGFR-mTFP and the distribution of the fluorescence lifetime *t* with false-colour look-up table (in ns) is shown. The acceptor fluorophore QC-1 does not emit light so its localization cannot be visualized.

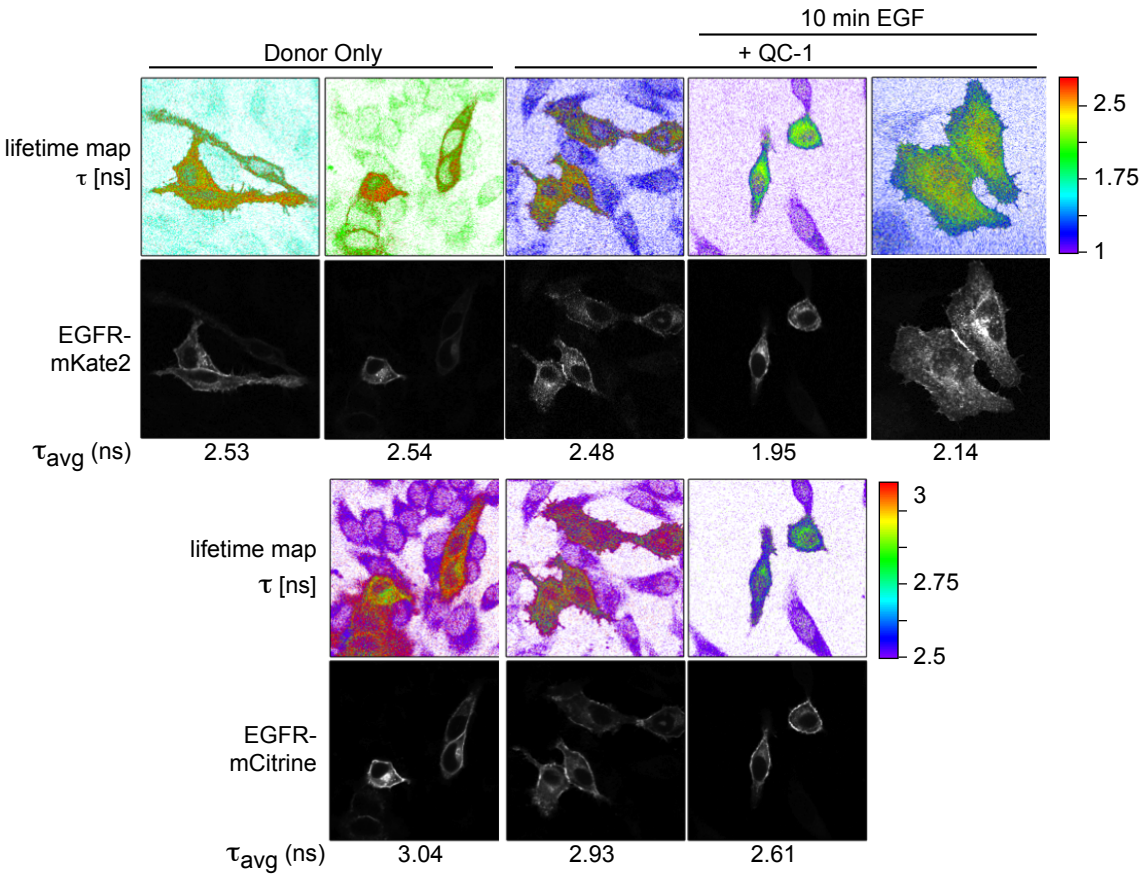

Figure 3.7: **QC1 as acceptor for mKate2.** To test the ability of QC-1 to undergo FRET with a red fluorescent protein, cells were transfected with EGFR-mKate2 alone or additionally co-transfected with EGFR-mCitrine. mCitrine was excitated at 470 nm and emission recorded at 517-533 nm. mKate2 was excitated at 532 nm and emission recorded between 610-680 nm.

To test the PTag-QC-1 also as acceptor for a red donor fluorophore, EGFR-mKate2 and additionally a dual donor measurement including EGFR-mCitrine and EGFR-mKate2 was set up (figure 3.7). EGFR-mKate2 alone or in co-expression with EGFR-mCitrine had an average lifetime of 2.54 ns, which was only subtly changed upon addition of the PTag-QC-1 complex. The induced EGFR phosphorylation by treatment with EGF, however, was reported by PTag-QC-1 with a lifetime change of 0.4-0.6 ns. Therefore, PTag-QC-1 can be applied to monitor the phosphorylation of proteins in a multi-donor FLIM approach.

4 Phospho-gradients in the yeast pheromone response

4.1 Influence of a Negative Feedback on the Fus3 Activity range in the Yeast Shmoo

4.1.1 Background

In yeast, an extracellular pheromone gradient is translated via the cell surface receptor occupation into an intracellular activity gradient of the MAPK Fus3 [Maeder et al., 2007]. The determining factors and the cellular role of this cytoplasmic ppMAPK gradient are still unknown. The Fus3 activity gradient might serve as an intracellular distance meter which aligns the nucleus and therefore maintains cell proportions [Maeder et al., 2007]. However, it is known that active Fus3 links the activation of the pheromone receptor to the polarization of the actin cytoskeleton [Matheos et al., 2004]. Therefore, the Fus3 activity distribution could define a spatial probability profile of growth and accordingly orient the mating projection.

In this chapter, the influence of the yeast MAPK network architecture on the Fus3 activity gradient was investigated using yeast strains in which a negative feedback phosphorylation from Fus3 on Ste11 is impaired [Hecker et al., 2014]. These mutant cells form broader, less well polarized mating projections and furthermore build more frequently a second mating projection [Hecker et al., 2014]. As described in chapter 1.3.3.3, computations on predictions on the activity gradients of single network elements show that the network architecture influences MAPK activity gradients. As described in chapter 1.3.3.3, an active molecule is distributed in a gradient, if forward and backward reaction of the activation cycle are spatially separated. Computational calculations on this spatial separation of the de-/activation cycle show that the spatial propagation of the active molecules also depends on the surrounding network architecture. A negative feedback can cause a lower amplitude and steeper decline of the gradients compared to cells without negative or with positive feedback (see figures 1.9 B-E and 1.10). Therefore, the impairment of the negative feedback in Ste11 mutant strains could cause the spreading of active Fus3. A correlation between the spatial Fus3 activity distribution and morphological changes during the pheromone response might point at a causal connection of these processes.

The negative feedback phosphorylation occurs in vegetatively growing cells on Ste11 Ser243 and Thr596, and is relieved in early time points after pheromone stimulation [Hecker et al., 2014]. Mutating the sites Ser243 and/or Thr596 in Ste11 to phospho-mimicking amino acids renders yeast insensitive to pheromone, while yeast expressing non-phosphorylatable Ste11 mutants react hypersensitive to pheromone [Hecker et al., 2014].

The non-phosphorylatable mutant Ste11-T596I was previously described as being constitutively active [Stevenson et al., 1992]. The phosphorylation of Ste11-Ser243 by Fus3 was shown to prevent the binding of Ste11 to scaffold Ste5 [Hecker et al., 2014]. The interaction Ste11-Ste5 is required for the recruitment of Ste11 to the active receptor and is thought to enhance the signal transduction to Ste7. The negative feedback from Fus3 to Ste11 therefore sets an activation threshold for the mating pathway which determines the sensitivity to pheromone. The negative feedback from Fus3 on Ste11, which impairs the association of Ste11 to Ste5, is therefore a further mechanism to prevent unspecific Fus3 activation by subthreshold concentrations of pheromone, Ste11 activation during cell cycle phases other than G1 or by other cross-talk signals (see also chapter 1.2). Additionally, the inhibition of the negative

feedback on Ste11-Ser243 renders the typically switch-like mating decision into a graded response. In conjunction with the ultrasensitive Ste5-Fus3 dissociation and Ste5 PM association upon pheromone stimulation, the regulated Ste5-Ste11 interaction optimizes the dose-response and the morphological transitions of the pheromone pathway.

In this context, the influence of the negative feedback from Fus3 on Ste11 on the spatial distribution of Fus3 activity was investigated in yeast expressing either the single mutant Ste11-S243A or the double mutant Ste11-S243A,Thr596I.

4.1.2 Imaging the Spatial Distribution of ppFus3

In order to measure the spatial distribution of Fus3 phosphorylation in yeast cells by FRET-FLIM, two phospho-specific Fus3 antibodies were tested in immunofluorescence as potential phospho-acceptors (figure 4.1).

Wild type (WT) yeast cells expressing Fus3- yeast enhanced monomeric (yem) -Citrine from the endogenous promoter were stimulated with 100 nM pheromone for 2.25 hours and fixed, as described in chapter 8.6.6. The anti-ppFus3 antibody from R&D Systems (AF1018) showed a clear projection tip and weak nuclear localization, while the Cell Signaling antibody strongly localized to the nucleus with a weak staining of the polarization tip, as shown in figure 4.1. As the R&D Systems anti-ppFus3 antibody was shown before to bind specifically the doubly phosphorylated form of Fus3, the strong nuclear localization of the Cell Signaling antibody might reflect affinity for the mono-phosphorylated Fus3 [Maeder et al., 2007]. Accordingly, AF1018 was labeled with Cy3.5 as acceptor fluorophore for FLIM of yemCitrine-tagged Fus3. Two batches of AF1018 were labeled with a 10 and 13 times excess of mono-functional dye

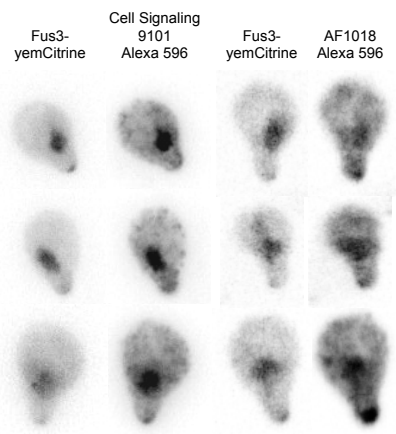

Figure 4.1: **Immunostaining of phosphorylated Fus3.** Yeast cells expressing Fus3-yemCitrine from the endogenous promoter were stimulated with 100 nM pheromone for 2.25 hours and subsequently fixed and permeabilized. To visualize ppFus3, cells were first incubated with anti-ppFus3 antibodies AF1018 from R&D Systems or 9101 from Cell Signaling and then with Alexa546-conjugated anti-rabbit antibody. Left half: Fluorescence intensity of Fus3-yemCitrine and Alexa546 after staining with ppFus3 antibody 9101 from Cell Signaling of three different cells. Right half: Fluorescence intensity of Fus3-yemCitrine and Alexa546 after staining with ppFus3 antibody from R&D Systems of three different cells.

as described in chapter 8.5.3, resulting in a dye per protein ratio of 4 and 7, respectively. Both labeled antibodies localized unspecifically to yeast cells (data not shown), showing that the antibody's binding affinity was lost during the labeling process.

Owing to the encountered issues with an antibody-based FRET-FLIM, which are the availability of suitable phospho-specific antibodies and the antibody's compatibility to the labeling process, PTag-FLIM was developed. PTag-FLIM enables the mapping of any phosphorylated protein with high signal-to-noise ratio but is simultaneously unselective for the accessible phosphosites in the protein of interest.

4.1.3 Influence of Network Architecture on Fus3 Activity Gradient

In order to map the Fus3 activity in WT, Ste11-S243A and Ste11-S243A,T596I yeast strains, the cells were stimulated for 3 hours with 100 ng/ml pheromone, fixed and stained as described in chapter 8.6.6. To quantify the distribution of Fus3 and ppFus3, cross-section profiles of intensity, excited state lifetime τ and phosphorylated fraction α were obtained from tip-to-end of the cell. Profile lengths of single cells were normalized to preserve cell proportions thus enabling the calculation of average profiles of intensity, lifetime τ and fraction α.

4.1.3.1 ppFus3 gradient detected by PTag-FLIM

Using PTag-FLIM, a steep ppFus3 gradient in the mating projection of WT yeast cells was detected (figure 4.2). The observed Fus3 phosphorylation gradient is consistent with previous data [Maeder et al., 2007], except for the detection of nuclear Fus3 phosphorylation. The newly obtained data showed an average difference in the lifetime τ between tip and cytoplasm of about 0.5 ns, in contrast to a difference of about 0.15 ns in the prior data [Maeder et al., 2007]. Theoretically, differences between the excited state lifetime maps using either PTag or the ppFus3 antibody could result from the detection of mono-phosphorylated Fus3 by the unselective PTag. The detection of phosphorylated Fus3 in the nucleus by PTag-FLIM is however supported by the result of the immunostaining with the anti-ppFus3 antibody AF1018 in figure 4.1 and can therefore be attributed to the high dynamic range of PTag-FLIM. The application of PTag-FLIM for Fus3 has therefore a superior signal-to-noise ratio and does not suffer from the unspecificity of PTag. PTag-FLIM is eminently suited to measure potentially subtle effects from changes in the MAPK network architecture on the ppFus3 gradient.

4.1.3.2 Inhibition of Feedback from Fus3 to Ste11 Extends the ppFus3 Gradient

The ppFus3 gradient in the shmoo region of Ste11-S243A expressing cells had a similar amplitude as in WT cells showing that the mutation S243A does not directly target the activity of Ste11 (figure 4.2 C and D). In the Ste11-S243A strain, the gradient's slope was slightly shallower than in the WT strain. Accordingly, the Fus3 activity gradient in Ste11-S243A cells extended further in the direction of the nucleus than in WT cells. Active Fus3 is therefore less constrained if the negative feedback on Ste11-S243 is impaired.

In the Ste11-S243A,T596I yeast strain, the phosphorylation of Fus3 is significantly elevated across the profile, relative to WT and Ste11-S243A cells. The increase in Fus3 phosphorylation can be attributed to mutation Ste11-T596I which renders Ste11 constitutively active. Like in Ste11-S243A cells, in Ste11-S243A,T596I cells the ppFus3 gradient's profile is extended to at least 20% of the cell's length. The results of the Ste11-S243A,T596I strains confirm the predictions that a relief of a negative feedback increases the basal level of phosphorylation and decreases the steepness of the gradient.

In regard of the shmoo morphology, the polarization tips in both Ste11 mutant expressing strains appeared to be broader than in WT cells. The intensity profiles of the different strains showed that the relative position of the nucleus seems to remain unchanged.

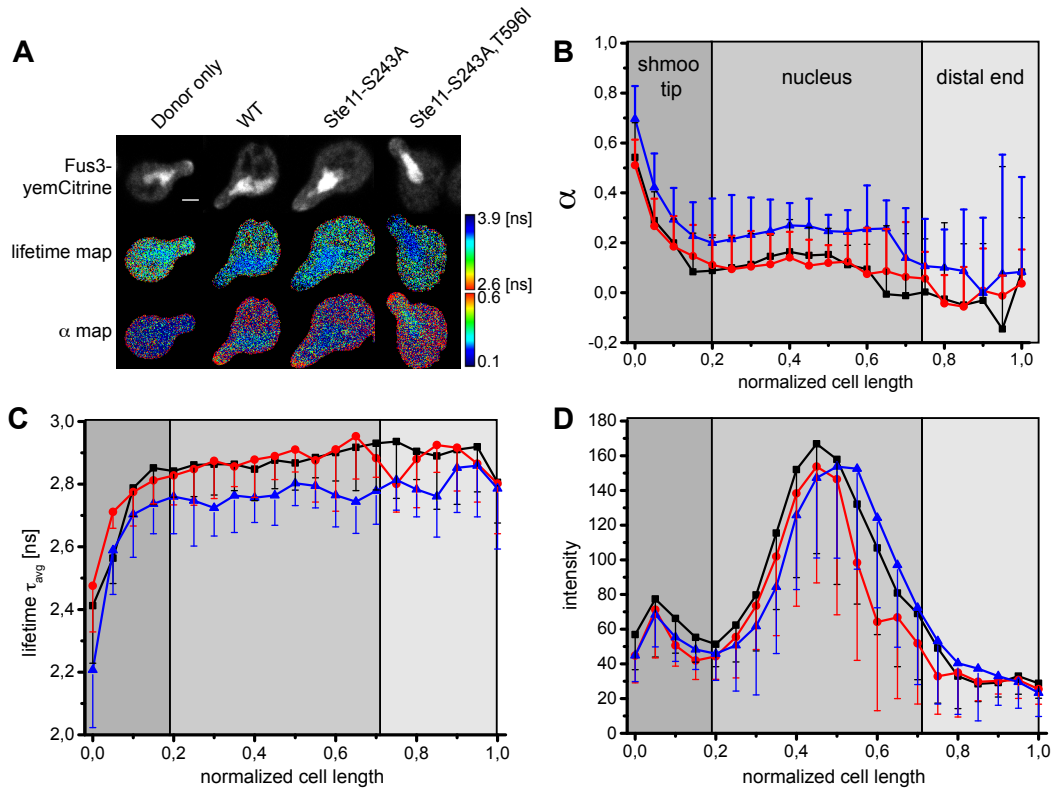

Figure 4.2: **Inhibition of Feedback Fus3 to Ste11 extends ppFus3 gradient.** (A) FLIM of phosphorylated Fus3 in stimulated WT (n = 20), Ste11-S243A (n = 9) or Ste11-S243A,T596I (n = 18) cells expressing Fus3-yemCitrine. Fixed and permeabilized yeast cells were incubated with the PTag-Cy3.5 complex. For each sample, the fluorescence intensity of Fus3-yemCitrine (donor), the distribution of donor fluorophore lifetime t and the spatial distribution of the fraction of interacting molecules α as determined by global analysis of FLIM data are shown. The false-color look-up table indicates the lifetime τ in ns or the fraction of phosphorylated protein, respectively. The tip-to-end profile of the fraction of phosphorylated Fus3, α, (B), donor fluorophore lifetime in ns (C) or the donor fluorophore intensity (D) averaged over several cells are shown with s.d. as function of the normalized distance. Asterisks indicate the probability of an unpaired, two-tailed t-test if the difference between WT and Ste11-S243A,T596I (blue) or Ste11-S243A and Ste11-S243A,T596I (red) are significant with $p \leq 0.05$ (1 asterisk), $p \leq 0.01$ (2 asterisks) or $p \leq 0.001$ (three asterisks). The average region of the nucleus and the shmoo tip are indicated.

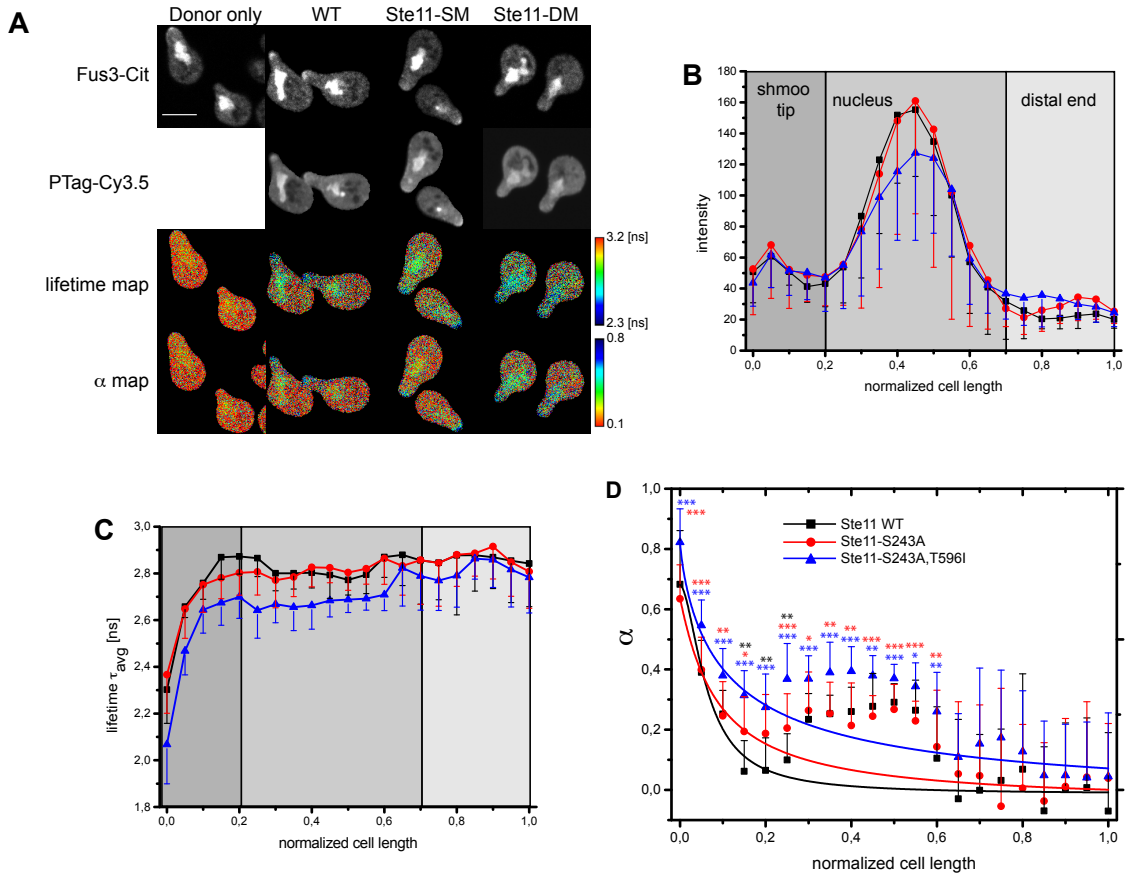

Figure 4.3: **Deletion of Kss1 strengthens effects of feedback impairment on the spatial ppFus3 profile.** (A) FLIM of phosphorylated Fus3 in stimulated (100 nM pheromone, 3h) ΔKSS1 (n = 18) , ΔKSS1, Ste11-S243A (n = 18) or ΔKSS1, Ste11-S243A,T596I (n = 13) cells expressing Fus3-yemCitrine. Fixed and permeabilized yeast cells were incubated with the PTag-Cy3.5 complex. For each sample, the fluorescence intensity of Fus3-yemCitrine (donor), PTag-Cy3.5 (acceptor), the distribution of donor fluorophore lifetime τ and the spatial distribution of the fraction of interacting molecules α as determined by global analysis of FLIM data are shown. The false-color look-up table indicates the lifetime τ in ns or the fraction of phosphorylated protein, respectively. The tip-to-end profile of the the donor fluorophore intensity (B), donor fluorophore lifetime in ns (C) or fraction of phosphorylated Fus3, α, (D) averaged over several cells are shown with s.d. as function of the normalized distance. The average position of the nucleus and the shmoo tip are indicated. α values from all datasets excluding the data points from the nuclear region were fitted with a logistic sigmoidal function and plotted as dashed lines. Asterisks indicate the probability of an unpaired, two-tailed t-test if the difference between WT and Ste11-S243A,T596I (blue) or Ste11-S243A and Ste11-S243A,T596I (red) are significant with $p \leq 0.05$ (1 asterisk), $p \leq 0.01$ (2 asterisks) or $p \leq 0.001$ (three asterisks).

4.1.3.3 Deletion of Kss1 Strengthens Effects of Feedback Impairment on ppFus3 Gradient

It was found that if Fus3 homologue Kss1 is deleted, the effects of mutations Ste11-S243A and Ste11-S243A,T596I on the cell morphology were enhanced [Hecker et al., 2014]. In a ΔKSS1 background, it was investigated if the stronger effect on the cell morphology caused by Ste11 mutations correlates with the Fus3 activity gradient.

Indeed, differences in the spatial Fus3 activity profile between WT and Ste11 mutant strains were qualitatively similar but more pronounced in strains deleted for Kss1 (compare figures 4.2 and 4.3). The fraction of phosphorylation α was increased for each ppFus3 profile in ΔKSS1 cells.

The steepness of the ppFus3 gradient in the tip region was significantly lower in both Ste11 mutant strains with $\Delta\alpha$ = 0.5 than in WT cells with $\Delta\alpha$ = 0.6 (figure 4.3). To visualize the cytoplasmic gradient exclusively, data points eliminating the nuclear region were fitted with a logistic sigmoidal function. Like in cells with Kss1, in yeast expressing Ste11-S243A,T596I, Fus3 was more phosphorylated throughout the cell. In the ΔKSS1 background, the Ste11 mutations caused a stronger defect in the morphology which correlated with a stronger affected Fus3 gradient [Hecker et al., 2014]. This correlation might be due to a causal dependency between Fus3 activity distribution and morphology.

The intensity profiles of the different strains without Kss1 showed that the relative position of the nucleus remains unchanged (figure 4.3 B). But, a comparison of intensity distributions of the WT versus ΔKSS1 background cells uncovers that the nucleus was slightly shifted to the front in cells lacking Kss1.

Concluding the results from strains with and without Kss1 it can be inferred that the network architecture is a determining factor of the MAPK activity gradient's properties. The experiments confirm simulations which predicted that a negative feedback decreases the amplitude and restricts the extent of the MAPK's activity. Furthermore, an increase in morphological defects, namely the formation of broader and more shmoo tips, correlates with an increase in the range of active Fus3.

4.2 Hierarchical phospho-gradients in the yeast pheromone response

In vegetatively growing yeast, Ste11 and Ste7 are homogeneously distributed in the yeast cell, partially excluding the nucleus [van Drogen et al., 2001, Maeder et al., 2007]. Upon pheromone stimulation both MAPK cascade proteins are accumulated at the projection tip and locally activated. Active Ste11 and Ste7 can be expected to be distributed in a phospho-gradient which emanates from the mating tip. For proteins which are activated in a hierarchical sequence, the activity gradients become shallower and extend with each hierarchy level (see figure 1.9 A). The activation of downstream Fus3 is however constrained to the PM by membrane-bound Ste5, which catalytically unlocks Fus3 for phosphorylation by Ste7 [Good et al., 2009]. An extended, shallower gradient due to a hierarchical effect should therefore appear only for Ste7. However, mapping of Ste7 and Ste11 phosphorylation by unselective PTag-FLIM might represent also other phophosites than the activating ones, for instance Ste11-pS243 or Ste11-pT596.

In vegetatively growing cells, Ste5 localizes throughout the cell [Maeder et al., 2007]. Upon pheromone stimulation it is enriched at the mating tip. The scaffold Ste5 specifies the signal from the pheromone receptor to Fus3 via regulated association with proteins and the PM. The Ste5 interactions are regulated by phosphorylation of Ste5 and/or its binding partners. For Ste5 8 CDK-dependent and 4 Fus3-targeted phosphosites are known. The Fus3 dependent sites become dephosphorylated within the first minutes after pheromone treatment and result in a switch-like dissociation of Fus3 from Ste5 (see also chapter 1.2). It is however not known if

Ste5 becomes phosphorylated by Fus3 or other proteins in the process of the mating response. If Ste5 becomes phosphorylated at the PM, a primary, steep gradient of phosphorylated Ste5 should emanate from the PM. The mapping of phosphorylated Ste5 in shmooing yeast by PTag-FLIM therefore may deliver a first glance on the spatial regulation of Ste5.

4.2.1 Phospho-mapping of MAPKKK Ste11 and MAPKK Ste7

Ste11 and Ste7 are 5 and 3 times less concentrated then Fus3 (Ste11 approx. 35 nM and Ste7 70 nm). Due to the low fluorescence intensity of Ste7- and Ste11-yemCitrine fusions the amounts of detected photons were too low to calculate reliable excited state lifetimes. Therefore, Ste11-yemCitrine and Ste7-yemCitrine were cloned under the artificial ADH promoter, which increases the concentration of the protein-FP fusion about 10 times [Chapman & Asthagiri, 2009]. This artificial increase in concentration of one protein might disturb the stoichiometry within the network of interacting proteins.

Under control of the ADH promoter, Ste7- and Ste11-yemCitrine were enriched at the shmoo tip and localized throughout the cytoplasm (figure 4.4 A and B). The increase in concentration did not affect the localization of Ste7- and Ste11-yemCitrine.

Ste11- and Ste7-yemCitrine indeed showed gradients of phosphorylation in the tip region, as shown in figure 4.4 C and D. The phospho-Ste11 gradient appeared to be very steep at the tip and decline slowly to a plateau of minimal phosphorylation. After roughly 3 μm the signal-to-noise ratio of the lifetime profile decreases due to a low fluorescence intensity in the rear shmoo, see figure 4.4 F. The strong noise impairs the exact determination of a plateau of Ste11 phosphorylation. The distribution of phosphorylated Ste7 showed a less steep slope in the projection

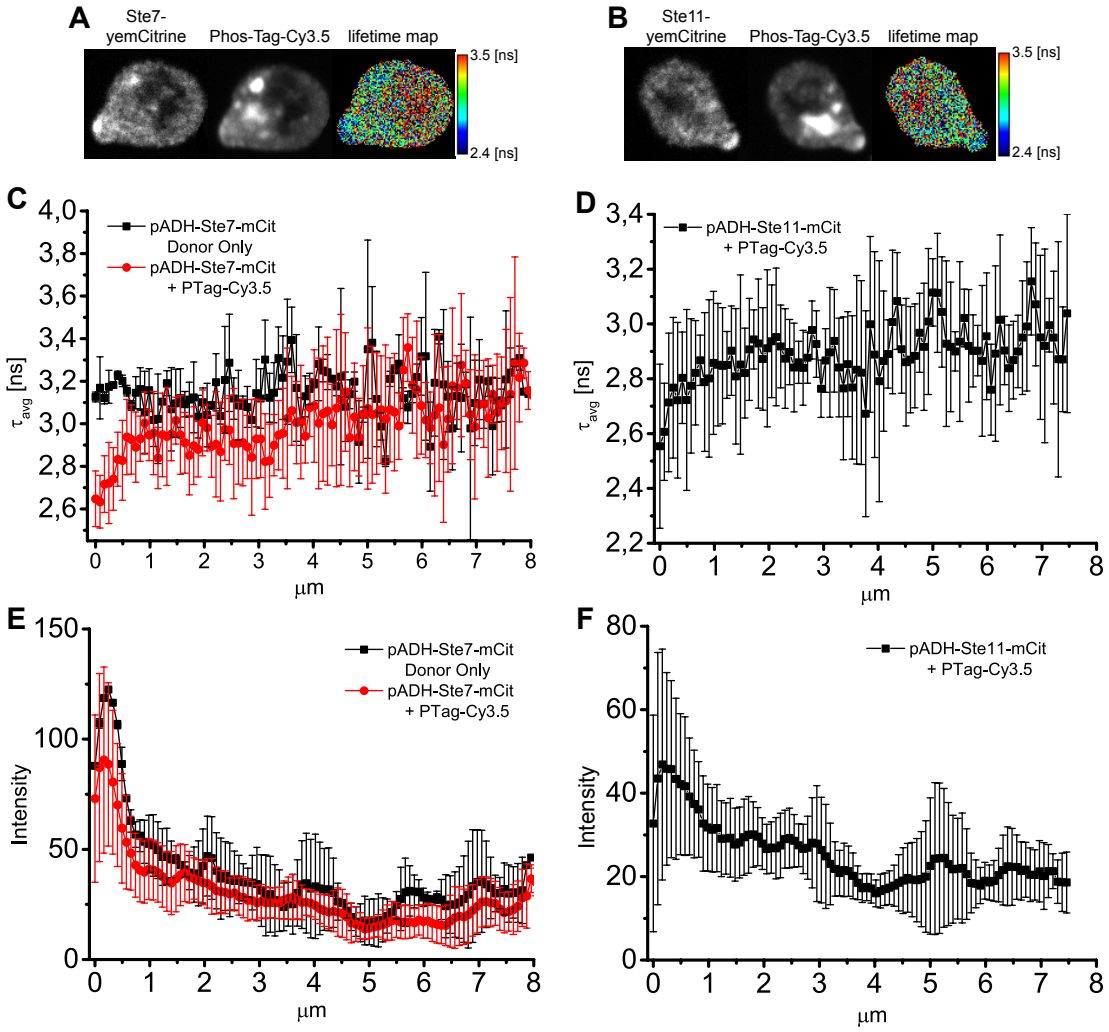

Figure 4.4: **Distribution of phosphorylated Ste7-yemCitrine or Ste11-yemCitrine in shmooing yeast.** Yeast expressing Ste7-yemCitrine (A) (n = 8) or Ste11-yemCitrine (B) (n = 6) from the ADH promoter were stimulated for 3 hours with 100 nM pheromone and subsequently fixed, permeabilized and stained with PTag-Cy3.5. For each sample, the fluorescence intensity of Ste7-yemCitrine (donor), PTag-Cy3.5 (acceptor), the distribution of donor fluorophore lifetime τ are shown. The false-color look-up table indicates the lifetime τ in ns. (C and D) The tip-to-end profile of the the donor fluorophore lifetime τ_{avg} in ns of Ste7-yemCitrine or Ste11-yemCitrine. (E and F) Tip-to-end profile of the the donor fluorophore intensity in arbitrary units of Ste7-yemCitrine or Ste11-yemCitrine.

tip which extended linearly to a constant level after 0.6 μm. To compare the gradients of the different yeast pheromone MAPK cascade elements the different profiles are shown in a single graph in figure 4.6.

4.2.2 Phospho-mapping of scaffold Ste5

Ste5 was over-expressed from the artificial ADH promoter. Unlike Ste5 expressed from its native promoter, ADH-Ste5-mCitrine was strongly enriched in the nucleus, as shown in figure 4.5 A and B. As expected, Ste5 further accumulated at the shmoo tip. Quantifying the localization of phosphorylated Ste5 revealed a steep phospho-Ste5 gradient, which extended over the first μm (see figure 4.5 C). The basal cytoplasmic phosphorylation level of scaffold Ste5 was

higher than the phosphorylation level of the kinases of the pheromone MAPK cascade (figure 4.6). PTag-FLIM showed a very good detection sensitivity for the phosphorylation of Ste5. The obtained data represents however generic information on Ste5 phosphorylation without the possibility to differentiate between phospho-sites with different functions.

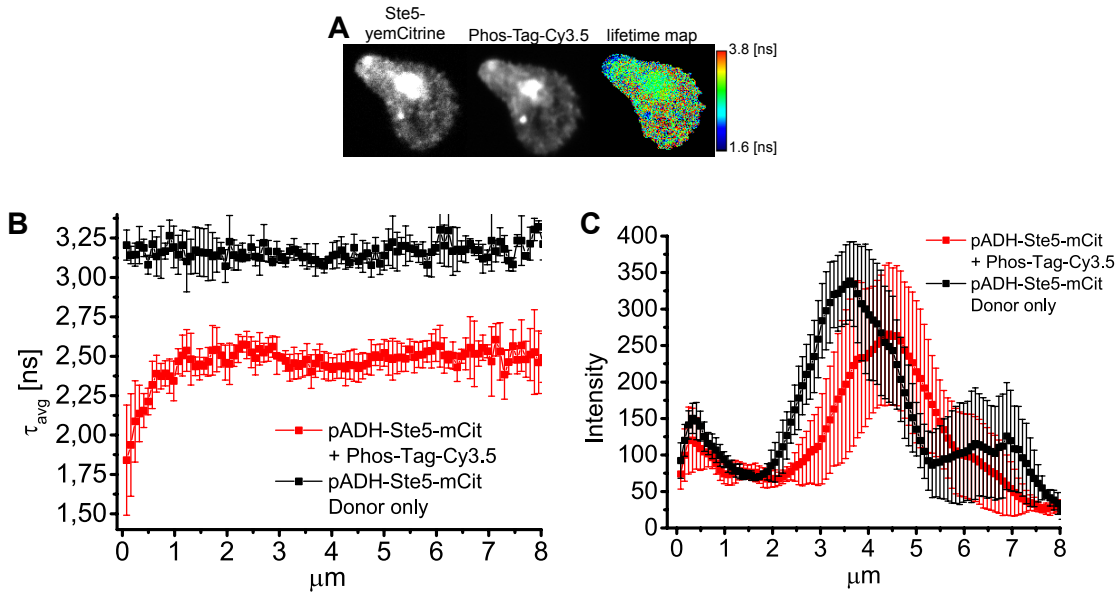

Figure 4.5: **Distribution of phosphorylated Ste5-yemCitrine in shmooing yeast.** Yeast expressing Ste5-yemCitrine from the ADH promoter were stimulated for 3 hours with 100 μM pheromone and subsequently fixed, permeabilized and stained with PTag-Cy3.5 (n = 6). (A) For each sample, the fluorescence intensity of Ste5-yemCitrine (donor), PTag-Cy3.5 (acceptor), the distribution of donor fluorophore lifetime τ are shown. The false-color look-up table indicates the lifetime τ in ns. The tip-to-end profile of the the donor fluorophore intensity (B) or donor fluorophore lifetime in ns (C).

4.2.3 Hierarchical phospho-gradients in the yeast shmoo

In the yeast pheromone MAPK network, Ste11 and Fus3 are activated directly at the PM, while the area of Ste7 activation is defined by the profile of active Ste11 and therefore extended in axial direction towards the nucleus. The comparison of phospho-profiles of the four main network components in the shmoo showed that except the phospho-Ste7 profile, all are steep, primary gradients as shown in figure 4.6. The Ste5 phosphorylation gradient points towards an unknown regulation of Ste5 interactions at the PM.

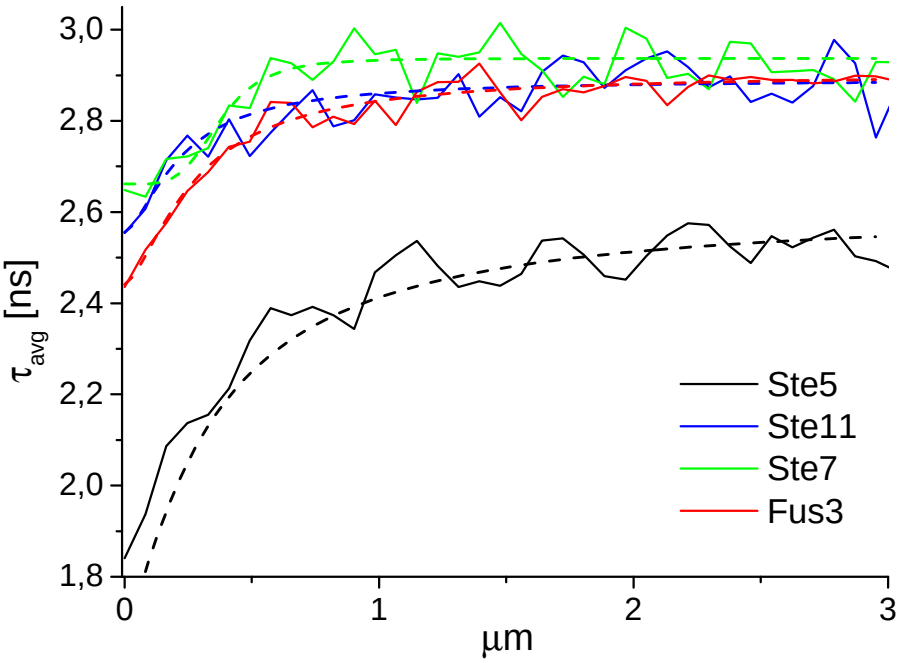

Figure 4.6: **Comparison of phospho-gradients of MAPK elements of the yeast pheromone response.** For details on the data see figures 4.2, 4.4 and 4.5. Each phospho-profile was fitted with a sigmoidal function.

5 Spatio-temporal regulation of Mek1 and ERK2 in MCF-7 cells

5.1 Differentiation of distinct MAPK functions

The core function of ERK1/2 activity is the initiation of transcription. In order to enter the nucleus on a short time scale, active ERK1/2 has to propagate through the cytoplasm despite the restriction by phosphatases. In contrast, targeting of ERK1/2 activity to specific functions in cytoplasm or organelles requires a sustained and localized ERK activity. Potentially multifaceted mechanisms enable the spatial differentiation of ERK1/2 functions in nucleus and cytoplasm.

Regarding the signal propagation from the PM to the nucleus within the dimensions of a mammalian cell, the hierarchical built-up of MAPK cascades may provide the necessary extension of activity gradients. Default signaling via the linear cascade might therefore be sufficient for ERK's global function, the initiation of transcription. However, if local ERK1/2 activity is required, the ERK1/2 activity range has to be targeted and confined by regulatory interactors. Scaffolds assemble signaling modules and target these to a supramolecular structure. This scaffolded catalysis of signal transduction within a confined space promotes the restraining of activity gradients. The use of several scaffolds for the divers cytoplasmic functions of ERK1/2 seems to be likely.

A classical example for the differentiation of MAPK functions is the HRG induced ERK1/2 activity in MCF-7 cells (see also chapter 1.3.4). In MCF-7 cells, stimulation with EGF causes proliferation, while HRG induces differentiation [Dong et al., 1992, Wosikowski et al., 1993, Nagashima et al., 2007]. In both cases the signal is channeled through the Raf/Mek/ERK cascade. The particular cell fate depends on the spatio-temporal ERK activity profile. Cells undergo proliferation, if the cytoplasmic ERK activity is transient, while sustained cytoplasmic ERK activity causes differentiation. The nuclear ERK activity is transient in both cases [Thottassery et al., 2004, Nagashima et al., 2007, Nakakuki et al., 2010]. The causal link between spatio-temporal ERK activity profile and cell fate is known: Only sustained ERK activity leads to phosphorylation and stabilization of the IEG cFos, which triggers differentiation. If cFos is not phosphorylated it becomes degraded and proliferation is programmed. The particular MAPK network compositions and topologies caused by the different GFs remain to be elucidated. Known is that EGF activates EGFR (ERB-B1) and HRG activates receptors ERB-B1, -B2, -B3 and -B4. While the stimulation with EGF causes the homo-dimerization of EGFR and subsequent endocytosis and degradation, the involvement of ERB-B3 and ERB-B2 in heterodimers causes the stabilization of these dimers and favours their recycling instead of degradation [Waterman et al., 1998, Lenferink et al., 1998]. The activation of ERB-B2 and ERB-B3 might therefore provide a mechanism for sustained cellular signaling. The activation of the whole ERB family by HRG induces additionally to the ERK pathway also the PI3K/AKT pathway, Rac-PAK signaling, PLCγ and subsequently Rap1 [Peles et al., 1991, Peles et al., 1992, Yang et al., 2006]. PLCγ can activate PKC, which was identified as distinctive factor for proliferation vs. differentiation in PC-12 cells [Santos et al., 2007]. Activation of PKC by PMA indeed prolongs ERK activity induced by EGF also in MCF-7 cells [Nakakuki et al., 2010]. However, PKC may directly activate Raf, so that a proof for PKC being integrated into the MAPK network upon HRG stimulation remains missing [Kolch et al., 1993].

The scaffold KSR1 has been associated with the determination of the MAPK signal en-

durance and localization in different cell types. KSR1 was shown to be required to maintain a prolonged ERK activity upon PDGF stimulation in mouse embryonic fibroblasts (MEFs) [Kortum & Lewis, 2004]. On the other hand, a negative feedback from active ERK on KSR1 was shown to promote transient MAPK cascade signaling in MEFs and fibroblasts [Razidlo et al., 2004, McKay et al., 2009, Canal et al., 2011]. After the homologue KSR2 was found to be catalytically active as a kinase for Mek1 sites of unknown function, also KSR1 is considered to be more than a pseudokinase [Brennan et al., 2011, Sibilski et al., 2013]. Regarding the GF-specific regulation of the scaffolding and the catalytic functions of KSR1 not much is known. It was however shown that Src can phosphorylate KSR1 on Tyr728 which "may regulate the transition between the scaffolding and the catalytic function of KSR1" [Sibilski et al., 2013]. KSR1 was shown to be required for localized activity of ERK in hippocampal neurons and lymphocytes [Canal et al., 2011, Giurisato et al., 2009].

In the first part of this chapter, EGF and HRG induced differential spatio-temporal Mek1 and ERK1/2 activity profiles were investigated in MCF-7 cells. In the second part the influence of scaffold KSR1 on EGF and HRG induced Mek1 and ERK2 activity was investigated. These considerations were approached by western blots (WB) of whole cell lysates detecting specifically Mek1 and ERK1/2 active forms and PTag-FLIM for imaging of active mCitrine-Mek1 and mCitrine-ERK2. The influence of KSR1 was investigated by ectopic overexpression of pECFP-KSR1, additionally to the endogenous protein.

5.2 Spatio-temporal regulation of Mek1 and ERK2 upon EGF/HRG stimulation in MCF-7

5.2.1 Temporal regulation of Mek and ERK in cell populations

In order to map Mek1 and ERK2 activity in MCF-7 cells by PTag-FLIM, both proteins were ectopically expressed as N-terminal mCitrine fusion. To test the functionality of these ectopically expressed FP fusions, the EGF-induced activation profile of the FP fusion constructs and the homologue endogenous proteins was compared by WB experiments.

In HeLa cells, EGF stimulation caused the typical transient response of mCitrine-Mek1 and mTurquoise-ERK2 as well as of the homologue endogenous proteins. The Mek1 and ERK2 FP fusion constructs were therefore functional. In MCF-7 cells however, the FP-tagged Mek1 and ERK2 did not show a clear EGF response, although the endogenous proteins showed the transient activity profile (figure 5.1). Noticeably, mTurquoise -ERK2 showed an offset in its initial phosphorylation level. Comparing the relative expression levels revealed that the endogenous and FP-tagged Mek1 and ERK2 are similarly strong expressed in HeLa cells, while in MCF-7 cells the FP-fused proteins were significantly stronger expressed than the endogenous homologues. This strong ectopic overexpression might saturate interacting proteins. Therefore, the expression levels of Mek1 and ERK2 -FP constructs were reduced in MCF-7 cells.

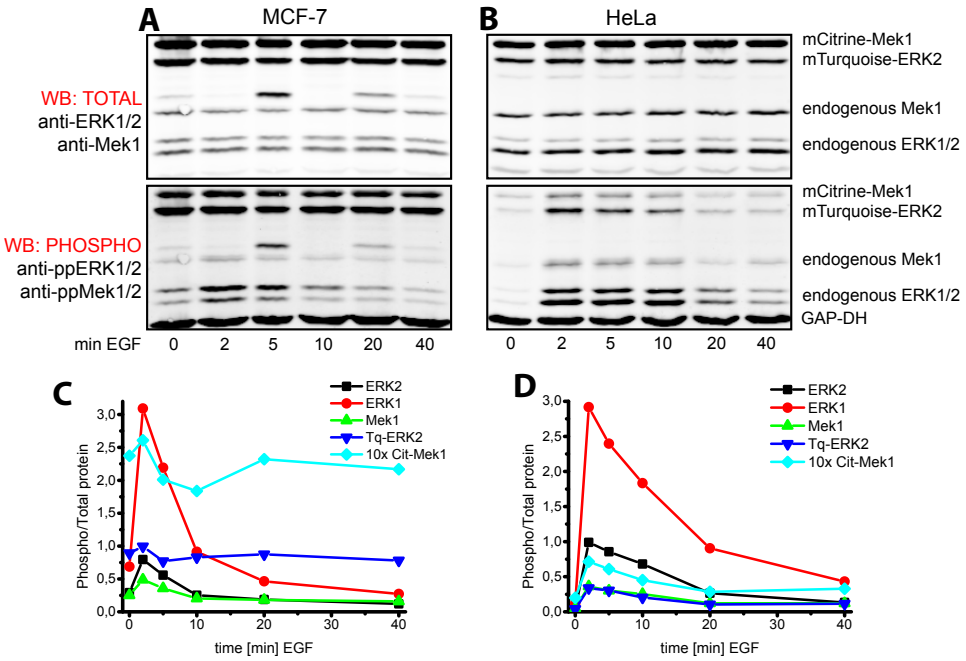

Figure 5.1: **Strong overexpression of FP-tagged Mek and ERK constructs in MCF-7 cells impedes their activation during EGF stimulation.** MCF-7 and HeLa cells expressing mCitrine-Mek1 and mTurquoise-ERK2 were stimulated with 100 ng/ml EGF for the indicated time points. Whole cell lysates of MCF-7 (A) and HeLa (B) cells were blotted for total and activating phospho-sites of Mek1/2 (pSer217/pSer221) and ERK1/2 (pThr202/pTyr204). The ratio of phosphorylated to total protein was quantified for MCF-7 (C) and HeLa (D).

The reduction of the expression level lead to comparable response profiles and amplitudes of ectopically expressed and endogenous Mek1 and ERK2 upon EGF stimulation, as shown in figure 5.2. Therefore, the EGF induced MAPK network in MCF-7 cells is sensitive to strong overexpression of Mek1 and ERK2. In subsequent microscopy experiments cells were selected against high fluorescence intensity. Furthermore, from the differential response profiles of endogenous and FP-tagged proteins it can be deduced that the FP tag renders the proteins distinguishable from the endogenous proteins.

Mek1 and ERK1/2 exhibited the known sustained activity profile upon HRG stimulation, as shown in figure 5.2 [Thottassery et al., 2004]. The FP-tagged proteins showed a sustained activation profile in response to HRG stimulation but with a lower amplitude than the endogenous proteins. The HRG induced response is therefore more sensitive than the EGF response, indicating that HRG signaling requires a different network architecture.

Upon EGF stimulation the activity of Mek1 and ERK1/2 reached a maximum after two minutes, while upon HRG treatment the maximal phosphorylation was shifted to five minutes. The subtly slower response of Mek1 and ERK1/2 upon HRG stimulation can be explained with slower activation kinetics of the ERB-B2 - B4 receptors compared to EGFR [Nagashima et al., 2007].

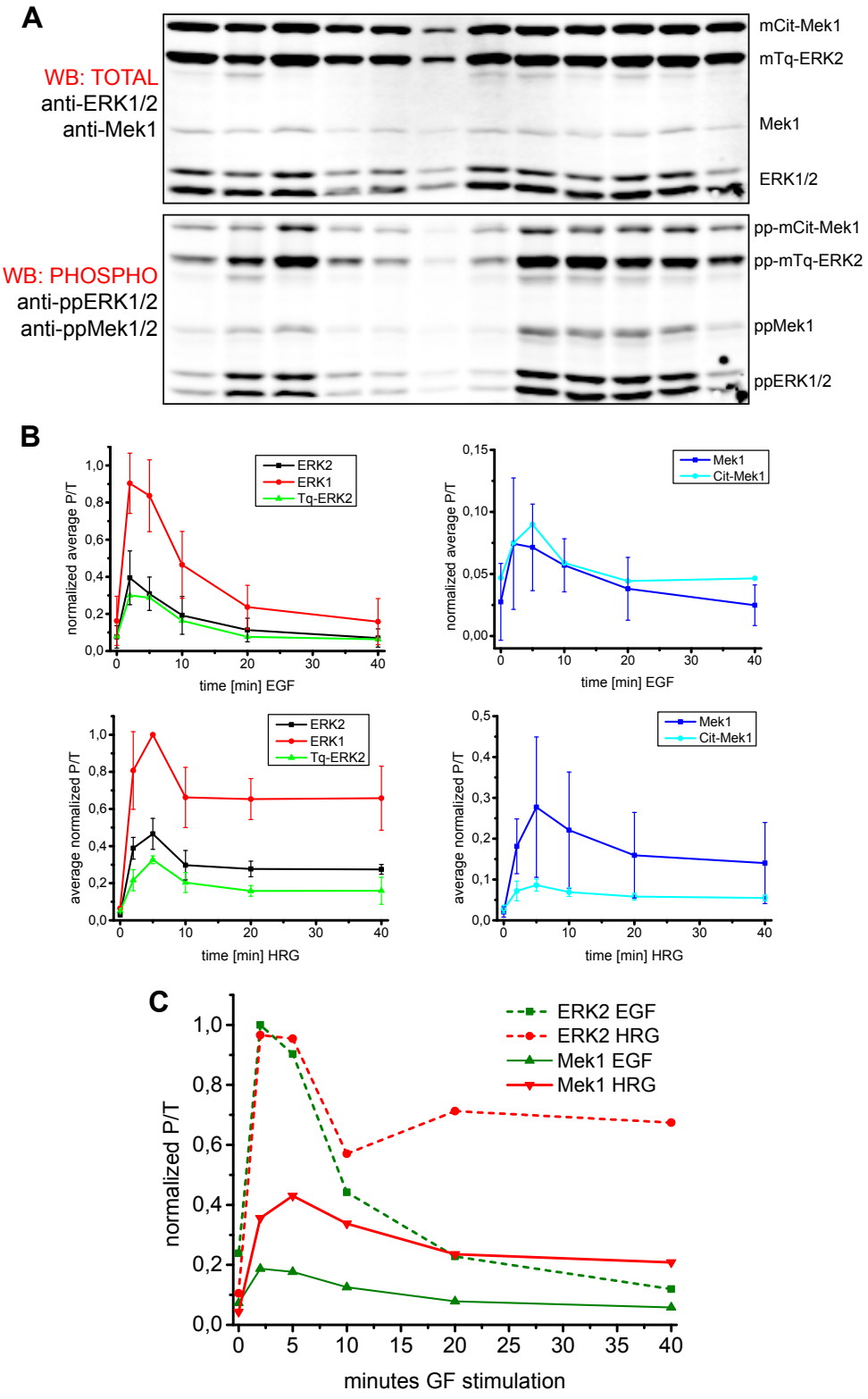

Figure 5.2: **Transient versus sustained response of Mek1 and ERK1/2 upon EGF or HRG treatment in MCF-7 cells.** Figure legend on the next page.

Figure 5.2: Transient versus sustained response of Mek1 and ERK1/2 upon EGF or HRG treatment in MCF-7 cells. (A) WB against total protein and activating phospho-sites of Mek1 and ERK1/2 stimulated with 100 ng/ml EGF or 100 ng/ml HRG for the indicated time points in MCF-7 cells. Ratios of phosphorylated/total (P/T) protein were calculated for

Mek1 and ERK1/2 and normalized to the peak value of the WB. (B) The average normalized ratios P/T of ERK1/2 or Mek1 were quantified between experiments (N = 5). (C) EGF and HRG cause differential response of ERK2 to the dose of pMek1. Although Mek1 is stronger activated by HRG, the amplitude of ppERK1/2 is similar.

Relative to the ERK1/2 response, the Mek1 response was stronger after HRG stimulation than after EGF treatment. In order to show that this differential conversion of Mek1 activity into ERK2 activity is not due to differential measurement parameter between experiments, like different antibody dilutions or instrument settings, a WB comprising both EGF and HRG stimulation time courses was conducted (see figure 5.2 C). This experiment showed that Mek1 is indeed about 2-fold stronger activated by HRG than by EGF. This higher fraction of active Mek1 is however not converted into a stronger fraction of active ERK1/2. The signal transduction from Mek1 to ERK1/2 is therefore differentially regulated by EGF and HRG stimulation.

5.2.2 Spatio-temporal regulation of Mek1 and ERK2 in single cells

Using PTag-FLIM, mCitrine-Mek1 and mCitrine-ERK2 activity was mapped in MCF-7 cells. To resolve nuclear from cytoplasmic activity and compare data from WB and PTag-FLIM, temporal activity profiles were calculated from the images of the phosphorylated fraction α, which was derived from global analysis of FLIM data.

Images were segmented based on the fluorescence intensity of mCitrine-Mek1 or mCitrine-ERK2 and the DNA stain DAPI to generate masks of the cell, cytoplasm or nucleus. To determine the temporal profile of Mek1 or ERK2 activity measured by PTag-FLIM, cumulative histograms of the distribution of α were computed and normalized to the peak value.

The EGF induced temporal profile of mCitrine-Mek1 activity followed an overall transient trend, except to an outlier at 5 minutes of EGF stimulation (compare figures 5.3 with 5.2). This outlier and the high standard error are likely due to the high biological variance between single cells, considering the number of measured cells (8-15 cells for each of the EGF stimulation time points). Despite the starvation of cells prior to stimulation, which is supposed to deprive cells from constant signaling and align cells in the G_0 phase of the cell cycle, the state of each single cell depends for instance on the local cell density.

The HRG induced response of mCitrine-Mek1 was strong enough to resolve the early peak at 2-5 minutes and a sustained response after 40 minutes of stimulation. PTag-FLIM experiments therefore confirm a stronger Mek1 phosphorylation upon HRG than after EGF stimulation.

As shown in figure 5.4, the mCitrine-ERK2 response upon EGF stimulation was transient in nucleus and cytoplasm with a maximal phosphorylation at 2 minutes. The temporal profile of mCitrine-ERK2 obtained by PTag-FLIM is consistent with WB data shown in figure 5.2.

The HRG induced peak of ERK2 phosphorylation appeared after 5 minutes. In contrast to EGF stimulation, HRG treatment induced a differential duration of ERK2 activity in nucleus and cytoplasm. The cytoplasmic ERK2 response was sustained within the observed time course, whereas the nuclear ERK2 response profile showed a bimodal trend. In the nucleus, the ERK2 response showed a maximal phosphorylation after 5 minutes and a delayed sustained response which appeared after 20 minutes and increased until 40 minutes of HRG stimulation. This bimodal activity profile in the nucleus hints towards different pools of active ERK2 in the cytoplasm induced by HRG stimulation. A sustained nuclear response contradicts results from a publication which found the nuclear response upon HRG stimulation in MCF-7 cells to be transient within 60 minutes [Nakakuki et al., 2010]. In this report the nuclear ERK2 activity was accessed by immunofluorescence, while the cytoplasmic ERK2 activity was determined by differential centrifugation of cell lysate and subsequent WB. PTag-FLIM is in contrast to immunofluorescence independent of the local protein concentration and provides a quantitative read-out over the whole cell. The ectopic expression of ERK-FP fusion constructs may however saturate interacting proteins and cause the release of excessive mCitrine-ERK2 which

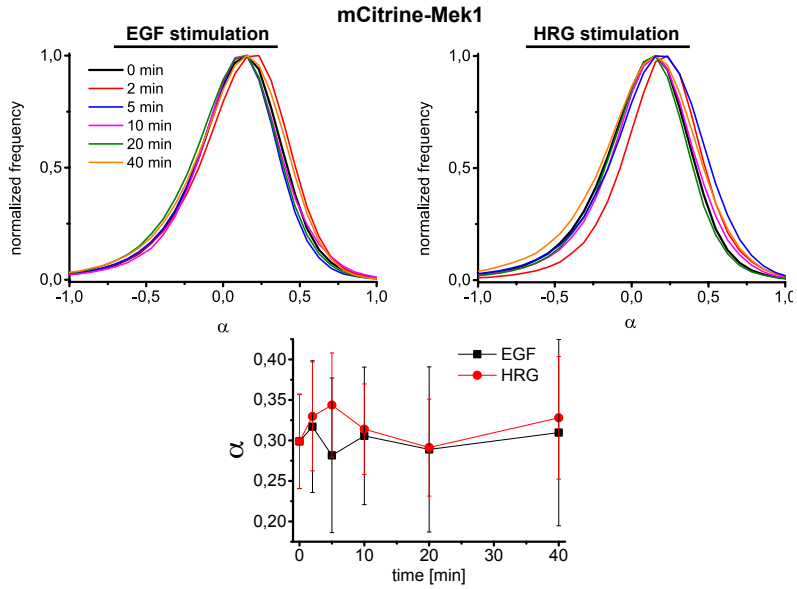

Figure 5.3: **EGF-induced Mek1 activity is transient, while HRG-induced MEK1 activity is sustained in the cytoplasm.** Quantification of mCitrine-Mek1 phosphorylation measured by PTag-FLIM in the whole cytoplasm upon EGF versus HRG stimulation in MCF-7 cells with s.e.m. Images of the phosphorylated fraction α were segmented for the cytoplasm. For each segmented image, cumulative histograms of the distribution of α were computed and normalized to the peak value. Number of cells stimulated either with EGF (0 min n = 27, 2 min n = 15, 5 min n = 9, 10 min n = 12, 20 min n = 9, 40 min n = 8) (top left) or with HRG (0 min n = 27, 2 min n = 17, 5 min n = 27, 10 min n = 28, 20 min n = 23, 40 min n = 20) (top right). Bottom: To visualize the temporal profile of Mek1 activity in the cytoplasm, the center of mass between 0-1 was calculated for each histogram and plotted for each timepoint.

subsequently accumulates in the nucleus.

Western blots and FLIM experiments revealed a fast ERK2 response upon EGF treatment (peak at 2 minutes in nucleus and cytoplasm) and a slow response upon HRG stimulation (peak at 5 minutes in nucleus and cytoplasm) (figures 5.2 and 5.9). The difference was less clear on western blots than in FLIM, which can be accounted for by the fixation in case of imaging but cooling down with ice-cold PBS for WB.

5.2.3 Phospho-mapping of Mek1 and ERK2

Images obtained by PTag-FLIM showed an elevation in the pMek1 fraction after 2 minutes of EGF stimulation, which was most pronounced at the PM and distributed into the interior cytoplasm (see figure 5.5). The resolution of such a gradual decrease in the phosphorylated fraction shows that PTag-FLIM provides a wide dynamic range of mCitrine-Mek1 phosphorylation. After 5 minutes of EGF stimulation the amplitude of the pMek1 gradient at the PM subtly decreased. From 10 minutes on, the pMek1 fraction returned to the initial level (0 minutes) and active Mek1 was no longer detected.

HRG stimulation caused after 2 minutes a strong and confined Mek1 activity at the PM (see figure 5.6). Within 5-10 minutes after HRG stimulation, the region of maximal pMek1 fraction seemed to spread into the cytoplasm causing a shallower distribution of Mek1. The width of this maximal pMek1 fraction correlated with the width of lamellipodia which can be observed in the fluorescence intensity image of mCitrine-Mek1. Upon 20 minutes of HRG stimulation, the strength of Mek1 activity decreased.

Compared to the EGF stimulation profile of Mek1 activity, HRG induced activity of Mek1 was persistent and stronger confined to the PM within 2-5 minutes. HRG stimulation might therefore recruit a regulatory interactor which confines MAPK signaling to the PM and therefore increases the steepness of a pMek1 gradient. On the contrary, EGF stimulation might induce default signaling via the linear cascade.

In order to quantify the cellular phospho-gradients, cells were computationally circularized and segmented into circular sections, as shown in figure 5.7.

The quantification of phospho-Mek1 distributions revealed pronounced gradients which emanated from the PM, as shown in figure 5.8. Therefore, Mek1 is generally activated in PM-proximal regions and the spreading of active Mek1 is constrained by phosphatases. Between 2-5 minutes, the HRG induced Mek1 activity gradients were subtly steeper than after EGF stimulation, while between 10-20 minutes the Mek1 activity steepness was comparable between both GF treatments. At 40 minutes of stimulation, the EGF induced Mek1 activity distribution was very shallow with a low amplitude in contrast to a sustained gradual decrease of Mek1 activity upon HRG stimulation.

Using PTag-FLIM, images of mCitrine-ERK2 phosphorylation were obtained, which showed a nuclear and cytoplasmic response of mCitrine-ERK2 between 2-10 minutes of EGF stimulation (shown in figure 5.9). mCitrine-ERK2 was more phosphorylated in the nucleus than in the cytoplasm.

The nuclear ERK2 phosphorylation was upon both stimuli distributed in gradients which emanated from the nuclear membrane in direction of the nucleus' center as shown in figures 5.9 and 5.10. A nuclear gradient has not been expected, because ERK2 activating proteins do not reside at the nuclear membrane. However, the nuclear import of ppERK2 through the two-dimensional nuclear membrane might be sufficient to generate a source of high ppERK2 concentration. Several nuclear ERK2 phosphatases, like MKP-1 and MKP-2 are known, which seem to prohibit the spreading of ppERK to the nucleus' center [Owens & Keyse, 2007].

In the cytoplasm, active ERK2 was distributed in a shallow gradient at 2 minutes of EGF stimulation. In the remaining stimulation time course ERK2 was distributed homogeneously between PM and nuclear membrane. At the 40 minutes time point ERK2 distribution was depolarized in comparison with the 0 minute time point. ERK2 distribution was shallower than

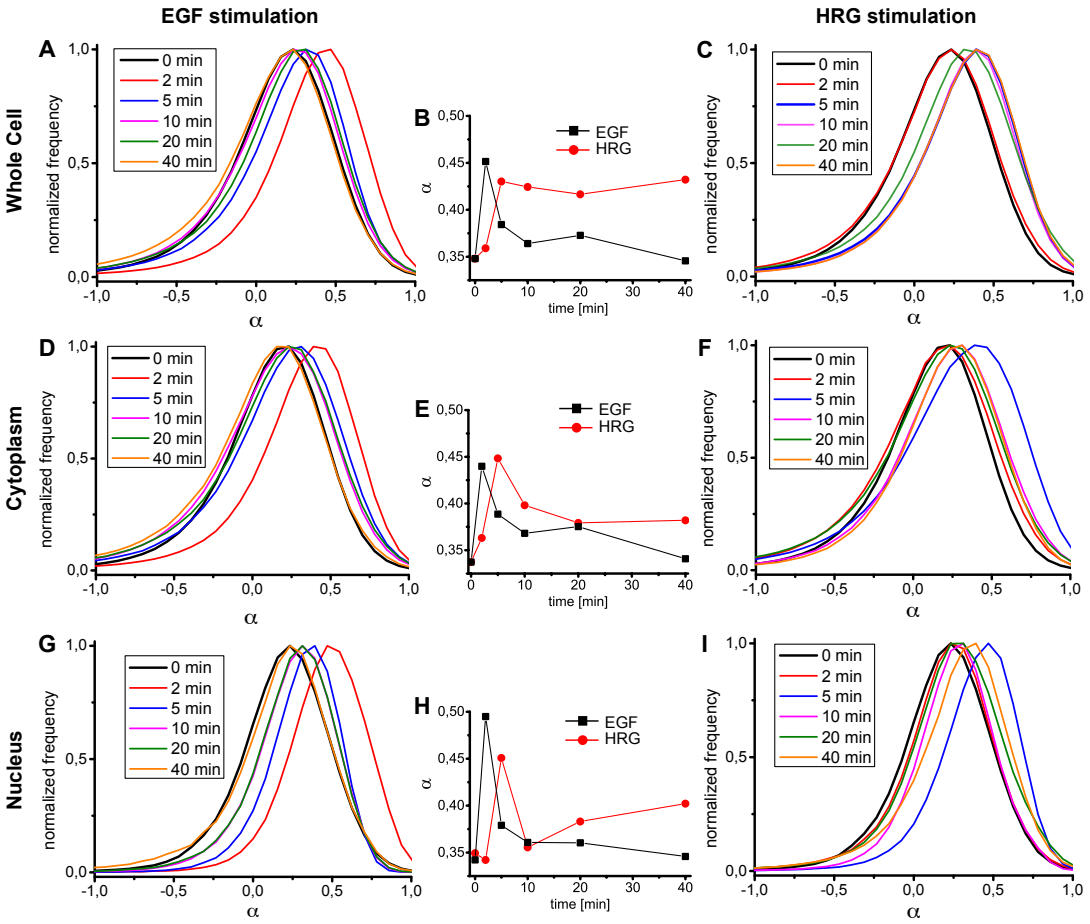

Figure 5.4: **EGF-induced ERK2 activity is transient, while HRG-induced ERK activity is sustained in the cytoplasm.** Quantification of mCitrine-ERK2 phosphorylation in the whole cell (top row) cytoplasm (middle row) or nucleus (bottom row) upon EGF versus HRG stimulation in MCF-7 cells with s.e.m. Images of the phosphorylated fraction α were segmented for the respective compartment. For each masked image, cumulative histograms of the distribution of α of cells stimulated with EGF (0 min n = 64, 2 min n = 20, 5 min n = 38, 10 min n = 42, 20 min n = 24, 40 min n = 24) (left column) or HRG (0 min n = 64, 2 min n = 43, 5 min n = 44, 10 min n = 40, 20 min n = 45, 40 min n = 27) (right column) were computed and normalized to the peak value. Middle column: To visualize the temporal profile of ERK activity in each compartment, the center of mass between 0 -1 was calculated for each histogram and plotted for each time point.

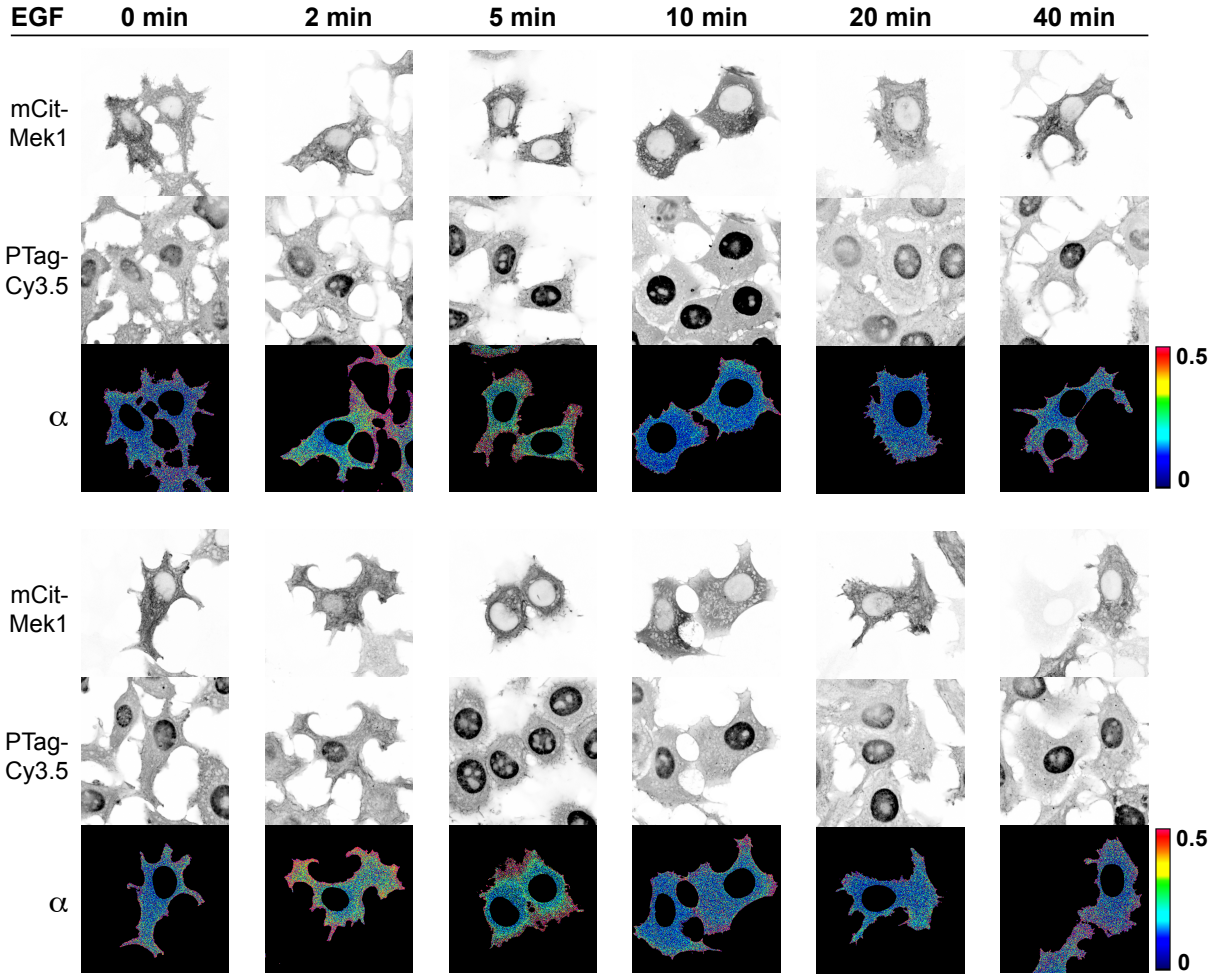

Figure 5.5: **EGF stimulation causes gradients of Mek1 activity in MCF-7 cells.** Representative images of EGF stimulation (100 ng/ml each) time course of MCF-7 cells transfected with mCitrine-Mek1 measured by PTag-FLIM. For each sample the intensity of mCitrine-Mek1, PTag-Cy3.5, the fraction of phosphorylated mCitrine-Mek1, α, with false-color look-up table are shown.

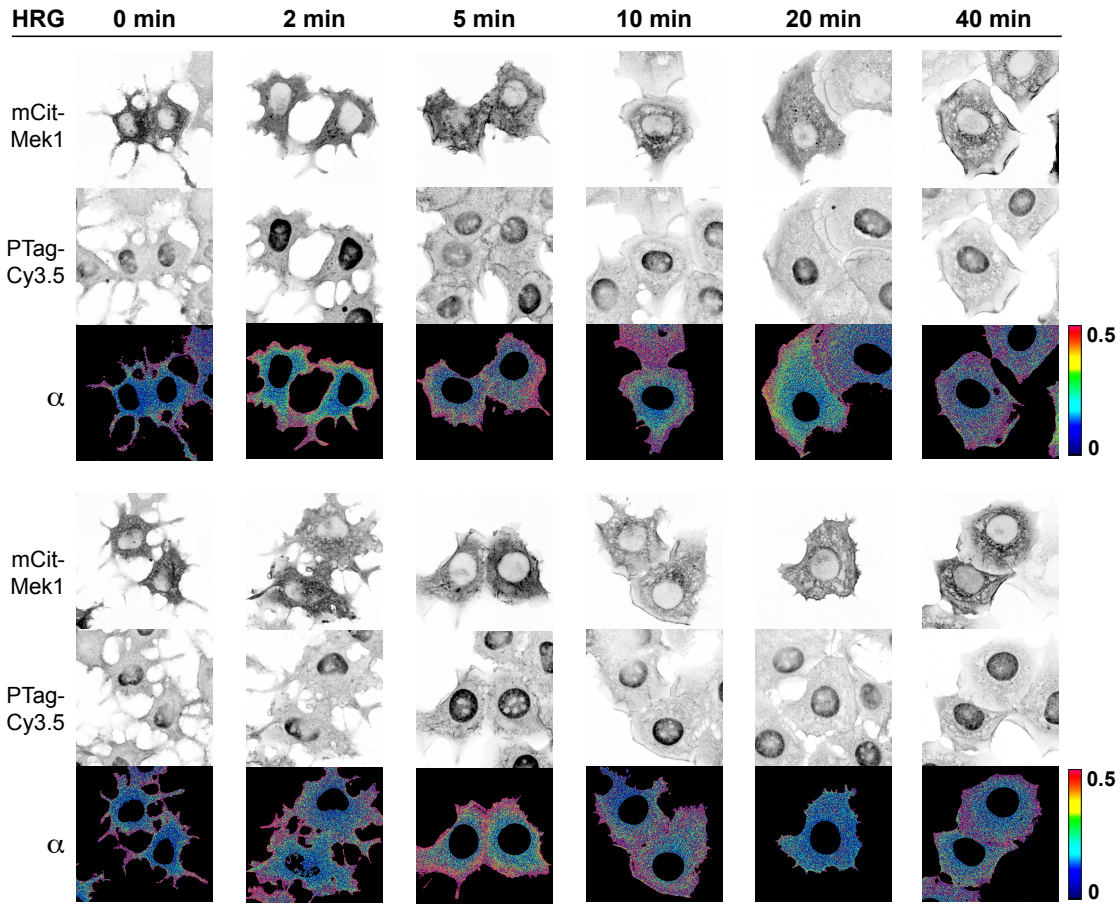

Figure 5.6: **HRG stimulation causes prolonged gradients of Mek1 activity in MCF-7 cells.** Representative images of HRG stimulation (100 ng/ml each) time course of MCF-7 cells transfected with mCitrine-Mek1 measured by PTag-FLIM. For each sample the intensity of mCitrine-Mek1, PTag-Cy3.5 and the fraction of phosphorylated mCitrine-Mek1, α, with false-color look-up table are shown.

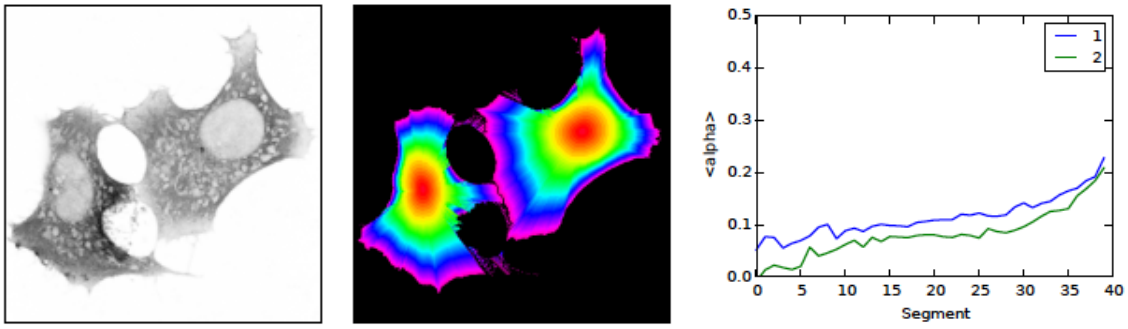

Figure 5.7: **Cell circularization and gradient quantification.** In order to quantify the cellular phospho-gradients, cells were computationally segmented into 10 circular sections in the nucleus and 30 sections in the cytoplasm. Shown is an example of 2 cells expressing mCitrine-Mek1 (left) with the circular segmentation mask (middle) and the obtained gradients (right).

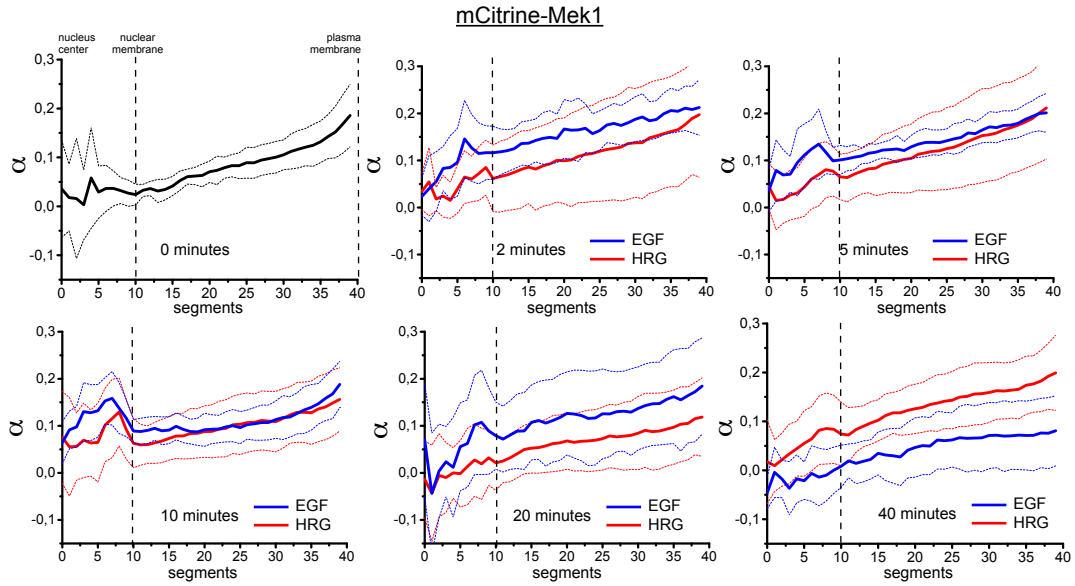

Figure 5.8: **Gradients of active mCitrine-Mek1 are steeper upon HRG than after EGF stimulation in MCF-7 cells.** To quantify the distribution of phosphorylated mCitrine-Mek1 in α maps, cells were circularized and segmented. 0 minutes n = 17 cells, 2 minutes EGF n = 13 cells, 5 minutes EGF n = 8 cells, 10 minutes EGF n = 12 cells, 20 minutes EGF n = 7 cells, 40 minutes EGF n = 6 cells. 2 minutes HRG n = 17 cells, 5 minutes HRG n = 25 cells, 10 minutes HRG n = 24 cells, 20 minutes HRG n = 20 cells, 40 minutes HRG n = 19 cells.

the Mek1 activity gradients throughout the time course, indicating that upon EGF stimulation ERK2 activation depends only on Mek1 and is not confined to the PM.

Round vesicles were visible in the mCitrine-ERK2 fluorescence image and the PTag-Cy3.5 channel. These might be endosomes which transport endocytosed receptors to the lysosome for degradation. In α maps these vesicles showed a subtly higher fraction of phosphorylated ERK2 than their environment. ERK2 might be either activated on these vesicles or ppERK2 which was activated at the PM is transported with the receptor and the remaining MAPK cascade to degradation.

HRG stimulation induced after 2 minutes a subtle elevation of the gradient's amplitude at the PM. Thereupon, HRG stimulation caused persistent cytoplasmic gradients of ppERK2, compared to EGF stimulation. Between 10-20 minutes of HRG stimulation the amplitude of the activity gradients was lower, but restrengthend after 40 minutes. The cytoplasmic ERK2 activity correlated with an increase in the nuclear ERK2 activity within 20-40 minutes. This result is consistent with the compartmental analysis for nuclear ERK activity which is shown shown in figure 5.4. Therefore, the late nuclear response might stem from ERK2 activated at the PM.

The quantification of ppERK2 distributions revealed that EGF caused mainly homogenous distributions of active ERK. Only after 2 minutes a gradual decrease can be observed. In contrast, HRG induced clear gradients of ppERK2 from the PM throughout the time course. The comparison of EGF and HRG induced ppERK distributions indicates that EGF causes default signaling through the cascade which results in the spatial extension and flattening of the ERK gradient. In contrast, HRG stimulation seems to restrain ERK2 activation to the PM, potentially by the recruitment of a scaffold.

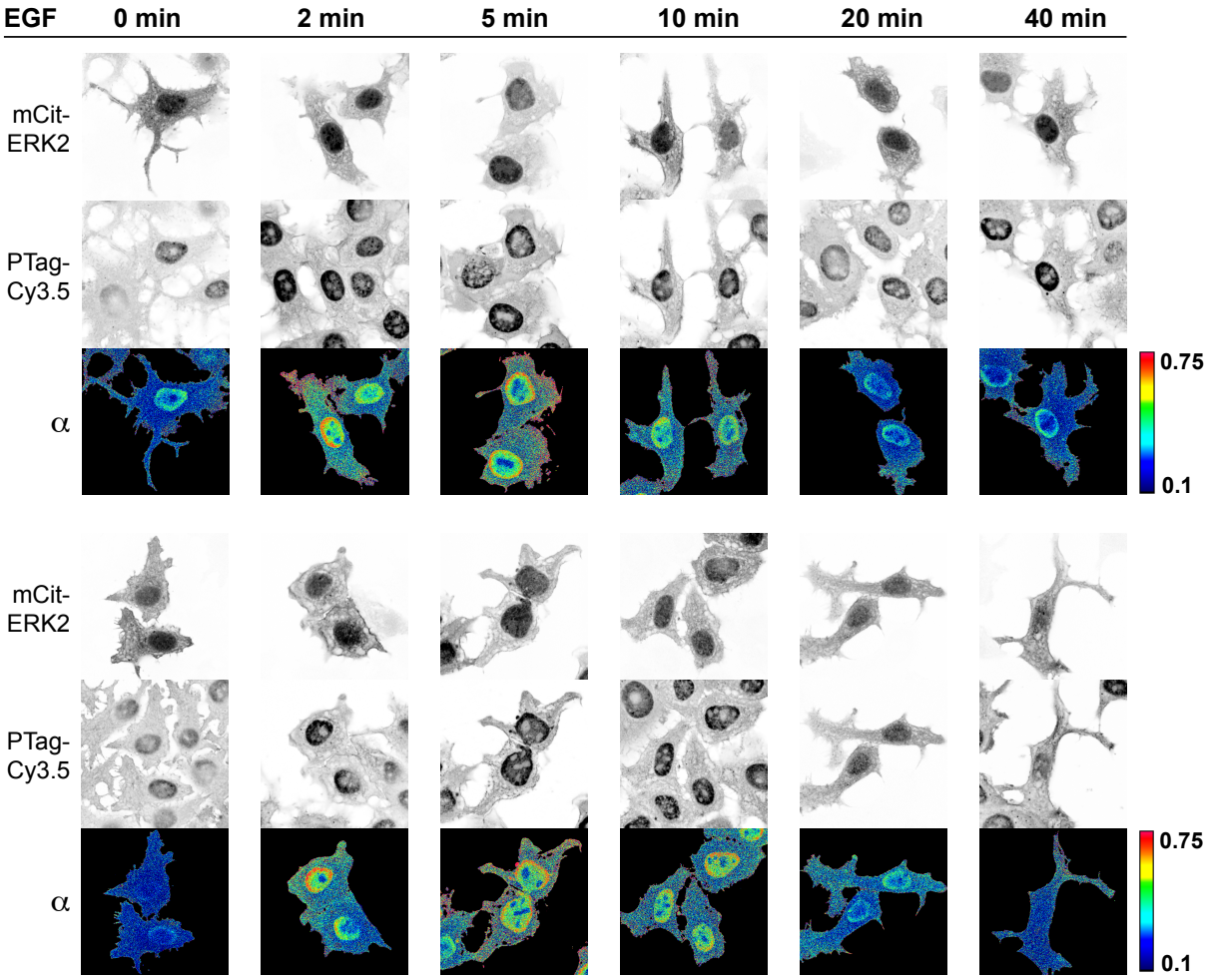

Figure 5.9: **ERK2 is transiently distributed in the cytoplasm of MCF-7 cells upon EGF stimulation.** Representative images of EGF stimulation (100 ng/ml each) time course of MCF-7 cells co-transfected with mCitrine-ERK2 and Mek1 measured by PTag-FLIM. For each sample the intensity of mCitrine-ERK, PTag-Cy3.5 and the fraction of phosphorylated mCitrine-ERK2, α, with false-color look-up table are shown.

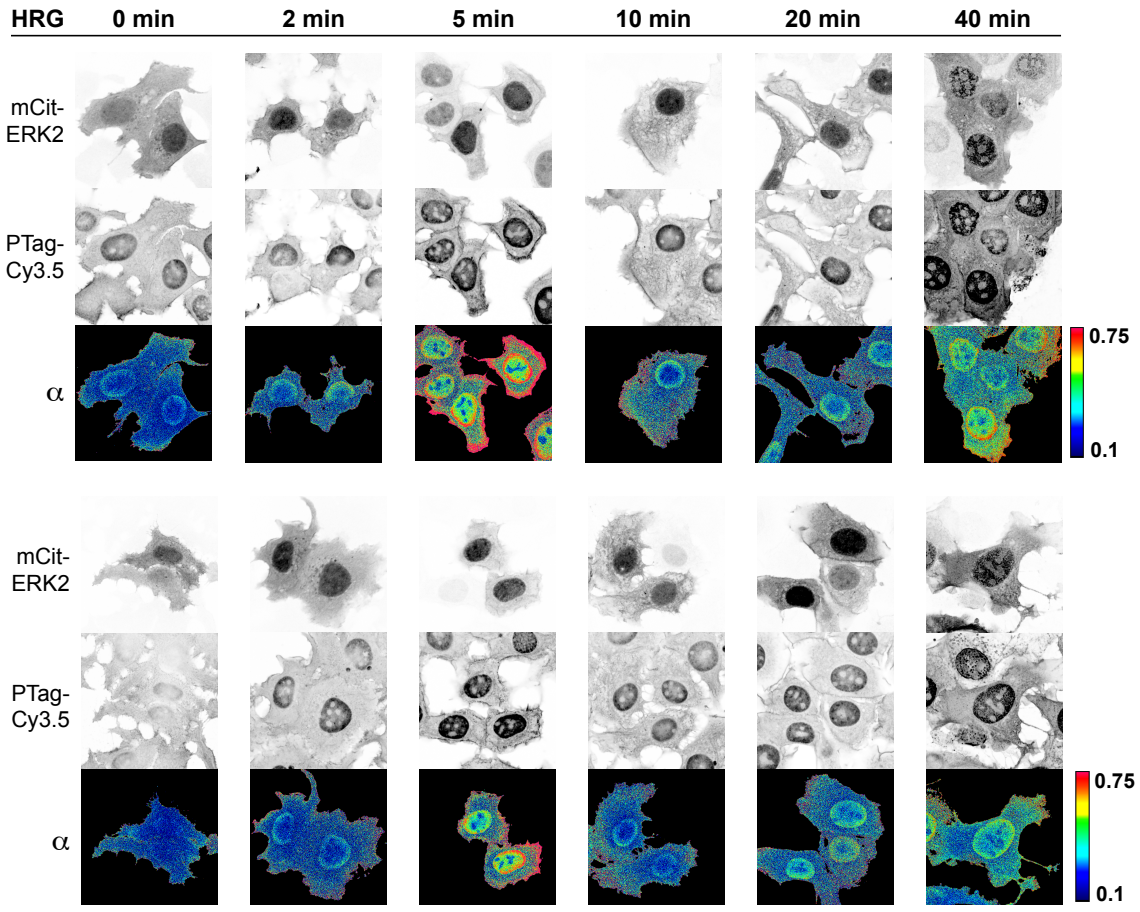

Figure 5.10: **HRG stimulation causes persistent and PM-confined ERK2 activity.** Representative images of stimulation (100 ng/ml each) time course of MCF-7 cells co-transfected with mCitrine-ERK2 and Mek1 measured by PTag-FLIM. For each sample the intensity of mCitrine-ERK, PTag-Cy3.5 and the fraction of phosphorylated mCitrine-ERK2, α, with false-color look-up table are shown.

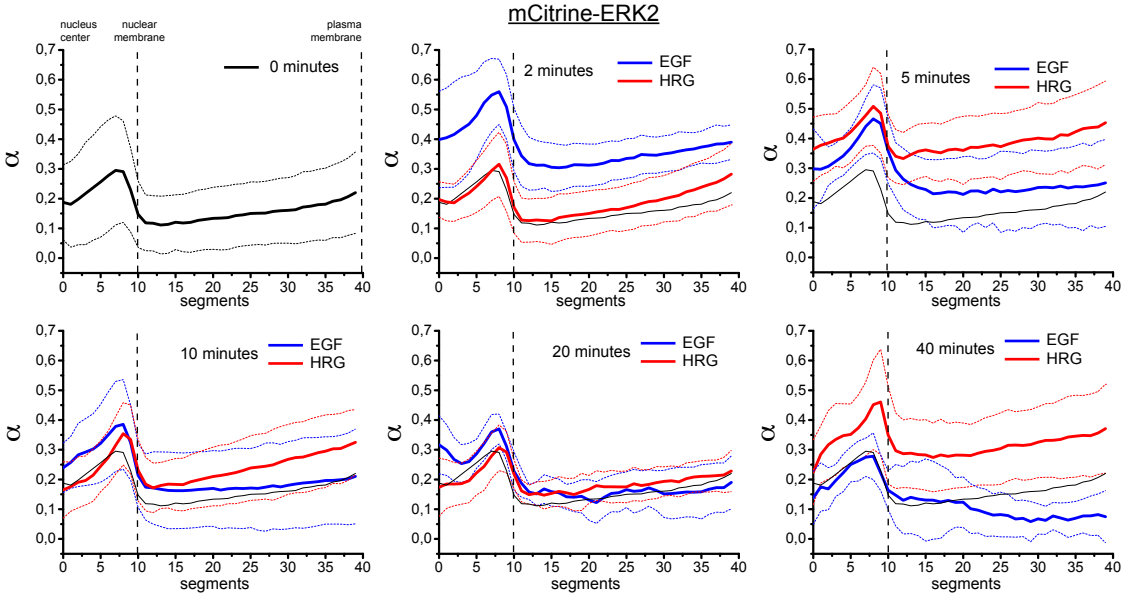

Figure 5.11: **Gradients of active mCitrine-ERK2 are steeper upon HRG than after EGF stimulation in MCF-7 cells.** To quantify the distribution of phosphorylated mCitrine-ERK2 in α maps, cells were circularized and segmented. 0 minutes n = 30 cells, 2 minutes EGF n = 14 cells, 5 minutes EGF n = 27 cells, 10 minutes EGF n = 22 cells, 20 minutes EGF n = 18 cells, 40 minutes EGF n = 16 cells. 2 minutes HRG n = 25 cells, 5 minutes HRG n = 21 cells, 10 minutes HRG n = 26 cells, 20 minutes HRG n = 25 cells, 40 minutes HRG n = 16 cells.

5.3 Influence of KSR1 on spatio-temporal Mek1 and ERK2 response

In the first part of this chapter we investigated the differences in the spatio-temporal Mek1 and ERK2 response caused be the growth factors EGF and HRG. In consistence with literature we found that EGF causes a transient and HRG induces a sustained cytoplasmic response of Mek1 and ERK2 [Nakakuki et al., 2010]. We also observed that the HRG induced response is susceptible to changes in the MAPK network stoichiometry, in contrast to the EGF response. Furthermore, in relation to Mek1 activity, the HRG induced ERK2 response was weaker than upon EGF stimulation. This suggests that a regulatory interactor, which is sensitive to changes in the MAP kinase concentration, influences the signal transduction from Mek1 to ERK2. HRG induced pronounced and persistent phospho-gradients from the PM of Mek1 and ERK2, while EGF caused shallow distributions of phosphorylated Mek1 and ERK2. Therefore, HRG stimulation seems to recruit a factor which promotes signaling at the PM and adapts the ERK2 response to the Mek1 dose. These differences in the MAPK response profile point at the involvement of KSR1 in the HRG response. KSR1 is a MAPK scaffold which is recruited to the PM upon GF stimulation and promotes local signaling through the MAPK cascade.

5.3.1 Influence of KSR1 on the temporal response profile of Mek and ERK

To investigate if KSR1 affects the EGF induced response in MCF-7 cells, KSR1 was ectopically expressed as ECFP fusion. In order to quantify the KSR1-dependent change in the Mek1 and ERK2 activity profiles, lysates of cells expressing elevated KSR were loaded with lysates from WT cells on one gel. ECFP-KSR1 was overexpressed to about 80-fold of the endogenous KSR1

level that furthermore induced the expression of endogenous KSR1 (see figure 5.12). The overexpression of ECFP-KSR1 caused a 25-fold stronger activation of Mek1 in starved cells. Probably due to the strong Mek1 preactivation, the EGF induced increase in Mek1 activity was weaker than in WT cells. KSR1 overexpression led furthermore to the appearance of a double ppMek1 band. The used antibody detects double as well as single phosphorylation on the Mek1 activation sites Ser217 and Ser221. The additional band might therefore be assigned to singly phosphorylated Mek1. The strong Mek activation and the double phospho-band show that KSR1 itself, or in interplay with Raf, strongly supports the phosphorylation of Mek1. In contrast, ERK2 was less strongly activated by EGF. Therefore, although Mek1 was strongly1 activated by the ectopic expression of KSR1, active Mek1 was impaired to activate ERK2. Strong overexpression of KSR was shown before to inhibit the activation of ERK2 due to an effect termed 'combinatorial inhibition' [Lin et al., 2009, Levchenko et al., 2000]. A high amount of KSR1 out-titrates the interaction between Mek1 and ERK2 due to sequestration of Mek1.

The ectopic overexpression of ECFP-KSR1 caused furthermore a delay of the early response of Mek1 and ERK1/2 from 2 to 5 minutes upon EGF stimulation. The response profile and the ratiometric comparison of KSR overexpression to WT show that Mek1 and ERK1/2 activity decreased slower and maintained a residual activity after 40 minutes of EGF stimulation. KSR1 might therefore indeed alter the temporal response profile of Mek1 and ERK2.

In order to prevent the combinatorial inhibition by strong ECFP-KSR1 expression, the expression level was lowered to the range of the endogenous proteins.

The expression of ECFP-KSR1 to 1.3-fold of the endogenous KSR1 level caused an elevated amplitude of the transient EGF response of Mek1 and ERK2 to about 2-fold. As expected, a subtle elevation of the KSR1 level promotes signaling through the MAPK cascade, in contrast to strong KSR1 overexpression. The profile peaks were delayed from 2 to 5 minutes, which can be attributed to the elevation of the response. The transient trend of the EGF response profiles was however unchanged by the ectopic expression of KSR1.

The HRG stimulation profile of Mek1 and ERK2 in MCF-7 cells was increased between 10-40 minutes by ectopic expression of ECFP-KSR1 (2-fold) (figure 5.14). In contrast to the EGF response profile, KSR1 strengthened the sustained response of Mek1 and ERK1/2 about 2-fold. KSR1 seems to amplify the Mek1 and ERK1/2 response without altering the trend of the response, consistent with an observation in T cells [Lin et al., 2009]. Additionally, the Mek1 and ERK1/2 phosphorylation peaks were delayed from 5 to 10 minutes upon HRG stimulation.

5.3.2 Influence of KSR1 on the spatial profile of Mek1 and ERK2

Using PTag-FLIM the influence of ectopic ECFP-KSR1 expression on the spatial distribution of ppMek1 and ppERK2 upon EGF stimulation was investigated.

mCitrine-Mek1 phosphorylation was elevated in cells with strong pECFP-KSR1 expression after EGF treatment (figure 5.15). Furthermore, phosphorylated Mek1 seemed to be homogeneously distributed throughout the cell in contrast to a clear phosphorylation gradient of Mek1 in WT cells as shown in figure 5.5. The quantification of Mek1 distribution shows that ECFP-KSR1 indeed distributed pMek1 in the cytoplasm, independently of EGF stimulation, as shown in figure 5.16. The obtained pMek1 maps may also represent the singly phosphorylated Mek1, due to Phos-Tag being unselective for different phosphorylated residues.

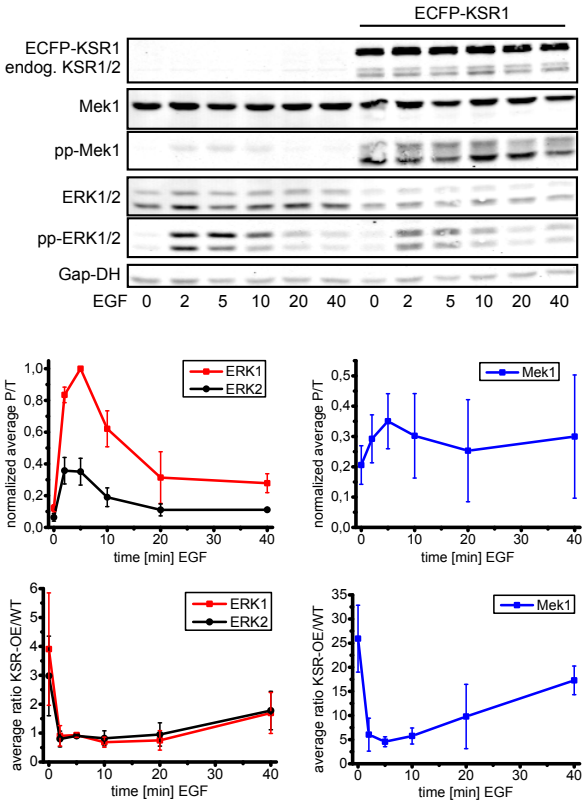

Figure 5.12: **Overexpression of ECFP-KSR1 elevates the late Mek1 and ERK2 response upon EGF stimulation in MCF-7 cells.** (Top) Representative Western Blot against total and activating phospho-sites of Mek1 and ERK1/2 in MCF-7 cells with or without ECFP-KSR1 overexpression (KSR1-OE) (n = 2). After starvation cell were stimulated with 100 ng/ml EGF for the indicated time points. (Middle) Quantification of the average normalized ratios of phosphorylated to total (P/T) ERK1/2 and Mek1 (n = 2). (D, E and I, J) Quantification of the average ratios of ERK1/2 and Mek1 between cells with or without KSR1 overexpression.

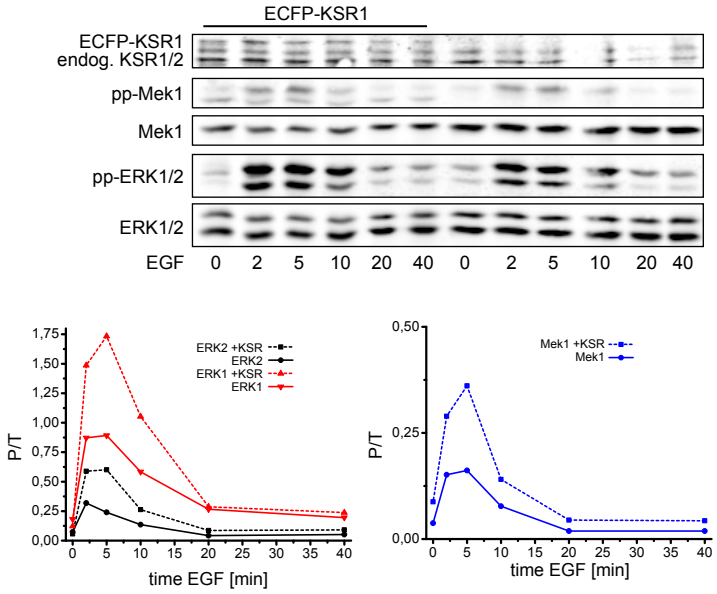

Figure 5.13: **KSR1 knockdown reduces Mek and ERK response, while a high level of KSR1 strongly increases the basal level of Mek and ERK activity and delays their early peak upon EGF stimulation in MCF-7 cells.** (A and F) Representative Western Blot against total and activating phospho-sites of Mek1 and ERK1/2 of MCF-7 cells exhibiting reduced (A), (n = 2), or elevated (F), (n = 2), levels of KSR1, stimulated with 100 ng/ml EGF or for the indicated time points. (B, C and G, H) Quantification of the average normalized ratios of phosphorylated to total ERK1/2 and Mek1 (n = 2) of KSR-KD (B, C) or KSR-OE (G, H) cells. (D, E and I, J) Quantification of the average ratios of ERK1/2 and Mek1 in modified KSR amount expressing cells to endogenous levels of KSR1 expressing cells.

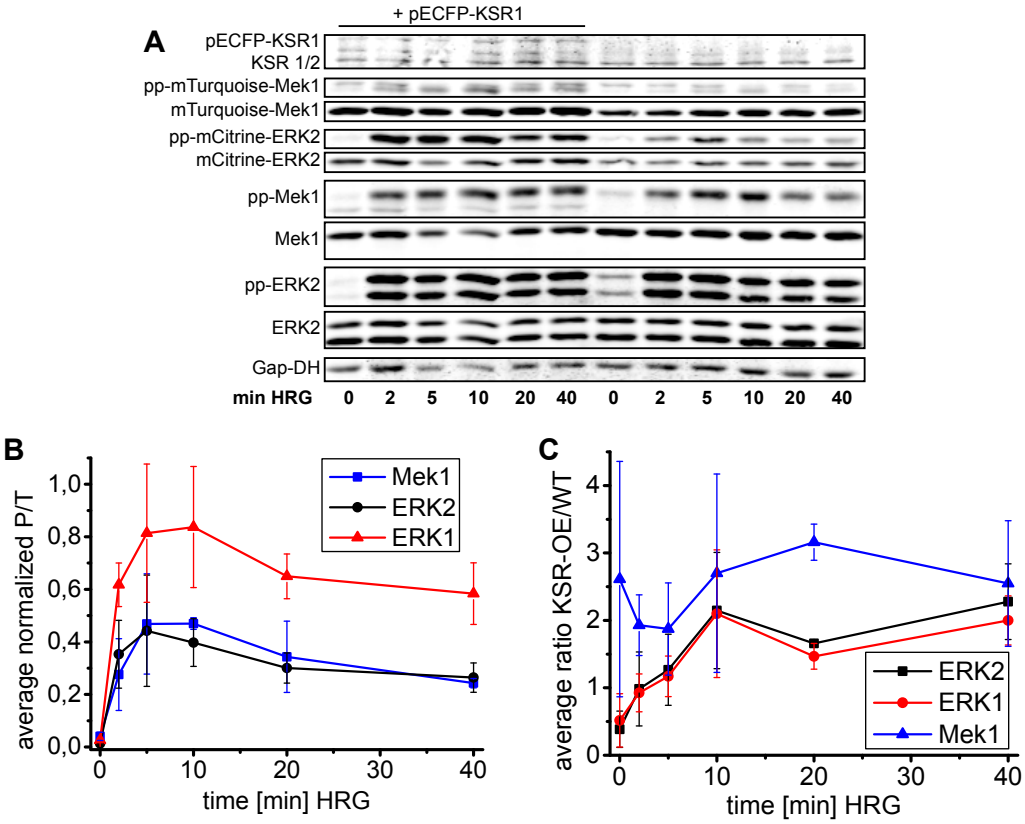

Figure 5.14: **KSR1 overexpression increases Mek and ERK response particularly at late time points of HRG stimulation.** (A) Representative Western Blot against total and activating phospho-sites of Mek1 and ERK1/2 of MCF-7 cells with or without overexpression of KSR1, stimulated with 100 ng/ml HRG for the indicated time points. (B) Quantification of the average normalized ratios of phosphorylated to total ERK1/2 and Mek1 (n = 2) of KSR-OE cells. (C) Quantification of the average ratios of ERK1/2 and Mek1 phosphorylation of KSR-OE to endogenous levels of KSR1 expressing cells .

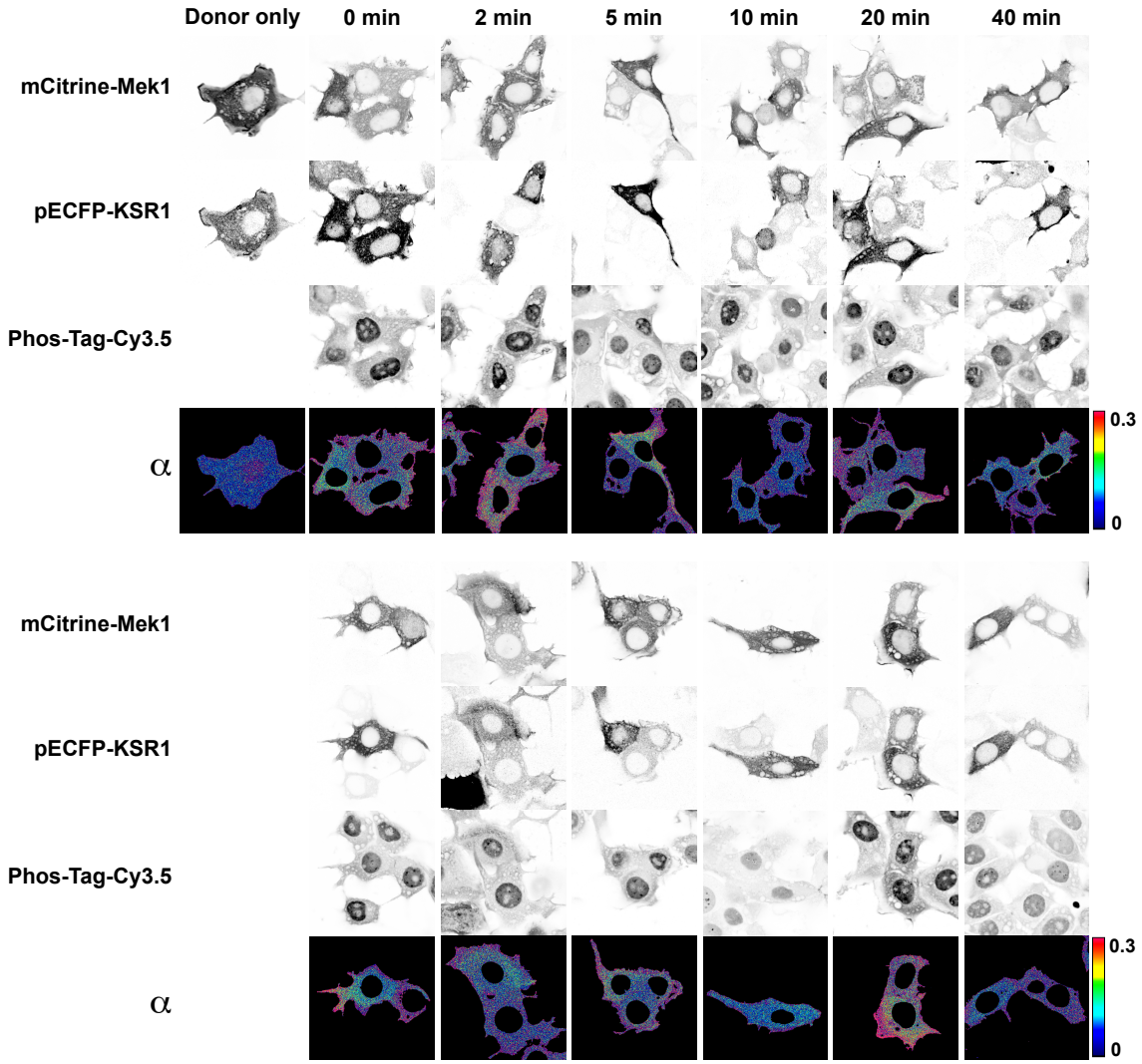

Figure 5.15: **ECFP-KSR1 expression promotes Mek1 phosphorylation and distributes phosphorylated Mek1.** Representative images of EGF stimulation (100 ng/ml each) time course of MCF-7 cells co-transfected with pECFP-KSR1 and mCitrine-Mek1. For each sample the intensity of mCitrine-Mek1, pECFP-KSR1, PTag-Cy3.5 and the fraction of phosphorylated mCitrine-ERK2, α, with false-color look-up table are shown.

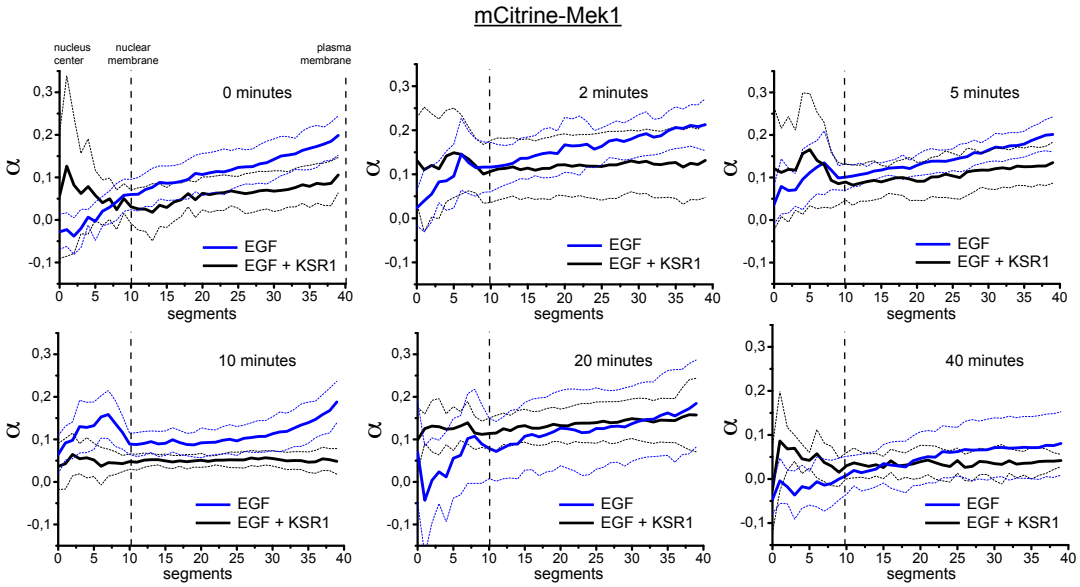

Figure 5.16: **KSR1 distributes phosphorylated Mek1.** To quantify the distribution of phosphorylated mCitrine-ERK2 in presence of ECFP-KSR1 in α maps, cells were circularized and segmented. 0 min n = 18, 2 min n = 18, 5 min n = 19, 10 min n = 14, 20 min n = 12, 40 min n = 16.

MCF-7 cells co-expressing pECFP-KSR1 and mCitrine-ERK2 revealed a reduced phosphorylation of mCitrine-ERK2 in cells with high ECFP-KSR1 amount. Furthermore, pERK2 seemed to be strongly confined to the PM in presence of ECFP-KSR1. Accordingly, nuclear mCitrine-ERK2 was less pronounced.

The quantification of ERK2 gradients showed that ERK2 is much less phosphorylated in cells with ECFP-KSR1. The concentration of KSR1 was therefore in the region of combinatorial inhibition. Therefore, KSR1 promotes Mek1 activation but inhibits the signal transduction to ERK2 by sequestering a major fraction of active Mek1. However, the gradients of active ERK2 were steeper if KSR1 was present, pointing at constrained activation of ERK2 at the PM. Regarding the KSR1 - ERK2 interaction it is known that only active ERK2 can bind to KSR1 via the DEF domain. This interaction is required to exhibit the negative feedback phosphorylation on KSR1, which forces the dissociation from Raf. A direct positive effect of KSR1 on ERK2 activation by Mek is not known.

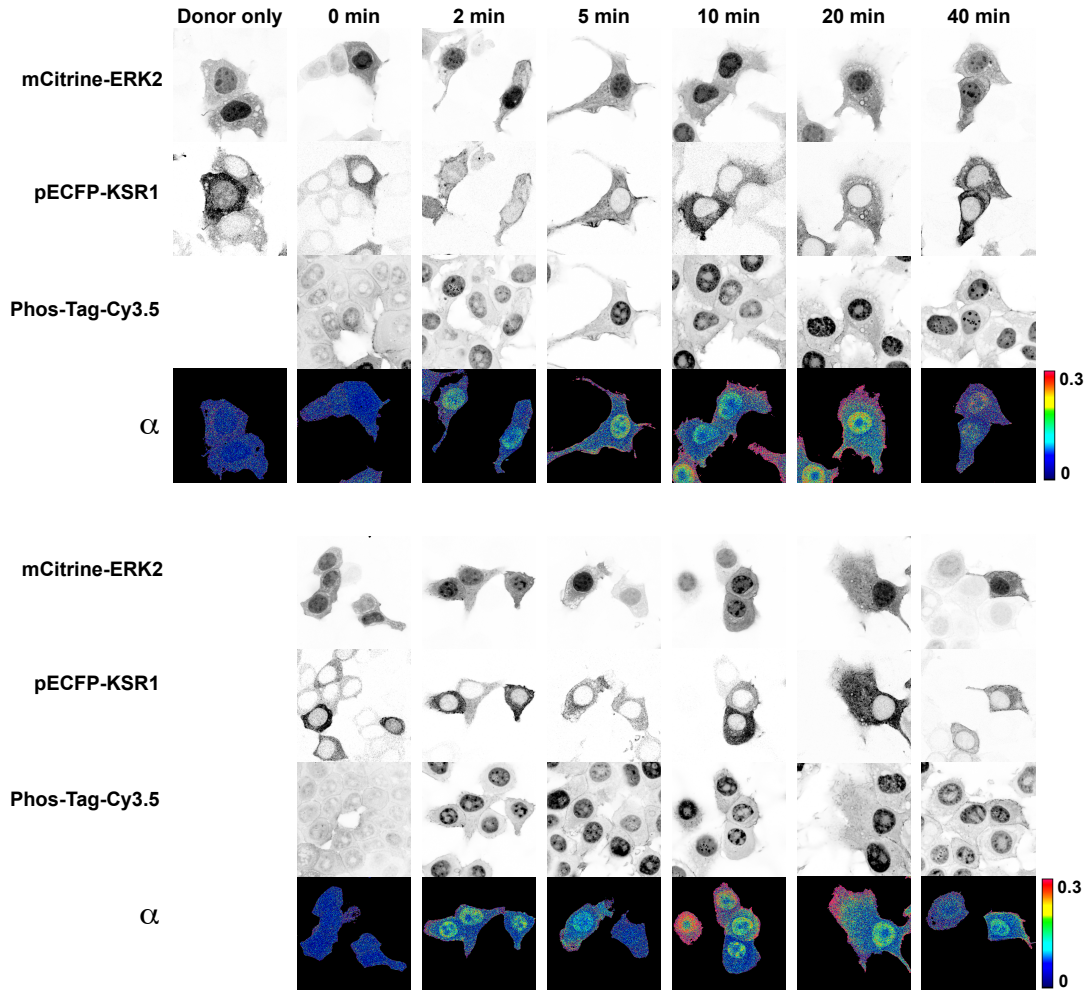

Figure 5.17: **KSR1 overexpression reduces ERK2 activity and constrains active ERK2.** Representative images of EGF stimulation (100 ng/ml) time course of MCF-7 cells co-transfected with pECFP-KSR1 and mCitrine-ERK2. For each sample the intensity of mCitrine-ERK2, pECFP-KSR1, PTag-Cy3.5 and the fraction of phosphorylated mCitrine-ERK2, α, with false-color look-up table are shown.

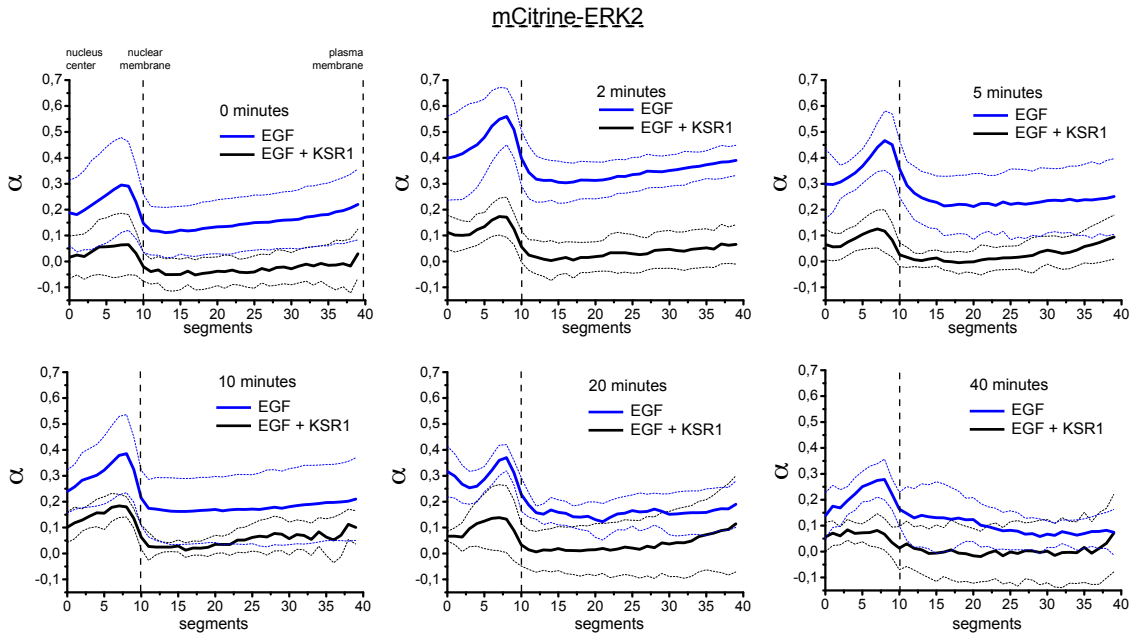

Figure 5.18: **KSR1 constrains phosphorylated ERK2 to PM-proximal regions.** To quantify the distribution of phosphorylated mCitrine-ERK2 in α maps, cells were circularized and segmented. 0 minutes n = 27 cells, 2 minutes EGF n = 9 cells, 5 minutes EGF n = 16 cells, 10 minutes EGF n = 17 cells, 20 minutes EGF n = 5 cells, 40 minutes EGF n = 11 cells.

6 Discussion

Signaling of MAPK modules determines cellular fate such as growth, differentiation or apoptosis. To respond appropriately to a stimulus, the MAPK activity is regulated in time and space by the context of the signaling network architecture. While the temporal MAPK response has been widely studied, a lack of quantitative imaging approaches made the investigation of spatial activity profiles impossible. Here, a versatile approach for the quantitative spatial profiling of MAPK activity was established, which allowed to study basic principles as well as specific aspects of MAPK activity organization in human cells as well as yeast.

6.1 PTag-Dye complex as activity sensor for MAPKs in FRET-FLIM

Common to all MAPKKs and MAPKs, like Mek1 and ERK2, is the activation by dual phosphorylation in their activation loop. These phosphorylation sites are a threonine and tyrosine of a conserved TXY motif in MAPKs and two serines in MAPKKs. In order to design a generic sensor for MAPK activity, an approach was required which detects protein phosphorylation irrespective of the kind of amino acid and maintains specificity towards the kinase of interest. These demands were fulfilled in PTag FLIM, which combines the universality of the phospho-binding reagent PTag with the specificity of donor fluorophore-based FRET by measuring the molecular proximity between the donor fluorophore fused kinase and the dye-coupled PTag. Single phosphorylation sites on the protein of interest cannot be distinguished from each other with PTag-FLIM. Although MAPKs have further phosphorylation sites than the activating ones, the major contribution on the detected decrease in the donor lifetime by PTag-FLIM comes from the activating phospho-sites. This was confirmed by mutating the respective sites in mCitrine-ERK2 and the reconstituted temporal activity profile of mCitrine-Mek1 and -ERK2. Therefore, the application of PTag-FLIM is under the applied, distinctive conditions a measure of the kinase activity. As a byproduct, PTag-FLIM is the first approach which can detect the overall phosphorylation of a specific protein of interest in a protein mixture. It can be applied to study the spatial distribution of any protein in its phosphorylated state.

PTag-FLIM resolved subcellular spatial activity gradients of Mek, ERK2, and the yeast pheromone MAPK module, demonstrating its versatility and a superior dynamic range over previously available imaging approaches. Individual activity sensors were beforehand only available for ERK. However, these ERK activity sensors (chapter 1.4.4) suffered from being indirect measures of ERK activity, did not provide sufficient signal-to-noise or required the modification with subcellular localization sequences. Immunostainings of active MAPKs do not show gradients because these deliver information on the total concentration of the active protein (active fraction times intensity). Only the fractional activity map can provide the locations of activation and deactivation of the observed protein.

A drawback of PTag-FLIM is the requirement of fixated and permeabilized cells. The fixation of cells impairs the observation of single cells throughout a time course and therefore the correlation between initial and subsequent states. Although it is technically possible to bring PTag-Dye into the cells, for instance by microinjection, the binding of PTag to all accessible phosphate-monoesters comprising phosphorylated proteins, ATP and 5'-ends of DNA and RNA would inhibit all phosphorylation dependent processes and presumably cause cell death.

6.2 Fus3 activity gradients in the yeast pheromone response

As many Fus3 targets are localized to the nucleus (e.g. transcription factor Ste12) it remains arguable how the fully active Fus3 reaches these substrates despite the phosphatases which restrain active Fus3 to PM-proximal areas. On the one hand the functions of active Fus3 relocate in the course of the pheromone response, on the other hand the spatial distribution of active Fus3 changes. The distance between tip and nucleus increases during growth of the mating projection. Early after pathway activation and symmetry breaking, the gradient of active Fus3 might extend enough to let a fraction of fully active Fus3 attain the nucleus and start mating specific transcription. This early transcriptional response induced by Fus3 might be the starting point for further delayed transcriptional responses which are independent of Fus3 activity. Further functions of Fus3 like cell cycle arrest via Far and polarization of the cytoskeleton via Bni1 and Bem1 are localized to the cytoplasm. Therefore, in late time points of the mating response, Fus3 activity might only be required in the shmoo region and no mechanism would be necessary to overcome the confinement of Fus3 activity. The conditions under which the Fus3 activity gradient forms change during the pheromone response. Additionally to diffusion and deactivation rate, an activity gradient is dependent on the cell's shape. The geometry of the cell determines the ratio of surface-to-volume and thereby the ratio of activation to deactivation. The surface of activation at the yeast mating tip can be assumed to be constant, while the volume changes during the growth of the mating projection. Early after polarization, the yeast morphology is still roundish with a small projection which could be mathematically approximated by a cone with a big radius and small height. In later time points the cone's radius decreases while the height increases. The ratio of surface-to-volume increases and accordingly does the rate of activation become stronger relative to deactivation. Therefore, the gradient might be more restrained in the beginning of polarized growth. However, phosphatase expression increases during the pheromone response which counteracts this geometrical effect.

The nuclear position could be adjusted by the steepness of the gradient or the total ppFus3 concentration. But the relative yeast cell proportions revealed from the intensity distributions in figures 4.2 and 4.3 are unaltered in each genetic background disregarding the differences in the Fus3 phosphorylation gradient. The ppFus3 gradient seemingly does not affect the position of the nucleus, as previously described [Maeder et al., 2007].

6.2.1 Interplay of network topology, Fus3 activity range and shmoo morphology

Using PTag-FLIM, the influence of a MAPK network architecture on the activity distribution of an embedded MAPK was examined for the first time. It was found that the inhibition of a negative feedback from Fus3 on Ste11 increases the extent of the Fus3 activity gradient. This broader range of Fus3 activity correlates with broader shmoo tips and an increase in the number of shmoo tips.

Computations on the dependence of the MAPK activity distribution on the network architecture are confirmed by results showing that the inhibition of the negative feedback from Fus3 on Ste11 causes a higher amplitude, at least for the double mutant Ste11-S243A,T596I, and shallower gradients. However, the determined differences in the gradient upon feedback inhibition are not as pronounced as expected from the simulations (see figure 1.3.3.3) [Sun et al., 2014]. The gradient simulations are based on a sequential activation of a three-step cascade in which only the activation of the MAPKKK is restricted to the PM. The MAPK being third in the hierarchy therefore builds a tertiary activity gradient. In yeast though, Fus3 activation depends on the MAPKK Ste7 *and* the PM-bound scaffold Ste5. Fus3 therefore builds a primary gradient so that the inhibition of the negative feedback allows only for a subtle extension of the Fus3 activity gradient.

In Ste11-Ser243Ala expressing cells, Fus3 is at the shmoo tip equally phosphorylated as in WT cells, demonstrating that the mutation Ser243Ala is not interfering with Ste11 activity. How can a negative feedback from MAPK to MAPKKK which does not affect the activity of the target cause a different spatial distribution of the active MAPK? The phosphorylation of Ste11-Ser243 inhibits the association with Ste5, so that the mutation Ser243Ala allows an unregulated interaction between Ste11 and Ste5 [Hecker et al., 2014]. The dependencies in the interplay of network topology, Fus3 activity range and shmoo morphology are discussed: The negative regulation of the Ste11-Ste5 complex by Fus3 phosphorylation in vegetatively growing cells decreases the sensitivity and maintains the switch-like response of the pheromone pathway [Hecker et al., 2014]. Fus3 also down-regulates the Ste5 PM recruitment, further elevating the threshold of activation [Yu et al., 2008]. Like the Ste11-Ste5 interaction, the Ste5 PM association and Ste5-Fus3 dissociation upon pheromone stimulation are required to maintain the switch-like mating decision [Malleshaiah et al., 2010]. It can be deduced that in the yeast pheromone pathway, ultrasensitivity is generated at the level of the MAPKKK and is not an inherent property of the sequential activation in the cascade, as for MAPK signaling in the maturation of *Xenopus* oocytes (see also chapter 1.3.3.1) [Huang & Ferrell, 1996]. Cooperative events of Ste5-Fus3 dissociation, Ste5-Ste11 association and Ste5-PM binding might cause the activation of the MAPK cascade in an all-or-none manner and further propagate the symmetry break from the PM to the MAPK cascade. A switch-like Ste11 recruitment to the PM would deplete a major amount of Ste11 from the cytoplasm, preventing the activation of Ste11 at multiple polarization clusters. The choice of a polarization cluster would be made after a "first come, first serve" strategy.

The lower threshold of activation in Ste11-S243A cells may cause a broadened distribution of Ste5 and Ste11 activation around the polarization core at the PM which results in the extension of the Fus3 activity gradient. Additionally, active Ste11 can diffuse in complex with Ste5 from the site of action without being regulated by Fus3. The diffusion further enables delocalized signaling to Ste7 and in turn to Fus3. Inhibiting the phosphorylation on Ste11-Ser243 may lead to a broadened area of active Ste11 which is transduced in a less focussed Fus3 activity.

The mutant Ste11-T596I was known before to be constitutively active [Stevenson et al., 1992]. The combination of mutation Ser243Ala with Thr596Ile renders Ste11 independent of any activating signal and enables the unspecific interaction with Ste5. This Ste11 mutant can therefore signal to each of the three MAPK pathways in which it participates.

The causal link between Fus3 and the polarization of the actin cytoskeleton is largely known [Matheos et al., 2004, Yu et al., 2008]. Interestingly, Fus3 activity controls the polarized localization of the actin scaffold Bni1, small GTPase Cdc42 and PAK Ste20 [Matheos et al., 2004, Yu et al., 2008]. The distribution of active Fus3 presumably defines a spatial probability distribution of growth. The broadened Fus3 activity causes outspread growth at the mating projection. Accordingly, the distribution of active Fus3 also orients the mating projection within the pheromone field. The three-dimensional Fus3 activity gradient would therefore serve as a cytoplasmic morphogen.

Apart from the theory that the increased range of active Fus3 in the Ste11 mutant strains stems from a delocalized, active Ste11, also an influence of the cell's geometry on the gradient can be considered. Let's assume that an unknown process which is associated with Ste11-Ser243 but independent of Fus3, causes the morphological defects, e.g. broader mating projections. The extension of the Fus3 activity gradient in Ste11-S243A cells might either be caused by an elevated total Fus3 level which saturates the phosphatase, or by a decreased phosphatase concentration. As revealed from the intensity profile in 4.2 and 4.3 total Fus3 levels stay constant. However, if the shmoo morphology of Ste11 mutant expressing cells is broader, the surface-to-volume ratio decreases in the tip region. Assuming that the expression rate of activating and deactivating proteins is unaffected by the Ste11 mutations, the phosphatase in the cytosol would become stronger diluted than the signaling molecules at the membrane of

the shmoo tip. So, the increase in ppFus3 activity range might be due to a dilution of the phosphatase in Ste11-S243A cells caused by the broader shmoos and a lower surface-to-volume ratio.

The broadened mating projection in Ste11 mutant expressing cells correlates with an extended and shallower ppFus3 gradient. The question what was first, the chicken or the egg or their causal dependence, respectively, could not be answered by the experiments presented. The general advantage of a pointed polarization might lie in the oeconomic viability. The broader the tip and bigger the volume of the cell, the more energy is required to synthesize the new cell wall and to maintain the cellular homeostasis, amongst others. If the growing mating tip is sharply polarized, it needs to be well oriented in the pheromone field to meet precisely the mating tip of the chosen mating partner. A broader projection can be less well oriented and still attain the opposite cell. However, further experiments of [Hecker et al., 2014] revealed that Ste11-SM and -DM cells frequently lyse during shmoo growth, supporting the theory that a broad shmoo is not favorable.

When Kss1 is deleted, effects of the Ste11 mutants on the gradient become even stronger, while the deletion of Kss1 alone is not sufficient to cause broader polarization tips. The stronger differences between the ppFus3 gradient in cells without Kss1 could simply be due to the higher phosphorylation amplitude. Fus3 and Kss1 are the only substrates of MAPKK Ste7. Their competition for Ste7 could increase the rate of Fus3 phosphorylation if Kss1 is deleted. An elevated amount of phosphorylated Fus3 could enhance the effects of the Ste11 mutations on the cell morphology.

Using PTag-FLIM, the first data on a three-step activation cascade was ascertained. Under overexpressing conditions, the kinases Ste7 and Ste11 as well as the scaffold Ste5 did show gradients of phosphorylation, emanating from the projection tip. This shows that Ste5 is also phosphorylated in late time points of the pheromone response. It is however unclear which phosphosites on Ste5 contribute to the steep gradient. A phosphorylation gradient point towards a regulation of Ste5 interactions at the PM.

Given that the respective phosphatases are in natural conditions working at or close to saturating level, the overexpression of the Ste-proteins might lead to an extension of the gradients towards the distal end of the cell. So, the endogenously expressed Ste7, Ste11 and Ste5 might in reality be sharply localized to the tip.

6.3 Spatio-temporal regulation of Mek1 and ERK2 in MCF-7 cells

6.3.1 Mek1 and ERK2 activity gradients

Using PTag-FLIM it was shown that the sequential design of the MAPK module indeed implicates extended MAPK activity gradients in mammalian cells, which have been postulated 15 years ago [Brown & Kholodenko, 1999, Kholodenko, 2006].

The cytoplasmic gradients of MAPKs might be just a byproduct of the required spatial signal propagation from the PM to the nucleus. In this view, the ERK activity gradient acts as a threshold which has to be overcome [Kholodenko, 2006, Kholodenko, 2002]. However, ERK has various functions outside of the nucleus, represented by the fact that half of the about 160 targets of ERK are non-nuclear [Yoon & Seger, 2006]. Additionally to the functions in cell fate decisions, ERK has specialized cytoplasmic roles, like cytoskeletal rearrangements, synaptical plasticity in neurons or golgi fragmentation [Reszka et al., 1995, Shalin et al., 2006, Acharya et al., 1998]. To target the soluble ERK specifically to one of these locations, it has to be locally activated and/or restrained in its diffusion in order to impair the uncontrolled phosphorylation of targets in the cytoplasm or nucleus. Activity gradients are therefore not only a threshold which needs to be vanquished, gradients allow to modulate the activity range of ERK.

Surprisingly, active ERK2 was in the nucleus also distributed in a gradient which emanated from the nuclear membrane towards the nucleus' center. This was unexpected because ERK2 activating proteins are not localized to the nuclear membrane. A source of high ppERK2 concentration might be generated by the transport of active ERK2 through the nuclear membrane. The mechanism of nuclear import and transient nuclear accumulation of active ERK2 is highly controversial (see chapter 1.1.3). However, the kinetics of nuclear import seem to correlate with the rate of ERK2 phosphorylation [Caunt & McArdle, 2010, Lidke et al., 2010]. Therefore, ppERK2 import is favored over ERK2 import, while several nuclear phosphatases, like DUSPs 1, 2, 4 and 5, might serve as a sink for active ERK2 and thereby restrain ppERK2 spreading in the nucleus [Owens & Keyse, 2007]. The nuclear ppERK2 gradient being much steeper than the cytoplasmic gradient shows that the nuclear source location of ppERK2 is the nuclear membrane, while in the cytoplasm the source of the ppERK2 gradient is outspread from the PM by the sequential built-up of the MAPK cascade. The nuclear gradient of ERK2 activity suggests that ERK2 activity is primarily required at the nuclear envelope. The nuclear envelope is partitioned in domains of heterochromatin with repression of transcription and nuclear pore complexes (NPCs) with high transcription [Steglich et al., 2013]. ERK1/2 was shown to directly and indirectly redistribute domains of heterochromatin by phosphorylating histone H3 and therefore regulate transcription on a higher level [Martin et al., 2010, Drobic et al., 2010, Brami-Cherrier et al., 2005, Wiegert & Bading, 2011]. Furthermore, ERK2 associates with the nuclear envelope protein lamin A, which was shown to have a dual effect [González et al., 2008, Rodríguez et al., 2010, Adler, 2010, Kwon et al., 2011]. The interaction of ERK2 with lamin promotes cell cycle entry in a mechanism independent of ERK1/2 kinase activity and additionally seems to facilitate the phosphorylation and release of cFos from lamin, resulting in the transcription of IEGs [González et al., 2008, Rodríguez et al., 2010, Adler, 2010]. Therefore, the higher fraction of ERK2 activity in the nuclear periphery might have various functions in proliferation, transcriptional induction and heterochromatin organization. If nuclear ERK2 interactions are primarily located at the nuclear periphery, ERK2 might show a decreased mobility in this region. Studies on the ERK2 mobility using FCS and FRAP did not find a difference between the nucleus and cytoplasm [Lidke et al., 2010]. However, it might be interesting to investigate the ERK2 mobility at higher spatial resolution than in the overall compartments.

The spatial profiling of mCitrine-pMek1 and -pERK revealed that pMek1 and pERK2 are early after GF stimulation often laterally polarized in the cytoplasm of HeLa as well as MCF-7 cells. This can be due to the polarized appearance of lamellipodia, which is a thin actin structure. If the distance between facing PMs, or rather the gradient sources, is smaller than the gradient's decay length, the complete structure will exhibit high activity which dissipates if the distance between membranes increases (see also figure 1.8). However, in the case of ERK2, the cytoplasmic polarization continued in a nuclear polarization of phosphorylated ERK2. The nucleus is thought to remain spherical, so here such a distortion of the nuclear shape is unlikely, the observed lateral polarity is therefore real. As the cell is exposed to a homogenous concentration of GFs, no extracellular GF gradients should occur which might cause the polarized activation of RTKs. The laterally polarized MAPK activation indicates therefore that spatial cues are prepolarized, which promote local RTK activation upon GF stimulation. These spatial cues might be the Rho GTPase family and PAK1, which are involved in cytoskeletal restructuring and are localized to sites of high actin turnover. Rho and PAK1 were further shown to support ERK1/2 signaling in response to EGFR activation [Eblen et al., 2004, Smith et al., 2008]. PAK1 for instance phosphorylates Mek on Thr298, priming it for the activation by Raf [Coles & Shaw, 2002]. In later time points, polarized MAPK activity was less often observed. The occurrence of local activation and lateral phosphorylation propagation was shown for EGFR [Reynolds et al., 2003]. The emergence of polarized MAPK activity gradients reflects first that the active receptor on the PM was activated in a polarized manner and second

that the phosphorylated MAPKs deactivated in axial as well as lateral direction.

6.3.2 Differences in EGF vs. HRG induced spatio-temporal activity profiles of Mek1 and ERK1/2 in MCF-7 cells

The observed difference in the strength of Mek1 activation upon EGF or HRG stimulation can be attributed to the activation of different receptors. The EGF induced ERB-B1 (EGFR) expresses in MCF-7 cells only to 5000 molecules per cell, which is very low compared to other cell lines [Goldenberg et al., 1989]. HRG induces additionally to EGFR also the activation of receptors ERB-B2 - B4 which are equally abundant and therefore might cause an elevated signal. EGFR is known to be degraded upon EGF binding, while ERB-B2 and B3 are primarily recycled [Waterman et al., 1998, Lenferink et al., 1998]. GF-specific receptor routing might affect the signaling dynamics of EGF and HRG in MCF-7 cells. However, the dynamic properties of signaling are thought to arise from the individual GF-specific context of signaling, instead of the intrinsic features of a specified protein, like the receptor [Santos et al., 2007]. In the analogues example of EGF vs. NGF signaling in PC-12 cells, a negative feedback from ERK on SOS upon EGF stimulation causes a transient ERK activity, while a positive feedback from ERK to Raf upon NGF treatment sustains the ERK activity [Santos et al., 2007]. The positive feedback is mediated by the integration of PKC into the NGF-induced network. It is likely that the same switch occurs in the MAPK network topology of MCF-7 cells upon EGF vs. HRG stimulation [Santos et al., 2007]. Indeed, MCF-7 cells stimulated with EGF and the PKC activator PMA showed sustained signaling, having reverted the EGF into the HRG dependent response [Nakakuki et al., 2010]. However, as PKC might directly activate Raf, the inverse experiment with inhibition of PKC upon HRG treatment is necessary to finally demonstrate that PKC is also in EGF vs. HRG signaling the distinctive factor of the ERK signal duration [Kolch et al., 1993]. The newly obtained data indicates that the HRG-induced response recruits a regulatory interactor which affects the signal transduction from Mek1 to ERK2, based on the following facts: First, HRG stimulation induced a stronger Mek1 activity than EGF stimulation, although ERK2 activity was equal for both GFs. Therefore, in the HRG induced response the dose of Mek1 activity was less efficiently converted into a response of ERK2 activity than in the EGF induced signaling. Such a differential relation between Mek1 and ERK2 activity indicates a different dose-response from active Mek1 on ERK activation. This could be explained with a shift in the threshold of activation or with ultrasensitivity from pMek to ERK activation in the case of EGF stimulation and a graded behaviour upon HRG stimulation. Ultrasensitivity can arise from the dual phosphorylation required to activate a MAPK, if the two phosphorylation reactions proceed in a distributive and cooperative manner (for further information on dose-responses of MAPKs see 1.3.3.1). The EGF induced dose-response might therefore represent the MAPK cascade inherent signaling mode. Consequently, a scaffold would modify the HRG induced response and render the ultrasensitive into a graded response. Scaffolds are indeed thought to promote a graded dose-response by binding the signaling molecules and favouring a processive dual phosphorylation. Second, the ectopic expression of Mek1 and ERK2 led to a reduced amplitude in the kinases activity upon HRG stimulation but not after EGF stimulation. This notion supports the theory of a scaffold in the HRG dependent response, because the relative levels between scaffold and kinases need to meet an optimum in order to promote signaling [Locasale et al., 2007]. The ectopic expression of the kinases might exhibit reduced signaling due to different relative levels between scaffold and kinases. Third, it was shown that the EGF induced gradients of ERK2 activity were shallower than HRG induced gradients, while the Mek1 activity gradients were comparable steep for EGF and HRG stimulation. Therefore, it can be deduced that in the EGF response the shallow ERK2 activity distribution results from being "passively" derived from the Mek1 activity gradient, while the scaffold in the HRG response promotes ERK2 activation in PM-proximal regions. This causes the spatial restriction of ERK2 activity relative to the Mek1 activity gradient. The differential regulation of Mek1

and ERK2 activity and especially the steep ERK2 activity gradients from the PM suggest that the PM scaffold KSR1 is integrated in the HRG induced response. KSR1 could be integrated additionally to PKC in the HRG-induced network architecture.

6.3.3 Spatio-temporal role of KSR1 in the MCF-7 MAPK response

The role of KSR1 on the spatio-temporal activity profiles of Mek1 and ERK2 was investigated by the ectopic expression of KSR1. Ectopic KSR1 expression delayed the ERK2 response for several minutes upon EGF as well as HRG treatment. The delay might be caused by prolonged KSR1-Raf interaction and signaling. The elevation of KSR1 expression might diminish the effect of the negative feedback phosphorylation from ERK on KSR1 which causes the KSR1 dissociation from Raf. Furthermore, the ectopic expression of ECFP-KSR1 elevated the activity amplitudes of Mek1 and ERK1/2 response upon EGF as well as upon HRG stimulation, without changing the fundamental transient or sustained trends. However, Mek1 activity was stronger elevated by KSR1 expression than the ERK2 activity after both GF treatments, showing that KSR1 might indeed be the scaffold responsible for the differential Mek1 and ERK2 activity observed after HRG stimulation. Therefore, KSR1 might not be a temporal switch, but regulate the spatial propagation of active ERK2.

PTag-FLIM results showed that Mek1 phosphorylation increased with the expression of KSR1 and was furthermore outspread in the cytoplasm. Therefore, KSR1 stimulates the activation of Mek1 and either protects Mek1 from dephosphorylation or activates Mek1 also in cytoplasm, thereby breaking the spatial separation of activation and deactivation. In contrast, ERK2 phosphorylation decreased with increasing KSR1 expression, showing that Mek1 which is bound to KSR1 is impaired to activate ERK2. Therefore, the reduced ERK2 activation due to overexpression of KSR1 is a case of combinatorial inhibition. However, it is unclear if KSR1 out-titrates only available active Mek1 or if KSR1 also binds to inactive ERK2 and thereby diminishes accessible ERK2. An interaction of KSR1 with the inactive ERK2 is however unknown. However, ERK2 showed a clear gradient with short decay length in presence of ECFP-KSR1, indicating that ERK2 was still activated at the PM. KSR1 is recruited to the PM upon GF stimulation and has a binding site for the active ERK2 [Dougherty et al., 2009]. Although the restriction of active ERK2 to the PM might only be caused by the interaction with KSR1, the gradient of ERK2 activity indicates that KSR1 has different effects at the PM and in the cytoplasm. The obtained results indicate that at the PM KSR1 supports, or at least does not hinder ERK2 activation, while in the cytoplasm KSR1 impairs the activation of ERK2. KSR1 might act as a sequestration factor for active Mek in regions close to the PM, which artificially constrains the gradient of active and accessible Mek1 and the derived ERK activity gradient. Therefore, KSR1 might restrain ERK activity doubly by allowing ERK activation at the PM and inhibiting it in the cytoplasm. The differential action of KSR1 at the PM and the cytoplasm is likely to depend on a conformational change of KSR1 upon membrane binding. It is known that in solution, KSR1 binds Mek1 in a mirror-imaged conformation which mutually occupies the active sites of their kinase's domain [Brennan et al., 2011]. On the contrary, the PM-bound dimer of KSR1 and Mek1 might take over an "open" conformation which promotes ERK2 activation. The negative feedback from ERK on KSR1 which causes the dissociation of KSR1 from the PM might therefore dynamically restrict ERK activation. Therefore, ERK2 constrains its own spatial propagation by the negative feedback. This mechanism does not depend on high KSR1 expression. Under physiologic conditions where KSR1 levels are low, KSR1 is strongly recruited to the PM upon GF stimulation causing locally a high concentration [Dougherty et al., 2009]. Furthermore, ectopic KSR1 expression induced the expression of endogenous KSR1. If KSR1 induces its own expression, active ERK might become increasingly confined to the membrane over time. The proposed theory of ERK2 confinement by KSR1 is supported by results from [Giurisato et al., 2009], who showed that a PM-binding mutant of KSR1 fails to localize active ERK2 to the synapse in T cells.

PTag-FLIM enables the comparison of scaffold mechanisms on the spatial distribution of MAPKs. The only other known intracellular gradient of a MAPK is the Fus3 activity gradient in the yeast shmoo tip, which is required to transform the pheromone receptor activation into a focussed mating projection. The scaffold Ste5 is essential to allosterically unlock Fus3 for the activation by Ste7 [Good et al., 2009]. It thereby completely controls the localization of Fus3 activation, connecting the symmetry break at the PM into a primary Fus3 activity gradient. This short and steep gradient does not impair the accumulation of active Fus3 in the nucleus due to the small size of the yeast cell (see also above 6.2). In the dimensions of a mammalian cell, such a strict confinement of the ERK activation would inhibit the global response of ERK in the nucleus. However, as Raf-Mek-ERK response can signal independently of a scaffold, domains of scaffolded and unscaffolded signaling will occur at the PM. The unscaffolded MAPK module propagates the ERK activity into the nucleus, while the scaffolded MAPK module confines ERK activity to the PM. This local inhomogeneity of scaffolded and unscaffolded signaling domains will result in alternate low and high ERK activity which might promote pattern formation, for example in differentiation. In this case the patterning does not depend on bi- or multi-stability in the network response but on scaffolded and unscaffolded signaling domains.

7 Future Perspectives

A third of the proteome is estimated to be phosphorylated and phosphorylation is often a switch for protein activity. Therefore, the integration of PTag-FLIM in high throughput screenings for drug discovery would allow to assay a key parameter of protein function. It might be used to detect the activity of the target protein or be a read-out for pathway activation. The phospho-imaging can be combined with redistribution measurements and morphological analyses to observe and correlate multiple properties of the cellular and protein state.

PTag-FLIM furthermore enables the investigation of MAPK phosphorylation on a larger scale. It's becoming more and more evident that the individual properties of scaffolds are required to appropriately modulate MAPK signaling. A screening of MAPK activity under the overexpression or knock-down of various scaffolds would give insight in the divers functions of scaffolds. Such a screen may be combined with the analysis of MAPK signaling from endosomes. It is expected, that internalized active receptors on endosomes function as signaling platforms.

In light of the technical optimization of PTag-FLIM, it is conceivable to establish a dual-donor FLIM using the dark acceptor QC-1 (see also chapter 3.6). With dual-donor FLIM, the activities of two proteins could be correlated in single cells. For instance, the interplay of EGFR and ERK activity could be monitored upon EGF stimulation.

In order to follow the phosphorylation of MAPKs in single cells over time, the PTag FLIM approach should be applied to live cells. The challenge is to circumvent the potential inhibition of all phosphorylation-dependent processes by binding of PTag. Ideally, the PTag-Dye complex would bind only to the donor FP fused protein of interest, if this is phosphorylated. PTag chelates Zn^{2+}, which coordinates to phosphate-monoesters. To circumvent the toxicity of the PTag-Zn^{2+} complex, the free, inactive PTag ligand, conjugated to a dye, might be microinjected into cells. To activate the PTag locally in small doses, a caged Zn^{2+} might be additionally administrated, which is uncaged by photo-activation. The free Zn^{2+} would then be chelated by the PTag ligand and bind to locally available phosphate-monoesters. Therefore the protein of interest as well as other phosphorylated molecules would be bound, but the toxicity reduced. To increase the probability of active PTag complex binding to the protein of interest, the release of Zn^{2+} might be induced by the emission of the donor FP fused to the kinase of interest. Then, active PTag complexes would be constituted only in the proximity to the kinase which would reduce the toxicity and increase the probability of binding to the kinase of interest. However, the FP emission is usually not intense enough to cause the uncaging of a chelator.

Furthermore, the Biotin-STV bond might be used to target PTag to the protein of interest. The protein of interest might be fused to a circular permuted FP, such as cpYFP. This fluorophore is sensitive to changes in its environment and can translate conformational changes into an increase in fluorophore emission. Additionally to the cpFP, the construct were further fused to STV on the genomic level. The free, inactive PTag-Biotin would be administrated to the cells. After binding to the STV, excess PTag would be washed out and free Zn^{2+} would be added. This approach is based on a conformational change between phosphorylated and un-phosphorylated construct. This approach would not enable the fractional observation of phosphorylated to total protein, which is possible with FRET. However, the PTag-Biotin reagent might be modified with a dye which would then serve as FRET acceptor. However, it remains to be elucidated if the binding of PTag is a reversible process. Reversibility is a requirement to profile the temporal phosphorylation of a protein.

The yeast MAPK networks provide an attractive model to study determinants of gradient

properties and the interplay between MAPK network topology and spatial MAPK activity organization. Yeast genomics open the possibility to manipulate single elements of the MAPK network, for instance by inhibiting single kinases with gatekeeper mutations, and measure the spatio-temporal response of the network. Simultaneous computations analyzing the system response would enable the testing of predictions.

8 Materials and Methods

8.1 Antibodies, Reagents and Enzymes

Primary antibodies	*Dilution WB*	*Company (Cat.No.)*
ERK1/2 (mouse)	1:2500	Abcam (ab36991)
ppERK1/2 (rabbit)	1:1000	Cell Signaling Technology (9101)
ppERK1/2 (rabbit)		R&D Systems (AF1018)
Mek1 (mouse)	1:1000	BD Biosciences (610121)
ppMek1 (rabbit)	1:1000	Cell Signaling Technology (9121)
anti-GapDH (mouse)	1:5000	
anti-KSR1 (rabbit)	1:1000	Abcam (ab68483)
Secondary antibodies	*Dilution WB*	*Company (Cat.No.)*
anti-rabbit IR-Dye 800CW (donkey)	1:5000	Licor Biosciences (926-32213)
anti-mouse IR-Dye 680RD (goat)	1:5000	Licor Biosciences (926-68070)
anti-rabbit Alexa-546		Cell Signaling
Phos-tag Biotin BTL-104		Wako Pure Chemical Industries
Streptavidin		Sigma-Aldrich
Fluorolink Cy3.5 Monofunctional Dye		GE Healthcare (PA23501)
IRDye QC-1 NHS Ester		Licor Biosciences (929-70031)
Enzymes and Hormones		
Platinum Pfx DNA Polymerase		Life Technologies
Accuprime Pfx DNA Polymerase		Life Technologies
Platinum Taq DNA Polymerase		Life Technologies
PfuUltra High-fidelity DNA Polymerase		Agilent Technologies
Lyticase		Sigma-Aldrich (L2524)
Epidermal Growth factor		Cell Signaling Technology
Heregulin-beta		Merck Millipore (01-201)

8.2 Media

Name	*Ingredients/Company*
LB	1 % Bact. Tryptophan, 0.5 % Yeast Extract, 1 % g NaCl
YPD	1 % Yeast Extract, 2 % Bacto-Peptone, 2 % Glucose
SC	0.7 % Yeast nitrogen base with amino acids, 2 % Glucose
DMEM	PAN Biotech GmbH (P04-03600)
l-Glutamine	Life Technology
FCS	PAN Biotech GmbH

8.3 Kits and Consumables

Name	*Company (Cat.No.)*
QIAprep Spin Miniprep Kit	Qiagen (27106)
Roti-prep Plasmid Mini	Roth (HP29)
Nucleo-Bond XtraMidi Plus EF	Macherey-Nagel (740422)
DNA clean and concentrator kit	Zymo Research (D4004)
Fugene 6	Roche (11814443001)
Dharmafect 1	Thermo Scientific (T-2001)
10x Cell lysis Buffer	Cell Signaling (9803S)
Phosphatase Inhibitor Cocktail 2	Sigma-Aldrich (P5726)
Phosphatase Inhibitor Cocktail 3	Sigma-Aldrich (P0044)
Protease Inhibitor Cocktail Tablets	Roche (04693132001)
5x siRNA Buffer	Thermo Scientific (B-002000-UB-100)
Zeba Spin Desalting Columns 40K MWCO	Thermo Scientific (87771)
PBS	PAN
PVDF membrane	Millipore
Odyssey blocking buffer	Licor Biosciences (927-40000)
Amicon 30 kD cut-off	
Protein Desalting Spin Columns	Thermo Scientific (89862)
Poly-L-Lysine	

8.4 Buffers and solutions

Buffer	*Ingredients*
SORB buffer	100 mM Lithiumacetat Tris/HCl pH 7.8
	10 mM EDTA/NaOH pH 8
	1 mM Sorbitol
	adjusted to pH 8 with acetic acid
PEG	100 mM Lithiumacetat
	10 mM Tris
	1 mM EDTA/NaOH pH 8
	1M PEG 4000
CarrierDNA	10 mg/ml Salmon sperm DNA
1 M KPO4	mix 1 M K2HPO4 and 1 M KH2PO4 to pH 6.5
SP	1.2 M Sorbitol
	0.1 M KPO4
PFA for yeast fixation	8% Paraformaldehyde
	Drop NaOH
	0.2 M KPO4
4% PFA	
1x TBS	10 mM Tris
	0.1 M NaCl
TBST	1x TBS
	0.1% Tween
5x SDS sample buffer	60 mM Tris/HCl pH 6.8
	25 % glycerol
	2 % SDS
	14.4 mM β-Mercaptoethanol
	0.1 % bromophenolblue
SDS running buffer	25 mM Tris
	192 mM Glycine
	0.1 % SDS
Separating gel buffer	1.5 M Tris-HCl pH 8.8
Stacking gel buffer	0.5 M Tris-HCl pH 6.8
Transfer buffer	25 mM Tris
	192 mM Glycine
	20 % Methanol

8.5 Molecular Biology Techniques

8.5.1 Cloning

DNA was amplified by PCR using “Accuprime Pfx Polymerase” or “Platinum Pfx Polymerase” according to the manufacturer’s protocol. Site-directed mutagenesis of DNA constructs was performed with PfuUltra HF Polymerase and subsequent Dpn1 digest. Oligonucleotides for PCR were ordered from Eurofins MWG Operon or Sigma-Aldrich. For the generation of new DNA constructs DNA was site-specifically cleaved with restriction enzymes and ligated by T4 DNA Ligase, enzymes purchased from New England Biolabs. DNA was analysed by electrophoresis in 1% agarose gels in TAE buffer and imaged under UV light. Isolation and concentration of DNA was done with the “DNA clean and concentrator Kit”. DNA constructs were cloned by transformation in chemically competent E. coli (XL10-Gold Agilent Technologies)

grown in LB medium with 100 mg/ml ampicillin or 50 mg/ml Kanamycin. For the purpose of cell transfection, plasmids were purified endotoxin-free from bacteria with the "Nucleo-Bond Xtra Midi Plus EF Kit" or else with the "Roti-prep Plasmid Mini". DNA was sequenced with the Sanger (chain termination) method using "Big dye terminator v3.1 cycle sequencing kit" and purification kit.

8.5.2 DNA constructs

Plasmid constructs coding for mCitrine-ERK2 and mCitrine-Mek1, KSR-CFP, EGFR-mCitrine have been described. mTurquoise and mTurquoise2 fusions of ERK2 and Mek1 were generated by cleavage of the coding sequence from mCit-erk2 and insertion into Clontech mTurquoise-N1 and Clontech mTurquoise2-N1. mCitrine-ERK2-TAYA was generated by site-directed mutagenesis. Yeast plasmids for homologue recombination were kindly provided by Michael Knop.

8.5.3 Labeling of Streptavidin (STV) and preparation of the Phos-Tag-Biotin-Streptavidin-Cy3.5 complex

Streptavidin (STV) was dissolved in PBS and washed two times with PBS using an Amicon 30 kD cut-off, resulting in a concentration of about 100 μM, determined by absorption at 280 nm. Protein concentration was calculated according to Lambert-Beer with an extinction coefficient of 165,000 $M^{-1}cm^{-1}$ for the tetrameric Streptavidin. Bicine (pH 9.3) was added to the STV solution yielding to a final concentration of 0.1 M. One vial of monofunctional Cy3.5 was dissolved in 10 μl DMF and the dye concentration determined by absorption measurement at its absorption peak at 581 nm. The dye was then added in a 10-fold molar excess to STV and the reaction incubated for 45 min at room temperature. The addition of Tris to 5 mM terminated the conjugation of Cy3.5 to STV. Streptavidin was purified two times by gel exclusion chromatography using Protein Desalting Spin Columns.

To obtain the Phos-Tag-Biotin-Streptavidin-Cy3.5 complex, Phos-Tag-Biotin was added in a 200-fold excess to Streptavidin-Cy3.5 in TBST containing 0.4 mM $Zn(NO_3)_2$. This solution was incubated for 30 minutes in the dark at room temperature and purified by gel exclusion chromatography with Zeba Spin Desalting columns 40kD cut-off.

8.5.4 Preparation of *in vitro* experiment

The glass beads were washed two times with TBST. Protein mixtures of phosphorylated and unphosphorylated EphA3 were washed once with TBS using a centrifugal filter (Amicon Ultra, 10 kD cut-off) and had a final concentration of 140 μM in 80 μl. 7.5 μl of each protein mix were removed for native PAGE. Glass beads were added to the protein mix to a final concentration of 0.5 mg/ml. The proteins were allowed to immobilize for one hour at 4řC, while shaking at 300 rpm. To wash excessive protein and block the beads, three wash steps with 0.01 mg/ml BSA in TBST were conducted. The beads were given in a microscopy dish with TBST to prevent drying of the beads. PTag-Cy3.5 was added in a concentration of and incubated for 30 minutes. After the staining, beads were washed once with TBST and kept at 4řC. FLIM measurement was conducted 16 hours later.

8.6 Cell Biology Techniques

8.6.1 Mammalian Cell culture

HeLa and MCF-7 cells were maintained in DMEM supplemented with 10% FBS and 1% L-Glutamine, while MCF-7 cell medium additionally contained 1% NEAA. Cells were incubated

at 37řC, 5 % CO_2 and 90 % humidity. To keep cells dividing, cultures were split before grown to confluency by separating cells with Trypsin/EDTA and reseeding in fresh media. Cells were counted with a Vi-CELL XR cell viability analyzer. Before growth factor stimulation, MCF-7 cells were starved for 5 hours in DMEM containing 1% L-Glutamine and 1% NEAA, Hela cells were starved over night in DMEM supplemented with 1% L-Glutamine. Transfection of DNA constructs was performed with Fugene-6 according to the manufacturer's protocol. Cells were stimulated with 100 ng/ml EGF or 100 ng/ml HRG.

8.6.2 Preparation of cell lysates

Cells were seeded in a density of 10^5 cells per well of a 6-well plate. After 72 hours growth, plasmid DNA was transfected over night. Cells were starved for 5 hours without serum and subsequently stimulated with growth factors. Stimulation was stopped by the addition of ice-cold PBS. Cells were scraped from the dish and harvested by centrifugation for 1 min at 800 rpm. The cell pellet was dissolved in 1xCell lysis buffer and homogenized using a Vortex mixer. The cell extract was centrifuged for 15 min at 14000xg in a cold microfuge and the supernatant transfered to a new tube. The concentration of the resulting cell lysate was measured by Bradford assay.

8.6.3 Western Blots

For SDS-PAGE with 15 wells, 20 μg protein lysate was mixed with 5x sample buffer and heated at 95řC for 5 minutes. The protein sample was then spun down for 15 seconds at maximum speed. Gel electrophoresis was performed in SDS running buffer using 10% SDS-polyacrylamid gels at 150 V until the leading front of the sample buffer reached the gel bottom. For subsequent immune detection, proteins were transfered to a PVDF membrane in transfer buffer at constant 200 mA for one hour. The PVDF membrane was incubated in Odyssey Blocking Buffer to prevent unspecific antibody binding for 3 hours at room temperature or over night at 4řC. Next, the membrane was incubated with primary antibodies diluted in Odyssey Blocking Buffer at 4řC for minimum 14 hours followed by three wash steps with TBST for 10 minutes each. Infrared fluorescent secondary antibodies diluted in Odyssey Blocking Buffer were added in the dark for one hour to the membrane and afterwards washed three times with TBST for 5 minutes. Antigen-antibody interactions were imaged using the Odyssey system at 680 nm and 800 nm set to "5" for both channels.

Western blots were analyzed using ImageJ. Background signal was subtracted from the whole image. For each band a rectangle was drawn, which was used as "region of interest" in both channels. The integrated density of each "region of interest" was computed and used for further calculations.

8.6.4 Mammalian Cell fixation for PTag FLIM

Cells were seeded in a density of 10^4 cells per well of an 8-well LabTek. After 24 hours of growth plasmid DNA was transfected over night. Cells were starved for 5 hours without serum and subsequently stimulated. Cells were fixed by the addition of cold 4 % PFA for 10 minutes. After three steps of washing with TBS cells, were permeabilized for 10 minutes with TBS containing 0.1 % Triton-X. Cells were washed 3 times with TBST and incubated with a 170 nM concentration of the Phos-Tag-Cy3.5 complex in TBST for one hour at room temperature, followed by a single wash step with TBST.

8.6.5 High efficiency transformation in Yeast for homologue Recombination

Yeast transformation was described elsewhere [Knop et al., 1999]. Genetic manipulations in yeast were performed using a PCR-based method described in [Janke et al., 2004].

8.6.6 Yeast fixation for PTag-FLIM

Yeast cells grown in liquid culture to an OD of 0.8 were stimulated with 100 ng/ml pheromone for 3h. Cells were fixed in the presence of 4% fresh formaldehyde solution and 0.1 M KPO_4 for 30 minutes at room temperature, followed by three wash steps with SP buffer. Cell walls were removed by incubation with 0.7 M Lyticase in SP buffer containing 20 mM β-Mercaptoethanol at 30řC for 30-45 minutes. Spheroblasts were washed 3 times with cold SP buffer and stored at 4řC. 8-well LabTek chambers were coated with Poly-L-Lysine for 30 minutes at room temperature and washed 3 times with water. Cells were allowed to immobilize in the coated chambers in TBS buffer for 30 minutes and subsequently permeabilized with TBS containing 0.1% Triton X-100, followed by 3 times washing with TBST. The chambers were incubated with a 170 nM concentration the PTag-Cy3.5 complex for 1h and washed once with TBST. Chambers were used forthrightly for microscopy.

8.6.7 Yeast immunofluorescence

Yeast cell fixation was performed as described 8.6.6. After permeabilizing yeast cells with TBS containing 0.1% Triton X-100 cells were blocked with 1% BSA in PBS. Antibodies were incubated in a dilution of 1:150 over night at 4řC in blocking buffer. After wahing of excess primary antibody the secondary antibody anti-rabbit carrying the dye Alexa-546 was added for one hour at room temperature.

8.7 Microscopy

Confocal images were acquired using a confocal laser-scanning microscope (Fluoview 1000, Olympus). mCitrine was excited with the 488 nm line of an Argon laser and its emission detected in the range of 500-550 nm. Cy3.5 was excited with the 561 nm line of a DPSS laser and its emission recorded at wavelengths 570-670 nm. Fluorescence signal was collected through a water objective (x60/1:35 UPlanSApo, Olympus) with a DM405/488/561/633 dichroic mirror. Emission light from mCitrine and Cy3.5 was separated by a beam splitter SDM560. ECFP was excited at 440 nm and its emission recorded in the range of 470-495 nm.

Fluorescence lifetime images were obtained using a confocal laser-scanning microscope (Fluoview 1000, Olympus) equipped with a TCSPC module (LSM Upgrade Kit, Picoquant). Photons were detected using a single-photon counting avalanche photodiode (PDM Series, MPD) and timed with a single-photon counting module (PicoHarp 300, Picoquant). Donor fluorophores were excited using pulsed diode lasers (Picoquant) with the appropriate wavelengths (see table) at 40 MHz repetition. Fluorescence signal was collected through a water objective (x60/1:35 UPlanSApo, Olympus) and spectrally filtered using narrow-band emission filters (see table).

8.7.1 FLIM data analysis

Excited state lifetimes in figures 3.3, 3.6 and 3.7 was analyzed by fitting the obtained fluorescence lifetime histograms using pFLIM [Walther et al., 2011].

Other presented FLIM data was analyzed by global analysis implemented in MatLab, for theoretical background see also chapter 1.4.3 [Grecco et al., 2009]. Briefly, for global analysis

Fluorophore	*Excitation*	*Emission*	
mTFP	440 nm	480/20	
mCitrine	470 nm	525/15	data from chapter 3
	510 nm	530/11	data from chapter 4 and 5
mKate2	532 nm		

Table 8.1: Excitation wavelengths and corresponding emission filters for FLIM.

the following steps were conducted: TCSPC histograms of a certain protein (Fus3-mCitrine, mCitrine-Mek1, mCitrine-ERK2) were pooled together. In the global analysis, pixels with low intensity were excluded from the analysis. The histograms were then Fourier transformed from the time domain to the frequency domain. After correction of the Fourier coefficients for the impulse response function of the instrument, the Fourier coefficients of each pixel are plotted in the Complex plane. The pixels are weighted according to the photon number to increase the signal-to-noise ratio. The fitting of a straight line through all pixels reveals the invariant lifetimes τ_D and τ_{DA} of the donor in presence and absence of the acceptor. The relative location of a pixel on this line reveals the fraction of molecules in complex with the acceptor, represented by α, from which an image was reconstructed.

9 Acknowledgement

First of all I would like to thank my supervisor Prof. Dr. Philippe I. H. Bastiaens for his guidance with my interesting project and the encouragement throughout the writing process.

I am very thankful to Prof. Dr. Roland Winter for taking over the second review.

My deepest thanks go to Dr. Christina-Maria Hecker for her outstanding constant support in all concerns during my stay at the MPI Dortmund.

I want to thank Dr. Ali Kinkhabwala and all former members of the yeast group for all the exciting discussions which I enjoyed a lot.

Dr. Astrid Krämer I want to thank for keeping the lab running and correcting my thesis. Furthermore I want to thank the IMPRS for funding and especially Christa Hornemann for always having an open ear.

I want to express special thanks to Klaus Schürmann, Aneta Koseska and Maja Sinn for last-minute help with my thesis.

Also special thanks goes to Kirsten Michel, Jutta Luig, Hendrike Schütz, Anette Langerak, Petra Glitz, Michael Reichl and Nimetka for being down-to-earth and understanding.

I am glad to have met so many interesting people in the Bastiaens lab, especially and without order Christina, Maja, Sven, Jana and Rabea, Björn, Johann, Ola, Amit, Dina, Jenny and the former colleagues Thies, Hernan, Yvonne, Pedro, Justine, Marton, Jian, Martin, Euli.

Finally, I want to thank my family, friends and Kai for their confidence.

Bibliography

[Abraham et al., 2000] Abraham, D., Podar, K., Pacher, M., Kubicek, M., Welzel, N., Hemmings, B. A., Dilworth, S. M., Mischak, H., Kolch, W., & Baccarini, M. (2000). Raf-1-associated Protein Phosphatase 2a as a Positive Regulator of Kinase Activation. *Journal of Biological Chemistry*, 275(29), 22300–22304. 6

[Acharya et al., 1998] Acharya, U., Mallabiabarrena, A., Acharya, J. K., & Malhotra, V. (1998). Signaling via mitogen-activated protein kinase kinase (MEK1) is required for Golgi fragmentation during mitosis. *Cell*, 92(2), 183–192. 84

[Adachi et al., 1999] Adachi, M., Fukuda, M., & Nishida, E. (1999). Two co-existing mechanisms for nuclear import of MAP kinase: passive diffusion of a monomer and active transport of a dimer. *The EMBO journal*, 18(19), 5347–5358. 9

[Adachi et al., 2000] Adachi, M., Fukuda, M., & Nishida, E. (2000). Nuclear export of MAP kinase (ERK) involves a MAP kinase kinase (MEK)-dependent active transport mechanism. *The Journal of cell biology*, 148(5), 849–856. 8

[Adler, 2010] Adler, E. M. (2010). ERKed About Lamin A. *Science Signaling*, 3(151), ec371–ec371. 85

[Ahn et al., 2004] Ahn, S., Shenoy, S. K., Wei, H., & Lefkowitz, R. J. (2004). Differential Kinetic and Spatial Patterns of -Arrestin and G Protein-mediated ERK Activation by the Angiotensin II Receptor. *Journal of Biological Chemistry*, 279(34), 35518–35525. 12

[Albeck et al., 2013] Albeck, J. G., Mills, G. B., & Brugge, J. S. (2013). Frequency-Modulated Pulses of ERK Activity Transmit Quantitative Proliferation Signals. *Molecular Cell*, 49(2), 249–261. 10, 21

[Anjum & Blenis, 2008] Anjum, R. & Blenis, J. (2008). The RSK family of kinases: emerging roles in cellular signalling. *Nature Reviews Molecular Cell Biology*, 9(10), 747–758. 10

[Aoki et al., 2013] Aoki, K., Kumagai, Y., Sakurai, A., Komatsu, N., Fujita, Y., Shionyu, C., & Matsuda, M. (2013). Stochastic ERK activation induced by noise and cell-to-cell propagation regulates cell density-dependent proliferation. *Molecular cell*, 52(4), 529–540. 10, 21

[Asthagiri & Lauffenburger, 2001] Asthagiri, A. R. & Lauffenburger, D. A. (2001). A computational study of feedback effects on signal dynamics in a mitogen-activated protein kinase (MAPK) pathway model. *Biotechnology progress*, 17(2), 227–239. 22

[Avraham & Yarden, 2011] Avraham, R. & Yarden, Y. (2011). Feedback regulation of EGFR signalling: decision making by early and delayed loops. *Nature reviews. Molecular cell biology*, 12(2), 104–117. 10, 22

[Balan et al., 2006] Balan, V., Leicht, D. T., Zhu, J., Balan, K., Kaplun, A., Singh-Gupta, V., Qin, J., Ruan, H., Comb, M. J., & Tzivion, G. (2006). Identification of novel in vivo Raf-1 phosphorylation sites mediating positive feedback Raf-1 regulation by extracellular signal-regulated kinase. *Molecular Biology of the Cell*, 17(3), 1141–1153. 27

[Baltanás et al., 2013] Baltanás, R., Bush, A., Couto, A., Durrieu, L., Hohmann, S., & Colman-Lerner, A. (2013). Pheromone-induced morphogenesis improves osmoadaptation capacity by activating the HOG MAPK pathway. *Science signaling*, 6(272), ra26. 14

[Bao et al., 2004] Bao, M. Z., Schwartz, M. A., Cantin, G. T., Yates, John R, r., & Madhani, H. D. (2004). Pheromone-dependent destruction of the Tec1 transcription factor is required for MAP kinase signaling specificity in yeast. *Cell*, 119(7), 991–1000. 16

[Bardwell et al., 2001] Bardwell, A. J., Flatauer, L. J., Matsukuma, K., Thorner, J., & Bardwell, L. (2001). A conserved docking site in MEKs mediates high-affinity binding to MAP kinases and cooperates with a scaffold protein to enhance signal transmission. *The Journal of biological chemistry*, 276(13), 10374–10386. 11

[Bashor et al., 2008] Bashor, C. J., Helman, N. C., Yan, S., & Lim, W. A. (2008). Using engineered scaffold interactions to reshape MAP kinase pathway signaling dynamics. *Science (New York, N.Y.)*, 319(5869), 1539–1543. 14

[Bastiaens et al., 2006] Bastiaens, P., Caudron, M., Niethammer, P., & Karsenti, E. (2006). Gradients in the self-organization of the mitotic spindle. *Trends in cell biology*, 16(3), 125–134. 22

[Bastiaens & Squire, 1999] Bastiaens, P. I. & Squire, A. (1999). Fluorescence lifetime imaging microscopy: spatial resolution of biochemical processes in the cell. *Trends in cell biology*, 9(2), 48–52. 5

[Bhalla et al., 2002] Bhalla, U. S., Ram, P. T., & Iyengar, R. (2002). MAP Kinase Phosphatase As a Locus of Flexibility in a Mitogen-Activated Protein Kinase Signaling Network. *Science*, 297(5583), 1018–1023. 18

[Bhattacharyya et al., 2006] Bhattacharyya, R. P., Reményi, A., Good, M. C., Bashor, C. J., Falick, A. M., & Lim, W. A. (2006). The Ste5 scaffold allosterically modulates signaling output of the yeast mating pathway. *Science (New York, N.Y.)*, 311(5762), 822–826. 17

[Brami-Cherrier et al., 2005] Brami-Cherrier, K., Valjent, E., Hervé, D., Darragh, J., Corvol, J.-C., Pages, C., Arthur, S. J., Simon, A. J., Girault, J.-A., & Caboche, J. (2005). Parsing molecular and behavioral effects of cocaine in mitogen- and stress-activated protein kinase-1-deficient mice. *The Journal of Neuroscience: The Official Journal of the Society for Neuroscience*, 25(49), 11444–11454. 85

[Bray & Lay, 1997] Bray, D. & Lay, S. (1997). Computer-based analysis of the binding steps in protein complex formation. *Proceedings of the National Academy of Sciences*, 94(25), 13493–13498. 20

[Brennan et al., 2011] Brennan, D. F., Dar, A. C., Hertz, N. T., Chao, W. C. H., Burlingame, A. L., Shokat, K. M., & Barford, D. (2011). A Raf-induced allosteric transition of KSR stimulates phosphorylation of MEK. *Nature*, 472(7343), 366–369. 12, 60, 87

[Brightman & Fell, 2000] Brightman, F. A. & Fell, D. A. (2000). Differential feedback regulation of the MAPK cascade underlies the quantitative differences in EGF and NGF signalling in PC12 cells. *FEBS letters*, 482(3), 169–174. 22

[Britson et al., 2009] Britson, J. S., Barton, F., Balko, J. M., & Black, E. P. (2009). Deregulation of DUSP activity in EGFR-mutant lung cancer cell lines contributes to sustained ERK1/2 signaling. *Biochemical and Biophysical Research Communications*, 390(3), 849–854. 10

[Brown & Kholodenko, 1999] Brown, G. C. & Kholodenko, B. N. (1999). Spatial gradients of cellular phospho-proteins. *FEBS letters*, 457(3), 452–454. 1, 3, 5, 22, 23, 43, 84

[Brunet et al., 1999] Brunet, A., Roux, D., Lenormand, P., Dowd, S., Keyse, S., & Pouysségur, J. (1999). Nuclear translocation of p42/p44 mitogen-activated protein kinase is required for growth factor-induced gene expression and cell cycle entry. *The EMBO journal*, 18(3), 664–674. 10

[Buchwalter et al., 2004] Buchwalter, G., Gross, C., & Wasylyk, B. (2004). Ets ternary complex transcription factors. *Gene*, 324, 1–14. 10

[Burack & Shaw, 2000] Burack, W. R. & Shaw, A. S. (2000). Signal transduction: hanging on a scaffold. *Current Opinion in Cell Biology*, 12(2), 211–216. 20

[Burack & Shaw, 2005] Burack, W. R. & Shaw, A. S. (2005). Live Cell Imaging of ERK and MEK: simple binding equilibrium explains the regulated nucleocytoplasmic distribution of ERK. *The Journal of biological chemistry*, 280(5), 3832–3837. 10

[Burnett & Kennedy, 1954] Burnett, G. & Kennedy, E. P. (1954). The Enzymatic Phosphorylation of Proteins. *Journal of Biological Chemistry*, 211(2), 969–980. 5

[Cacace et al., 1999] Cacace, A. M., Michaud, N. R., Therrien, M., Mathes, K., Copeland, T., Rubin, G. M., & Morrison, D. K. (1999). Identification of constitutive and ras-inducible phosphorylation sites of KSR: implications for 14-3-3 binding, mitogen-activated protein kinase binding, and KSR overexpression. *Molecular and cellular biology*, 19(1), 229–240. 12

[Canagarajah et al., 1997] Canagarajah, B. J., Khokhlatchev, A., Cobb, M. H., & Goldsmith, E. J. (1997). Activation mechanism of the MAP kinase ERK2 by dual phosphorylation. *Cell*, 90(5), 859–869. 9

[Canal et al., 2011] Canal, F., Palygin, O., Pankratov, Y., Corrêa, S. A. L., & Müller, J. (2011). Compartmentalization of the MAPK scaffold protein KSR1 modulates synaptic plasticity in hippocampal neurons. *FASEB journal: official publication of the Federation of American Societies for Experimental Biology*, 25(7), 2362–2372. 12, 60

[Carraway et al., 1994] Carraway, K. L., Sliwkowski, M. X., Akita, R., Platko, J. V., Guy, P. M., Nuijens, A., Diamonti, A. J., Vandlen, R. L., Cantley, L. C., & Cerione, R. A. (1994). The erbB3 gene product is a receptor for heregulin. *Journal of Biological Chemistry*, 269(19), 14303–14306. 27

[Casar et al., 2008] Casar, B., Pinto, A., & Crespo, P. (2008). Essential role of ERK dimers in the activation of cytoplasmic but not nuclear substrates by ERK-scaffold complexes. *Molecular cell*, 31(5), 708–721. 10

[Casar et al., 2009] Casar, B., Pinto, A., & Crespo, P. (2009). ERK dimers and scaffold proteins: unexpected partners for a forgotten (cytoplasmic) task. *Cell cycle (Georgetown, Tex.)*, 8(7), 1007–1013. 10, 13

[Catalanotti et al., 2009] Catalanotti, F., Reyes, G., Jesenberger, V., Galabova-Kovacs, G., de Matos Simoes, R., Carugo, O., & Baccarini, M. (2009). A Mek1–Mek2 heterodimer determines the strength and duration of the Erk signal. *Nature Structural & Molecular Biology*, 16(3), 294–303. 8

[Caunt & Keyse, 2013] Caunt, C. J. & Keyse, S. M. (2013). Dual-specificity MAP kinase phosphatases (MKPs): shaping the outcome of MAP kinase signalling. *The FEBS journal*, 280(2), 489–504. 10

[Caunt & McArdle, 2010] Caunt, C. J. & McArdle, C. A. (2010). Stimulus-induced uncoupling of extracellular signal-regulated kinase phosphorylation from nuclear localization is dependent on docking domain interactions. *Journal of cell science*, 123(Pt 24), 4310–4320. 9, 85

[Chalfie et al., 1994] Chalfie, M., Tu, Y., Euskirchen, G., Ward, W. W., & Prasher, D. C. (1994). Green fluorescent protein as a marker for gene expression. *Science*, 263(5148), 802–805. 28

[Chan et al., 2012] Chan, C., Liu, X., Wang, L., Bardwell, L., Nie, Q., & Enciso, G. (2012). Protein Scaffolds Can Enhance the Bistability of Multisite Phosphorylation Systems. *PLoS Comput Biol*, 8(6), e1002551. 20, 21

[Chang & Herskowitz, 1990] Chang, F. & Herskowitz, I. (1990). Identification of a gene necessary for cell cycle arrest by a negative growth factor of yeast: FAR1 is an inhibitor of a G1 cyclin, CLN2. *Cell*, 63(5), 999–1011. 16

[Chapman & Asthagiri, 2009] Chapman, S. A. & Asthagiri, A. R. (2009). Quantitative effect of scaffold abundance on signal propagation. *Molecular Systems Biology*, 5. 11, 55

[Chen & Thorner, 2007] Chen, R. E. & Thorner, J. (2007). Function and regulation in MAPK signaling pathways: lessons learned from the yeast Saccharomyces cerevisiae. *Biochimica et biophysica acta*, 1773(8), 1311–1340. 6, 14

[Chen et al., 2001] Chen, Z., Gibson, T. B., Robinson, F., Silvestro, L., Pearson, G., Xu, B.-e., Wright, A., Vanderbilt, C., & Cobb, M. H. (2001). MAP Kinases. *Chemical Reviews*, 101(8), 2449–2476. 5, 6

[Choi et al., 1994] Choi, K. Y., Satterberg, B., Lyons, D. M., & Elion, E. A. (1994). Ste5 tethers multiple protein kinases in the MAP kinase cascade required for mating in S. cerevisiae. *Cell*, 78(3), 499–512. 16

[Chou et al., 2004] Chou, S., Huang, L., & Liu, H. (2004). Fus3-regulated Tec1 degradation through SCFCdc4 determines MAPK signaling specificity during mating in yeast. *Cell*, 119(7), 981–990. 16

[Chuderland et al., 2008] Chuderland, D., Konson, A., & Seger, R. (2008). Identification and characterization of a general nuclear translocation signal in signaling proteins. *Molecular cell*, 31(6), 850–861. 9

[Clarke et al., 1990] Clarke, R., Dickson, R. B., & Brünner, N. (1990). The process of malignant progression in human breast cancer. *Annals of Oncology*, 1(6), 401–407. 27

[Clegg, 2006] Clegg, R. M. (2006). The History of Fret. In C. D. Geddes & J. R. Lakowicz (Eds.), *Reviews in Fluorescence 2006*, number 2006 in Reviews in Fluorescence (pp. 1–45). Springer US. 28

[Cochet et al., 1988] Cochet, C., Kashles, O., Chambaz, E. M., Borrello, I., King, C. R., & Schlessinger, J. (1988). Demonstration of epidermal growth factor-induced receptor dimerization in living cells using a chemical covalent cross-linking agent. *The Journal of biological chemistry*, 263(7), 3290–3295. 27

[Cohen, 2002] Cohen, P. (2002). The origins of protein phosphorylation. *Nature cell biology*, 4(5), E127–130. 5

[Cohen, 1983] Cohen, S. (1983). The receptor for epidermal growth factor functions as a tyrosyl-specific kinase. *Progress in nucleic acid research and molecular biology*, 29, 245–247. 27

[Cohen et al., 1980] Cohen, S., Carpenter, G., & King, L, J. (1980). Epidermal growth factor-receptor-protein kinase interactions. Co-purification of receptor and epidermal growth factor-enhanced phosphorylation activity. *The Journal of biological chemistry*, 255(10), 4834–4842. 27

[Coles & Shaw, 2002] Coles, L. C. & Shaw, P. E. (2002). PAK1 primes MEK1 for phosphorylation by Raf-1 kinase during cross-cascade activation of the ERK pathway. *Oncogene*, 21(14), 2236–2244. 8, 85

[Cook et al., 1997] Cook, J. G., Bardwell, L., & Thorner, J. (1997). Inhibitory and activating functions for MAPK Kss1 in the S. cerevisiae filamentous-growth signalling pathway. *Nature*, 390(6655), 85–88. 16

[Corbit et al., 2003] Corbit, K. C., Trakul, N., Eves, E. M., Diaz, B., Marshall, M., & Rosner, M. R. (2003). Activation of Raf-1 Signaling by Protein Kinase C through a Mechanism Involving Raf Kinase Inhibitory Protein. *Journal of Biological Chemistry*, 278(15), 13061–13068. 13, 25

[Cullis et al., 2014] Cullis, J., Meiri, D., Sandi, M. J., Radulovich, N., Kent, O. A., Medrano, M., Mokady, D., Normand, J., Larose, J., Marcotte, R., Marshall, C. B., Ikura, M., Ketela, T., Moffat, J., Neel, B. G., Gingras, A.-C., Tsao, M.-S., & Rottapel, R. (2014). The RhoGEF GEF-H1 Is Required for Oncogenic RAS Signaling via KSR-1. *Cancer Cell*, 25(2), 181–195. 12

[Daub et al., 2008] Daub, H., Olsen, J. V., Bairlein, M., Gnad, F., Oppermann, F. S., Körner, R., Greff, Z., Kéri, G., Stemmann, O., & Mann, M. (2008). Kinase-selective enrichment enables quantitative phosphoproteomics of the kinome across the cell cycle. *Molecular cell*, 31(3), 438–448. 45

[DeFea et al., 2000] DeFea, K., Zalevsky, J., Thoma, M., Dery, O., Mullins, R., & Bunnett, N. (2000). -Arrestin-dependent endocytosis of proteinase-activated receptor 2 is required for intracellular targeting of activated ERK1/2. *Journal of Cell Biology*, 148(6), 1267–1281. 12

[Deiss et al., 2012] Deiss, K., Kisker, C., Lohse, M. J., & Lorenz, K. (2012). Raf Kinase Inhibitor Protein (RKIP) Dimer Formation Controls Its Target Switch from Raf1 to G Protein-coupled Receptor Kinase (GRK) 2. *Journal of Biological Chemistry*, 287(28), 23407–23417. 13

[Denouel-Galy et al., 1998] Denouel-Galy, A., Douville, E. M., Warne, P. H., Papin, C., Laugier, D., Calothy, G., Downward, J., & Eychène, A. (1998). Murine Ksr interacts with MEK and inhibits Ras-induced transformation. *Current Biology*, 8(1), 46–55. 12

[Dent et al., 1992] Dent, P., Haser, W., Haystead, T. A., Vincent, L. A., Roberts, T. M., & Sturgill, T. W. (1992). Activation of mitogen-activated protein kinase kinase by v-Raf in NIH 3t3 cells and in vitro. *Science (New York, N.Y.)*, 257(5075), 1404–1407. 8

[Dong et al., 1992] Dong, X. F., Berthois, Y., Dussert, C., Isnardon, D., Palmari, J., & Martin, P. M. (1992). Mode of EGF action on cell cycle kinetics in human breast cancer cell line MCF-7: some evidence that EGF acts as a "progression factor". *Anticancer research*, 12(6B), 2085–2092. 27, 59

[Dougherty et al., 2009] Dougherty, M. K., Ritt, D. A., Zhou, M., Specht, S. I., Monson, D. M., Veenstra, T. D., & Morrison, D. K. (2009). KSR2 is a calcineurin substrate that promotes ERK cascade activation in response to calcium signals. *Molecular cell*, 34(6), 652–662. 11, 87

[Drobic et al., 2010] Drobic, B., Pérez-Cadahía, B., Yu, J., Kung, S. K.-P., & Davie, J. R. (2010). Promoter chromatin remodeling of immediate-early genes is mediated through H3 phosphorylation at either serine 28 or 10 by the MSK1 multi-protein complex. *Nucleic Acids Research*, 38(10), 3196–3208. 85

[Dushek et al., 2011] Dushek, O., van der Merwe, P. A., & Shahrezaei, V. (2011). Ultrasensitivity in Multisite Phosphorylation of Membrane-Anchored Proteins. *Biophysical Journal*, 100(5), 1189–1197. 20

[Eblen et al., 2004] Eblen, S. T., Slack-Davis, J. K., Tarcsafalvi, A., Parsons, J. T., Weber, M. J., & Catling, A. D. (2004). Mitogen-Activated Protein Kinase Feedback Phosphorylation Regulates MEK1 Complex Formation and Activation during Cellular Adhesion. *Molecular and Cellular Biology*, 24(6), 2308–2317. 8, 42, 85

[Eckert et al., 2008] Eckert, A., Böck, B. C., Tagscherer, K. E., Haas, T. L., Grund, K., Sykora, J., Herold-Mende, C., Ehemann, V., Hollstein, M., Chneiweiss, H., Wiestler, O. D., Walczak, H., & Roth, W. (2008). The PEA-15/PED protein protects glioblastoma cells from glucose deprivation-induced apoptosis via the ERK/MAP kinase pathway. *Oncogene*, 27(8), 1155–1166. 13, 14

[Elion, 1995] Elion, E. A. (1995). Ste5: a meeting place for MAP kinases and their associates. *Trends in cell biology*, 5(8), 322–327. 11

[Elion et al., 1991] Elion, E. A., Brill, J. A., & Fink, G. R. (1991). Functional redundancy in the yeast cell cycle: FUS3 and KSS1 have both overlapping and unique functions. *Cold Spring Harbor symposia on quantitative biology*, 56, 41–49. 16

[Farley et al., 1999] Farley, F. W., Satterberg, B., Goldsmith, E. J., & Elion, E. A. (1999). Relative dependence of different outputs of the Saccharomyces cerevisiae pheromone response pathway on the MAP kinase Fus3p. *Genetics*, 151(4), 1425–1444. 16

[Feng et al., 1998] Feng, Y., Song, L. Y., Kincaid, E., Mahanty, S. K., & Elion, E. A. (1998). Functional binding between Gbeta and the LIM domain of Ste5 is required to activate the MEKK Ste11. *Current biology: CB*, 8(5), 267–278. 16

[Ferrell & Xiong, 2001] Ferrell, J. E. & Xiong, W. (2001). Bistability in cell signaling: How to make continuous processes discontinuous, and reversible processes irreversible. *Chaos (Woodbury, N.Y.)*, 11(1), 227–236. 20, 21

[Ferrell, 2002] Ferrell, Jr, J. E. (2002). Self-perpetuating states in signal transduction: positive feedback, double-negative feedback and bistability. *Current opinion in cell biology*, 14(2), 140–148. 20, 21

[Ferrell Jr, 1996] Ferrell Jr, J. E. (1996). Tripping the switch fantastic: how a protein kinase cascade can convert graded inputs into switch-like outputs. *Trends in Biochemical Sciences*, 21(12), 460–466. 19

[Fiddes et al., 1995] Fiddes, R. J., Janes, P. W., Sanderson, G. M., Sivertsen, S. P., Sutherland, R. L., & Daly, R. J. (1995). Heregulin (HRG)-induced mitogenic signaling and cytotoxic activity of a HRG/PE40 ligand toxin in human breast cancer cells. *Cell growth & differentiation: the molecular biology journal of the American Association for Cancer Research*, 6(12), 1567–1577. 27

[Formstecher et al., 2001] Formstecher, E., Ramos, J. W., Fauquet, M., Calderwood, D. A., Hsieh, J. C., Canton, B., Nguyen, X. T., Barnier, J. V., Camonis, J., Ginsberg, M. H., & Chneiweiss, H. (2001). PEA-15 mediates cytoplasmic sequestration of ERK MAP kinase. *Developmental cell*, 1(2), 239–250. 13

[Förster, 1948] Förster, T. (1948). Zwischenmolekulare Energiewanderung und Fluoreszenz. *Annalen der Physik*, 437(1-2), 55–75. 28

[Fujioka et al., 2006] Fujioka, A., Terai, K., Itoh, R. E., Aoki, K., Nakamura, T., Kuroda, S., Nishida, E., & Matsuda, M. (2006). Dynamics of the Ras/ERK MAPK cascade as monitored by fluorescent probes. *The Journal of biological chemistry*, 281(13), 8917–8926. 19

[Fukuda et al., 1996] Fukuda, M., Gotoh, I., Gotoh, Y., & Nishida, E. (1996). Cytoplasmic localization of mitogen-activated protein kinase kinase directed by its NH2-terminal, leucine-rich short amino acid sequence, which acts as a nuclear export signal. *The Journal of biological chemistry*, 271(33), 20024–20028. 8, 43

[Fukuda et al., 1997] Fukuda, M., Gotoh, Y., & Nishida, E. (1997). Interaction of MAP kinase with MAP kinase kinase: its possible role in the control of nucleocytoplasmic transport of MAP kinase. *The EMBO Journal*, 16(8), 1901–1908. 8, 9

[Fürthauer et al., 2002] Fürthauer, M., Lin, W., Ang, S.-L., Thisse, B., & Thisse, C. (2002). Sef is a feedback-induced antagonist of Ras/MAPK-mediated FGF signalling. *Nature Cell Biology*, 4(2), 170–174. 13

[Galli et al., 2009] Galli, S., Jahn, O., Hitt, R., Hesse, D., Opitz, L., Plessmann, U., Urlaub, H., Poderoso, J. J., Jares-Erijman, E. A., & Jovin, T. M. (2009). A new paradigm for MAPK: structural interactions of hERK1 with mitochondria in HeLa cells. *PloS one*, 4(10), e7541. 10

[Garnett et al., 2005] Garnett, M. J., Rana, S., Paterson, H., Barford, D., & Marais, R. (2005). Wild-Type and Mutant B-RAF Activate C-RAF through Distinct Mechanisms Involving Heterodimerization. *Molecular Cell*, 20(6), 963–969. 8

[Gaumont-Leclerc et al., 2004] Gaumont-Leclerc, M.-F., Mukhopadhyay, U. K., Goumard, S., & Ferbeyre, G. (2004). PEA-15 is inhibited by adenovirus E1a and plays a role in ERK nuclear export and Ras-induced senescence. *The Journal of biological chemistry*, 279(45), 46802–46809. 13

[Ge et al., 2003] Ge, L., Ly, Y., Hollenberg, M., & DeFea, K. (2003). A beta-arrestin-dependent scaffold is associated with prolonged MAPK activation in pseudopodia during protease-activated receptor-2-induced chemotaxis. *The Journal of biological chemistry*, 278(36), 34418–34426. 25

[Ginty & Segal, 2002] Ginty, D. & Segal, R. (2002). Retrograde neurotrophin signaling: Trk-ing along the axon. *Current Opinion in Neurobiology*, 12(3), 268–274. 25

[Giurisato et al., 2009] Giurisato, E., Lin, J., Harding, A., Cerutti, E., Cella, M., Lewis, R. E., Colonna, M., & Shaw, A. S. (2009). The Mitogen-Activated Protein Kinase Scaffold KSR1 Is Required for Recruitment of Extracellular Signal-Regulated Kinase to the Immunological Synapse. *Molecular and Cellular Biology*, 29(6), 1554–1564. 60, 87

[Glading et al., 2007] Glading, A., Koziol, J. A., Krueger, J., & Ginsberg, M. H. (2007). PEA-15 inhibits tumor cell invasion by binding to extracellular signal-regulated kinase 1/2. *Cancer research*, 67(4), 1536–1544. 13

[Goldbeter & Koshland, 1981] Goldbeter, A. & Koshland, Jr, D. E. (1981). An amplified sensitivity arising from covalent modification in biological systems. *Proceedings of the National Academy of Sciences of the United States of America*, 78(11), 6840–6844. 19

[Goldenberg et al., 1989] Goldenberg, A., Masui, H., Divgi, C., Kamrath, H., Pentlow, K., & Mendelsohn, J. (1989). Imaging of human tumor xenografts with an indium-111-labeled anti-epidermal growth factor receptor monoclonal antibody. *Journal of the National Cancer Institute*, 81(21), 1616–1625. 27, 86

[González et al., 2008] González, J. M., Navarro-Puche, A., Casar, B., Crespo, P., & Andrés, V. (2008). Fast regulation of AP-1 activity through interaction of lamin A/C, ERK1/2, and c-Fos at the nuclear envelope. *The Journal of Cell Biology*, 183(4), 653–666. 85

[Good et al., 2009] Good, M., Tang, G., Singleton, J., Reményi, A., & Lim, W. A. (2009). The Ste5 scaffold directs mating signaling by catalytically unlocking the Fus3 MAP kinase for activation. *Cell*, 136(6), 1085–1097. 11, 16, 54, 88

[Good et al., 2011] Good, M. C., Zalatan, J. G., & Lim, W. A. (2011). Scaffold proteins: hubs for controlling the flow of cellular information. *Science (New York, N.Y.)*, 332(6030), 680–686. 11

[Gopalbhai et al., 2003] Gopalbhai, K., Jansen, G., Beauregard, G., Whiteway, M., Dumas, F., Wu, C., & Meloche, S. (2003). Negative Regulation of MAPKK by Phosphorylation of a Conserved Serine Residue Equivalent to Ser212 of MEK1. *Journal of Biological Chemistry*, 278(10), 8118–8125. 8

[Graus-Porta et al., 1997] Graus-Porta, D., Beerli, R. R., Daly, J. M., & Hynes, N. E. (1997). ErbB-2, the preferred heterodimerization partner of all ErbB receptors, is a mediator of lateral signaling. *The EMBO journal*, 16(7), 1647–1655. 27

[Grecco et al., 2010] Grecco, H. E., Roda-Navarro, P., Girod, A., Hou, J., Frahm, T., Truxius, D. C., Pepperkok, R., Squire, A., & Bastiaens, P. I. H. (2010). In situ analysis of tyrosine phosphorylation networks by FLIM on cell arrays. *Nature methods*, 7(6), 467–472. 5, 31

[Grecco et al., 2009] Grecco, H. E., Roda-Navarro, P., & Verveer, P. J. (2009). Global analysis of time correlated single photon counting FRET-FLIM data. *Optics express*, 17(8), 6493–6508. 31, 96

[Green & Pflum, 2007] Green, K. D. & Pflum, M. K. H. (2007). Kinase-Catalyzed Biotinylation for Phosphoprotein Detection. *Journal of the American Chemical Society*, 129(1), 10–11. 32

[Green & Pflum, 2009] Green, K. D. & Pflum, M. K. H. (2009). Exploring Kinase Cosubstrate Promiscuity: Monitoring Kinase Activity through Dansylation. *ChemBioChem*, 10(2), 234–237. 32

[Grønborg et al., 2002] Grønborg, M., Kristiansen, T. Z., Stensballe, A., Andersen, J. S., Ohara, O., Mann, M., Jensen, O. N., & Pandey, A. (2002). A mass spectrometry-based proteomic approach for identification of serine/threonine-phosphorylated proteins by enrichment with phospho-specific antibodies: identification of a novel protein, Frigg, as a protein kinase A substrate. *Molecular & cellular proteomics: MCP*, 1(7), 517–527. 32

[Gunawardena, 2005] Gunawardena, J. (2005). Multisite protein phosphorylation makes a good threshold but can be a poor switch. *Proceedings of the National Academy of Sciences of the United States of America*, 102(41), 14617–14622. 19

[Gustin et al., 1998] Gustin, M. C., Albertyn, J., Alexander, M., & Davenport, K. (1998). MAP kinase pathways in the yeast Saccharomyces cerevisiae. *Microbiology and molecular biology reviews: MMBR*, 62(4), 1264–1300. 14

[Hammet et al., 2003] Hammet, A., Pike, B., McNees, C., Conlan, L., Tenis, N., & Heierhorst, J. (2003). FHA Domains as Phospho-Threonine Binding Modules in Cell Signaling. *IUBMB Life*, 55(1), 23–27. 32

[Hartwell, 1980] Hartwell, L. H. (1980). Mutants of Saccharomyces cerevisiae unresponsive to cell division control by polypeptide mating hormone. *The Journal of cell biology*, 85(3), 811–822. 11

[Hatzivassiliou et al., 2010] Hatzivassiliou, G., Song, K., Yen, I., Brandhuber, B. J., Anderson, D. J., Alvarado, R., Ludlam, M. J. C., Stokoe, D., Gloor, S. L., Vigers, G., Morales, T., Aliagas, I., Liu, B., Sideris, S., Hoeflich, K. P., Jaiswal, B. S., Seshagiri, S., Koeppen, H., Belvin, M., Friedman, L. S., & Malek, S. (2010). RAF inhibitors prime wild-type RAF to activate the MAPK pathway and enhance growth. *Nature*, 464(7287), 431–435. 6

[Hecker et al., 2014] Hecker, C.-M., Johann Jarzombek, Wieczorek, J., Karajannis, L. S., Ickstadt, K., & Bastiaens, P. (2014). A negative feedback loop between Fus3 and Ste11 regulates pheromone induced formation of the mating projection. 1, 3, 49, 54, 83, 84

[Heidecker et al., 1990] Heidecker, G., Huleihel, M., Cleveland, J. L., Kolch, W., Beck, T. W., Lloyd, P., Pawson, T., & Rapp, U. R. (1990). Mutational activation of c-raf-1 and definition of the minimal transforming sequence. *Molecular and Cellular Biology*, 10(6), 2503–2512. 6

[Heidorn et al., 2010] Heidorn, S. J., Milagre, C., Whittaker, S., Nourry, A., Niculescu-Duvas, I., Dhomen, N., Hussain, J., Reis-Filho, J. S., Springer, C. J., Pritchard, C., & Marais, R. (2010). Kinase-dead BRAF and oncogenic RAS cooperate to drive tumor progression through CRAF. *Cell*, 140(2), 209–221. 6

[Heldin et al., 1997] Heldin, C.-H., Miyazono, K., & ten Dijke, P. (1997). TGF- signalling from cell membrane to nucleus through SMAD proteins. *Nature*, 390(6659), 465–471. 32

[Herrmann et al., 1995] Herrmann, C., Martin, G. A., & Wittinghofer, A. (1995). Quantitative analysis of the complex between p21ras and the Ras-binding domain of the human Raf-1 protein kinase. *The Journal of biological chemistry*, 270(7), 2901–2905. 6

[Howe et al., 1992] Howe, L. R., Leevers, S. J., Gómez, N., Nakielny, S., Cohen, P., & Marshall, C. J. (1992). Activation of the MAP kinase pathway by the protein kinase raf. *Cell*, 71(2), 335–342. 8

[Hu et al., 2013] Hu, J., Stites, E. C., Yu, H., Germino, E. A., Meharena, H. S., Stork, P. J. S., Kornev, A. P., Taylor, S. S., & Shaw, A. S. (2013). Allosteric activation of functionally asymmetric RAF kinase dimers. *Cell*, 154(5), 1036–1046. 8

[Hu et al., 2011] Hu, J., Yu, H., Kornev, A. P., Zhao, J., Filbert, E. L., Taylor, S. S., & Shaw, A. S. (2011). Mutation that blocks ATP binding creates a pseudokinase stabilizing the scaffolding function of kinase suppressor of Ras, CRAF and BRAF. *Proceedings of the National Academy of Sciences of the United States of America*, 108(15), 6067–6072. 8, 12

[Huang & Ferrell, 1996] Huang, C. Y. & Ferrell, Jr, J. E. (1996). Ultrasensitivity in the mitogen-activated protein kinase cascade. *Proceedings of the National Academy of Sciences of the United States of America*, 93(19), 10078–10083. 19, 20, 22, 83

[Humphreys et al., 2013] Humphreys, J. M., Piala, A. T., Akella, R., He, H., & Goldsmith, E. J. (2013). Precisely Ordered Phosphorylation Reactions in the p38 Mitogen-activated Protein (MAP) Kinase Cascade. *Journal of Biological Chemistry*, 288(32), 23322–23330. 19

[Inouye et al., 1997] Inouye, C., Dhillon, N., & Thorner, J. (1997). Ste5 RING-H2 domain: role in Ste4-promoted oligomerization for yeast pheromone signaling. *Science (New York, N.Y.)*, 278(5335), 103–106. 16

[Jameson et al., 2013] Jameson, K. L., Mazur, P. K., Zehnder, A. M., Zhang, J., Zarnegar, B., Sage, J., & Khavari, P. A. (2013). IQGAP1 scaffold-kinase interaction blockade selectively targets RAS-MAP kinase-driven tumors. *Nature Medicine*, 19(5), 626–630. 13

[Janke et al., 2004] Janke, C., Magiera, M. M., Rathfelder, N., Taxis, C., Reber, S., Maekawa, H., Moreno-Borchart, A., Doenges, G., Schwob, E., Schiebel, E., & Knop, M. (2004). A versatile toolbox for PCR-based tagging of yeast genes: new fluorescent proteins, more markers and promoter substitution cassettes. *Yeast (Chichester, England)*, 21(11), 947–962. 14, 96

[Johnson & Lewis, 2001] Johnson, L. N. & Lewis, R. J. (2001). Structural basis for control by phosphorylation. *Chemical reviews*, 101(8), 2209–2242. 5

[Johnson et al., 2009] Johnson, M., Sharma, M., & Henderson, B. R. (2009). IQGAP1 regulation and roles in cancer. *Cellular Signalling*, 21(10), 1471–1478. 13

[Kamerlin et al., 2013] Kamerlin, S. C. L., Sharma, P. K., Prasad, R. B., & Warshel, A. (2013). Why nature really chose phosphate. *Quarterly Reviews of Biophysics*, 46(01), 1–132. 19

[Khmelinskii et al., 2012] Khmelinskii, A., Keller, P. J., Bartosik, A., Meurer, M., Barry, J. D., Mardin, B. R., Kaufmann, A., Trautmann, S., Wachsmuth, M., Pereira, G., Huber, W., Schiebel, E., & Knop, M. (2012). Tandem fluorescent protein timers for in vivo analysis of protein dynamics. *Nature Biotechnology*, 30(7), 708–714. 28

[Khokhlatchev et al., 1998] Khokhlatchev, A. V., Canagarajah, B., Wilsbacher, J., Robinson, M., Atkinson, M., Goldsmith, E., & Cobb, M. H. (1998). Phosphorylation of the MAP kinase ERK2 promotes its homodimerization and nuclear translocation. *Cell*, 93(4), 605–615. 9

[Kholodenko, 2000] Kholodenko, B. N. (2000). Negative feedback and ultrasensitivity can bring about oscillations in the mitogen-activated protein kinase cascades. *European journal of biochemistry / FEBS*, 267(6), 1583–1588. 22

[Kholodenko, 2002] Kholodenko, B. N. (2002). MAP kinase cascade signaling and endocytic trafficking: a marriage of convenience? *Trends in cell biology*, 12(4), 173–177. 84

[Kholodenko, 2006] Kholodenko, B. N. (2006). Cell-signalling dynamics in time and space. *Nature Reviews Molecular Cell Biology*, 7(3), 165–176. 5, 23, 24, 84

[Kholodenko et al., 2010] Kholodenko, B. N., Hancock, J. F., & Kolch, W. (2010). Signalling ballet in space and time. *Nature reviews. Molecular cell biology*, 11(6), 414–426. 22

[Kinoshita et al., 2006] Kinoshita, E., Kinoshita-Kikuta, E., Takiyama, K., & Koike, T. (2006). Phosphate-binding tag, a new tool to visualize phosphorylated proteins. *Molecular & cellular proteomics: MCP*, 5(4), 749–757. 1, 33

[Kinoshita et al., 2004] Kinoshita, E., Takahashi, M., Takeda, H., Shiro, M., & Koike, T. (2004). Recognition of phosphate monoester dianion by an alkoxide-bridged dinuclear zinc(II) complex. *Dalton transactions (Cambridge, England: 2003)*, (8), 1189–1193. 32, 33

[Klein et al., 2000] Klein, S., Reuveni, H., & Levitzki, A. (2000). Signal transduction by a nondissociable heterotrimeric yeast G protein. *Proceedings of the National Academy of Sciences of the United States of America*, 97(7), 3219–3223. 16

[Klüßendorf, 2011] Klüßendorf, T. (2011). Development of a FRET-Based Fluorescent Biosensor for ERK2 Activity. 32

[Knop et al., 1999] Knop, M., Siegers, K., Pereira, G., Zachariae, W., Winsor, B., Nasmyth, K., & Schiebel, E. (1999). Epitope tagging of yeast genes using a PCR-based strategy: more tags and improved practical routines. *Yeast (Chichester, England)*, 15(10B), 963–972. 96

[Kolch et al., 1993] Kolch, W., Heidecker, G., Kochs, G., Hummel, R., Vahidi, H., Mischak, H., Finkenzeller, G., Marmé, D., & Rapp, U. R. (1993). Protein kinase C activates RAF-1 by direct phosphorylation. *Nature*, 364(6434), 249–252. 27, 59, 86

[Komatsu et al., 2011] Komatsu, N., Aoki, K., Yamada, M., Yukinaga, H., Fujita, Y., Kamioka, Y., & Matsuda, M. (2011). Development of an optimized backbone of FRET biosensors for kinases and GTPases. *Molecular biology of the cell*, 22(23), 4647–4656. 10

[Kornev et al., 2008] Kornev, A. P., Taylor, S. S., & Eyck, L. F. T. (2008). A helix scaffold for the assembly of active protein kinases. *Proceedings of the National Academy of Sciences*, 105(38), 14377–14382. 8

[Kornfeld et al., 1995] Kornfeld, K., Hom, D. B., & Horvitz, H. R. (1995). The ksr-1 gene encodes a novel protein kinase involved in Ras-mediated signaling in C. elegans. *Cell*, 83(6), 903–913. 11, 12

[Kortum & Lewis, 2004] Kortum, R. L. & Lewis, R. E. (2004). The Molecular Scaffold KSR1 Regulates the Proliferative and Oncogenic Potential of Cells. *Molecular and Cellular Biology*, 24(10), 4407–4416. 60

[Koveal et al., 2012] Koveal, D., Schuh-Nuhfer, N., Ritt, D., Page, R., Morrison, D. K., & Peti, W. (2012). A CC-SAM, for coiled coil-sterile motif, domain targets the scaffold KSR-1 to specific sites in the plasma membrane. *Science signaling*, 5(255), ra94. 12

[KREBS & FISCHER, 1955] KREBS, E. G. & FISCHER, E. H. (1955). Phosphorylase activity of skeletal muscle extracts. *The Journal of biological chemistry*, 216(1), 113–120. 5

[Kwon et al., 2011] Kwon, H., Jeong, K., Hwang, E. M., Park, J.-Y., & Pak, Y. (2011). A novel domain of caveolin-2 that controls nuclear targeting: regulation of insulin-specific ERK activation and nuclear translocation by caveolin-2. *Journal of Cellular and Molecular Medicine*, 15(4), 888–908. 85

[Kyriakis et al., 1992] Kyriakis, J. M., App, H., Zhang, X. F., Banerjee, P., Brautigan, D. L., Rapp, U. R., & Avruch, J. (1992). Raf-1 activates MAP kinase-kinase. *Nature*, 358(6385), 417–421. 8

[Lander et al., 2001] Lander, E. S., Linton, L. M., Birren, B., Nusbaum, C., Zody, M. C., Baldwin, J., Devon, K., Dewar, K., Doyle, M., FitzHugh, W., Funke, R., Gage, D., Harris, K., Heaford, A., Howland, J., Kann, L., Lehoczky, J., LeVine, R., McEwan, P., McKernan, K.,

Meldrim, J., Mesirov, J. P., Miranda, C., Morris, W., Naylor, J., Raymond, C., Rosetti, M., Santos, R., Sheridan, A., Sougnez, C., Stange-Thomann, N., Stojanovic, N., Subramanian, A., Wyman, D., Rogers, J., Sulston, J., Ainscough, R., Beck, S., Bentley, D., Burton, J., Clee, C., Carter, N., Coulson, A., Deadman, R., Deloukas, P., Dunham, A., Dunham, I., Durbin, R., French, L., Grafham, D., Gregory, S., Hubbard, T., Humphray, S., Hunt, A., Jones, M., Lloyd, C., McMurray, A., Matthews, L., Mercer, S., Milne, S., Mullikin, J. C., Mungall, A., Plumb, R., Ross, M., Shownkeen, R., Sims, S., Waterston, R. H., Wilson, R. K., Hillier, L. W., McPherson, J. D., Marra, M. A., Mardis, E. R., Fulton, L. A., Chinwalla, A. T., Pepin, K. H., Gish, W. R., Chissoe, S. L., Wendl, M. C., Delehaunty, K. D., Miner, T. L., Delehaunty, A., Kramer, J. B., Cook, L. L., Fulton, R. S., Johnson, D. L., Minx, P. J., Clifton, S. W., Hawkins, T., Branscomb, E., Predki, P., Richardson, P., Wenning, S., Slezak, T., Doggett, N., Cheng, J. F., Olsen, A., Lucas, S., Elkin, C., Uberbacher, E., Frazier, M., Gibbs, R. A., Muzny, D. M., Scherer, S. E., Bouck, J. B., Sodergren, E. J., Worley, K. C., Rives, C. M., Gorrell, J. H., Metzker, M. L., Naylor, S. L., Kucherlapati, R. S., Nelson, D. L., Weinstock, G. M., Sakaki, Y., Fujiyama, A., Hattori, M., Yada, T., Toyoda, A., Itoh, T., Kawagoe, C., Watanabe, H., Totoki, Y., Taylor, T., Weissenbach, J., Heilig, R., Saurin, W., Artiguenave, F., Brottier, P., Bruls, T., Pelletier, E., Robert, C., Wincker, P., Smith, D. R., Doucette-Stamm, L., Rubenfield, M., Weinstock, K., Lee, H. M., Dubois, J., Rosenthal, A., Platzer, M., Nyakatura, G., Taudien, S., Rump, A., Yang, H., Yu, J., Wang, J., Huang, G., Gu, J., Hood, L., Rowen, L., Madan, A., Qin, S., Davis, R. W., Federspiel, N. A., Abola, A. P., Proctor, M. J., Myers, R. M., Schmutz, J., Dickson, M., Grimwood, J., Cox, D. R., Olson, M. V., Kaul, R., Raymond, C., Shimizu, N., Kawasaki, K., Minoshima, S., Evans, G. A., Athanasiou, M., Schultz, R., Roe, B. A., Chen, F., Pan, H., Ramser, J., Lehrach, H., Reinhardt, R., McCombie, W. R., de la Bastide, M., Dedhia, N., Blöcker, H., Hornischer, K., Nordsiek, G., Agarwala, R., Aravind, L., Bailey, J. A., Bateman, A., Batzoglou, S., Birney, E., Bork, P., Brown, D. G., Burge, C. B., Cerutti, L., Chen, H. C., Church, D., Clamp, M., Copley, R. R., Doerks, T., Eddy, S. R., Eichler, E. E., Furey, T. S., Galagan, J., Gilbert, J. G., Harmon, C., Hayashizaki, Y., Haussler, D., Hermjakob, H., Hokamp, K., Jang, W., Johnson, L. S., Jones, T. A., Kasif, S., Kaspryzk, A., Kennedy, S., Kent, W. J., Kitts, P., Koonin, E. V., Korf, I., Kulp, D., Lancet, D., Lowe, T. M., McLysaght, A., Mikkelsen, T., Moran, J. V., Mulder, N., Pollara, V. J., Ponting, C. P., Schuler, G., Schultz, J., Slater, G., Smit, A. F., Stupka, E., Szustakowski, J., Thierry-Mieg, D., Thierry-Mieg, J., Wagner, L., Wallis, J., Wheeler, R., Williams, A., Wolf, Y. I., Wolfe, K. H., Yang, S. P., Yeh, R. F., Collins, F., Guyer, M. S., Peterson, J., Felsenfeld, A., Wetterstrand, K. A., Patrinos, A., Morgan, M. J., de Jong, P., Catanese, J. J., Osoegawa, K., Shizuya, H., Choi, S., Chen, Y. J., Szustakowki, J., & International Human Genome Sequencing Consortium (2001). Initial sequencing and analysis of the human genome. *Nature*, 409(6822), 860–921. 5

[Lavoie et al., 2013] Lavoie, H., Thevakumaran, N., Gavory, G., Li, J. J., Padeganeh, A., Guiral, S., Duchaine, J., Mao, D. Y. L., Bouvier, M., Sicheri, F., & Therrien, M. (2013). Inhibitors that stabilize a closed RAF kinase domain conformation induce dimerization. *Nature Chemical Biology*, 9(7), 428–436. 6, 8

[Lee et al., 2004] Lee, T., Hoofnagle, A. N., Kabuyama, Y., Stroud, J., Min, X., Goldsmith, E. J., Chen, L., Resing, K. A., & Ahn, N. G. (2004). Docking motif interactions in MAP kinases revealed by hydrogen exchange mass spectrometry. *Molecular cell*, 14(1), 43–55. 9

[Lenferink et al., 1998] Lenferink, A. E. G., PinkasKramarski, R., Poll, M. L. M. v. d., Vugt, M. J. H. v., Klapper, L. N., Tzahar, E., Waterman, H., Sela, M., Zoelen, E. J. J. v., & Yarden, Y. (1998). Differential endocytic routing of homo and heterodimeric ErbB tyrosine kinases confers signaling superiority to receptor heterodimers. *The EMBO Journal*, 17(12), 3385–3397. 27, 59, 86

[Levchenko et al., 2000] Levchenko, A., Bruck, J., & Sternberg, P. W. (2000). Scaffold proteins may biphasically affect the levels of mitogen-activated protein kinase signaling and reduce its threshold properties. *Proceedings of the National Academy of Sciences*, 97(11), 5818–5823. 20, 25, 73

[Levkowitz et al., 1998] Levkowitz, G., Waterman, H., Zamir, E., Kam, Z., Oved, S., Langdon, W. Y., Beguinot, L., Geiger, B., & Yarden, Y. (1998). c-Cbl/Sli-1 regulates endocytic sorting and ubiquitination of the epidermal growth factor receptor. *Genes & Development*, 12(23), 3663–3674. 27

[Li et al., 2000] Li, S., Wang, Q., Chakladar, A., Bronson, R. T., & Bernards, A. (2000). Gastric Hyperplasia in Mice Lacking the Putative Cdc42 Effector IQGAP1. *Molecular and Cellular Biology*, 20(2), 697–701. 13

[Lidke et al., 2010] Lidke, D. S., Huang, F., Post, J. N., Rieger, B., Wilsbacher, J., Thomas, J. L., Pouysségur, J., Jovin, T. M., & Lenormand, P. (2010). ERK Nuclear Translocation Is Dimerization-independent but Controlled by the Rate of Phosphorylation. *Journal of Biological Chemistry*, 285(5), 3092–3102. 9, 10, 85

[Light et al., 2002] Light, Y., Paterson, H., & Marais, R. (2002). 14-3-3 Antagonizes Ras-Mediated Raf-1 Recruitment to the Plasma Membrane To Maintain Signaling Fidelity. *Molecular and Cellular Biology*, 22(14), 4984–4996. 6

[Lin et al., 2009] Lin, J., Harding, A., Giurisato, E., & Shaw, A. S. (2009). KSR1 modulates the sensitivity of mitogen-activated protein kinase pathway activation in T cells without altering fundamental system outputs. *Molecular and cellular biology*, 29(8), 2082–2091. 73

[Liu et al., 2010] Liu, X., Bardwell, L., & Nie, Q. (2010). A Combination of Multisite Phosphorylation and Substrate Sequestration Produces Switchlike Responses. *Biophysical Journal*, 98(8), 1396–1407. 20

[Locasale et al., 2007] Locasale, J. W., Shaw, A. S., & Chakraborty, A. K. (2007). Scaffold proteins confer diverse regulatory properties to protein kinase cascades. *Proceedings of the National Academy of Sciences*, 104(33), 13307–13312. 20, 86

[Lorenz et al., 2003] Lorenz, K., Lohse, M. J., & Quitterer, U. (2003). Protein kinase C switches the Raf kinase inhibitor from Raf-1 to GRK-2. *Nature*, 426(6966), 574–579. 13

[Lorenz et al., 2009] Lorenz, K., Schmitt, J. P., Schmitteckert, E. M., & Lohse, M. J. (2009). A new type of ERK1/2 autophosphorylation causes cardiac hypertrophy. *Nature medicine*, 15(1), 75–83. 45

[Lowenstein et al., 1992] Lowenstein, E. J., Daly, R. J., Batzer, A. G., Li, W., Margolis, B., Lammers, R., Ullrich, A., Skolnik, E. Y., Bar-Sagi, D., & Schlessinger, J. (1992). The SH2 and SH3 domain-containing protein GRB2 links receptor tyrosine kinases to ras signaling. *Cell*, 70(3), 431–442. 6

[Lu et al., 1999] Lu, P.-J., Zhou, X. Z., Shen, M., & Lu, K. P. (1999). Function of WW Domains as Phosphoserine- or Phosphothreonine-Binding Modules. *Science*, 283(5406), 1325–1328. 32

[Luo et al., 1996] Luo, Z., Tzivion, G., Belshaw, P. J., Vavvas, D., Marshall, M., & Avruch, J. (1996). Oligomerization activates c-Raf-1 through a Ras-dependent mechanism. *Nature*, 383(6596), 181–185. 8

[Luttrell et al., 1999] Luttrell, L. M., Ferguson, S. S. G., Daaka, Y., Miller, W. E., Maudsley, S., Rocca, G. J. D., Lin, F.-T., Kawakatsu, H., Owada, K., Luttrell, D. K., Caron, M. G., & Lefkowitz, R. J. (1999). -Arrestin-Dependent Formation of 2 Adrenergic Receptor-Src Protein Kinase Complexes. *Science*, 283(5402), 655–661. 13

[Luttrell et al., 2001] Luttrell, L. M., Roudabush, F. L., Choy, E. W., Miller, W. E., Field, M. E., Pierce, K. L., & Lefkowitz, R. J. (2001). Activation and targeting of extracellular signal-regulated kinases by -arrestin scaffolds. *Proceedings of the National Academy of Sciences*, 98(5), 2449–2454. 13

[Mace et al., 2013] Mace, P. D., Wallez, Y., Egger, M. F., Dobaczewska, M. K., Robinson, H., Pasquale, E. B., & Riedl, S. J. (2013). Structure of ERK2 bound to PEA-15 reveals a mechanism for rapid release of activated MAPK. *Nature Communications*, 4, 1681. 14

[Maeder et al., 2007] Maeder, C. I., Hink, M. A., Kinkhabwala, A., Mayr, R., Bastiaens, P. I. H., & Knop, M. (2007). Spatial regulation of Fus3 MAP kinase activity through a reaction-diffusion mechanism in yeast pheromone signalling. *Nature cell biology*, 9(11), 1319–1326. 1, 3, 16, 17, 49, 50, 51, 54, 82

[Maleri et al., 2004] Maleri, S., Ge, Q., Hackett, E. A., Wang, Y., Dohlman, H. G., & Errede, B. (2004). Persistent activation by constitutive Ste7 promotes Kss1-mediated invasive growth but fails to support Fus3-dependent mating in yeast. *Molecular and cellular biology*, 24(20), 9221–9238. 16

[Malleshaiah et al., 2010] Malleshaiah, M. K., Shahrezaei, V., Swain, P. S., & Michnick, S. W. (2010). The scaffold protein Ste5 directly controls a switch-like mating decision in yeast. *Nature*, 465(7294), 101–105. 17, 83

[Mangan et al., 2003] Mangan, S., Zaslaver, A., & Alon, U. (2003). The Coherent Feedforward Loop Serves as a Sign-sensitive Delay Element in Transcription Networks. *Journal of Molecular Biology*, 334(2), 197–204. 22

[Manning et al., 2002] Manning, G., Whyte, D. B., Martinez, R., Hunter, T., & Sudarsanam, S. (2002). The protein kinase complement of the human genome. *Science (New York, N.Y.)*, 298(5600), 1912–1934. 5

[Markevich et al., 2006] Markevich, N. I., Tsyganov, M. A., Hoek, J. B., & Kholodenko, B. N. (2006). Long-range signaling by phosphoprotein waves arising from bistability in protein kinase cascades. *Molecular systems biology*, 2, 61. 21, 23, 24, 25

[Martin et al., 2010] Martin, C., Chen, S., Heilos, D., Sauer, G., Hunt, J., Shaw, A. G., Sims, P. F. G., Jackson, D. A., & Lovrić, J. (2010). Changed Genome Heterochromatinization Upon Prolonged Activation of the Raf/ERK Signaling Pathway. *PLoS ONE*, 5(10), e13322. 85

[Martin et al., 2003] Martin, K., Steinberg, T. H., Cooley, L. A., Gee, K. R., Beechem, J. M., & Patton, W. F. (2003). Quantitative analysis of protein phosphorylation status and protein kinase activity on microarrays using a novel fluorescent phosphorylation sensor dye. *Proteomics*, 3(7), 1244–1255. 32

[Matheos et al., 2004] Matheos, D., Metodiev, M., Muller, E., Stone, D., & Rose, M. D. (2004). Pheromone-induced polarization is dependent on the Fus3p MAPK acting through the formin Bni1p. *The Journal of Cell Biology*, 165(1), 99–109. 49, 83

[Matsubayashi et al., 2001] Matsubayashi, Y., Fukuda, M., & Nishida, E. (2001). Evidence for Existence of a Nuclear Pore Complex-mediated, Cytosol-independent Pathway of Nuclear Translocation of ERK MAP Kinase in Permeabilized Cells. *Journal of Biological Chemistry*, 276(45), 41755–41760. 9

[McCaffrey et al., 1987] McCaffrey, G., Clay, F. J., Kelsay, K., & Sprague, Jr, G. F. (1987). Identification and regulation of a gene required for cell fusion during mating of the yeast Saccharomyces cerevisiae. *Molecular and cellular biology*, 7(8), 2680–2690. 16

[McKay et al., 2009] McKay, M. M., Ritt, D. A., & Morrison, D. K. (2009). Signaling dynamics of the KSR1 scaffold complex. *Proceedings of the National Academy of Sciences of the United States of America*, 106(27), 11022–11027. 8, 12, 60

[McNulty et al., 2011] McNulty, D. E., Li, Z., White, C. D., Sacks, D. B., & Annan, R. S. (2011). MAPK Scaffold IQGAP1 Binds the EGF Receptor and Modulates Its Activation. *Journal of Biological Chemistry*, 286(17), 15010–15021. 13

[Melen et al., 2005] Melen, G. J., Levy, S., Barkai, N., & Shilo, B.-Z. (2005). Threshold responses to morphogen gradients by zero-order ultrasensitivity. *Molecular systems biology*, 1, 2005.0028. 23

[Meyer et al., 1997] Meyer, D., Yamaai, T., Garratt, A., Riethmacher-Sonnenberg, E., Kane, D., Theill, L. E., & Birchmeier, C. (1997). Isoform-specific expression and function of neuregulin. *Development (Cambridge, England)*, 124(18), 3575–3586. 27

[Meyers et al., 2006] Meyers, J., Craig, J., & Odde, D. J. (2006). Potential for Control of Signaling Pathways via Cell Size and Shape. *Current Biology*, 16(17), 1685–1693. 23

[Müller et al., 2001] Müller, J., Ory, S., Copeland, T., Piwnica-Worms, H., & Morrison, D. K. (2001). C-TAK1 regulates Ras signaling by phosphorylating the MAPK scaffold, KSR1. *Molecular cell*, 8(5), 983–993. 12

[Murphy et al., 2002] Murphy, L. O., Smith, S., Chen, R.-H., Fingar, D. C., & Blenis, J. (2002). Molecular interpretation of ERK signal duration by immediate early gene products. *Nature cell biology*, 4(8), 556–564. 10, 22

[Nada et al., 2009] Nada, S., Hondo, A., Kasai, A., Koike, M., Saito, K., Uchiyama, Y., & Okada, M. (2009). The novel lipid raft adaptor p18 controls endosome dynamics by anchoring the MEK-ERK pathway to late endosomes. *The EMBO Journal*, 28(5), 477–489. 14

[Nada et al., 1993] Nada, S., Yagi, T., Takeda, H., Tokunaga, T., Nakagawa, H., Ikawa, Y., Okada, M., & Aizawa, S. (1993). Constitutive activation of Src family kinases in mouse embryos that lack Csk. *Cell*, 73(6), 1125–1135. 6

[Nagashima et al., 2007] Nagashima, T., Shimodaira, H., Ide, K., Nakakuki, T., Tani, Y., Takahashi, K., Yumoto, N., & Hatakeyama, M. (2007). Quantitative transcriptional control of ErbB receptor signaling undergoes graded to biphasic response for cell differentiation. *The Journal of biological chemistry*, 282(6), 4045–4056. 1, 17, 27, 59, 61

[Nakakuki et al., 2010] Nakakuki, T., Birtwistle, M. R., Saeki, Y., Yumoto, N., Ide, K., Nagashima, T., Brusch, L., Ogunnaike, B. A., Okada-Hatakeyama, M., & Kholodenko, B. N. (2010). Ligand-specific c-Fos expression emerges from the spatiotemporal control of ErbB network dynamics. *Cell*, 141(5), 884–896. 22, 27, 59, 63, 72, 86

[Nguyen et al., 1993] Nguyen, T. T., Scimeca, J. C., Filloux, C., Peraldi, P., Carpentier, J. L., & Van Obberghen, E. (1993). Co-regulation of the mitogen-activated protein kinase, extracellular signal-regulated kinase 1, and the 90-kDa ribosomal S6 kinase in PC12 cells. Distinct effects of the neurotrophic factor, nerve growth factor, and the mitogenic factor, epidermal growth factor. *The Journal of biological chemistry*, 268(13), 9803–9810. 6, 17

[Offterdinger et al., 2004] Offterdinger, M., Georget, V., Girod, A., & Bastiaens, P. I. H. (2004). Imaging phosphorylation dynamics of the epidermal growth factor receptor. *The Journal of biological chemistry*, 279(35), 36972–36981. 32

[Olsen et al., 2006] Olsen, J. V., Blagoev, B., Gnad, F., Macek, B., Kumar, C., Mortensen, P., & Mann, M. (2006). Global, in vivo, and site-specific phosphorylation dynamics in signaling networks. *Cell*, 127(3), 635–648. 5

[Olsen et al., 2010] Olsen, J. V., Vermeulen, M., Santamaria, A., Kumar, C., Miller, M. L., Jensen, L. J., Gnad, F., Cox, J., Jensen, T. S., Nigg, E. A., Brunak, S., & Mann, M. (2010). Quantitative phosphoproteomics reveals widespread full phosphorylation site occupancy during mitosis. *Science signaling*, 3(104), ra3. 5

[Ortega et al., 2006] Ortega, F., Garcés, J. L., Mas, F., Kholodenko, B. N., & Cascante, M. (2006). Bistability from double phosphorylation in signal transduction. *FEBS Journal*, 273(17), 3915–3926. 21

[Ory et al., 2003] Ory, S., Zhou, M., Conrads, T. P., Veenstra, T. D., & Morrison, D. K. (2003). Protein phosphatase 2a positively regulates Ras signaling by dephosphorylating KSR1 and Raf-1 on critical 14-3-3 binding sites. *Current biology: CB*, 13(16), 1356–1364. 12

[Owens & Keyse, 2007] Owens, D. M. & Keyse, S. M. (2007). Differential regulation of MAP kinase signalling by dual-specificity protein phosphatases. *Oncogene*, 26(22), 3203–3213. 10, 65, 85

[Paliwal et al., 2007] Paliwal, S., Iglesias, P. A., Campbell, K., Hilioti, Z., Groisman, A., & Levchenko, A. (2007). MAPK-mediated bimodal gene expression and adaptive gradient sensing in yeast. *Nature*, 446(7131), 46–51. 17

[Park et al., 2005] Park, S., Yeung, M. L., Beach, S., Shields, J. M., & Yeung, K. C. (2005). RKIP downregulates B-Raf kinase activity in melanoma cancer cells. *Oncogene*, 24(21), 3535–3540. 13

[Patschinsky & Bister, 1988] Patschinsky, T. & Bister, K. (1988). Structural analysis of normal and transforming mil(raf) proteins: effect of 5'-truncation on phosphorylation in vivo or in vitro. *Oncogene*, 3(4), 357–364. 6

[Payne et al., 1991] Payne, D. M., Rossomando, A. J., Martino, P., Erickson, A. K., Her, J. H., Shabanowitz, J., Hunt, D. F., Weber, M. J., & Sturgill, T. W. (1991). Identification of the regulatory phosphorylation sites in pp42/mitogen-activated protein kinase (MAP kinase). *The EMBO journal*, 10(4), 885–892. 9

[Peisajovich et al., 2010] Peisajovich, S. G., Garbarino, J. E., Wei, P., & Lim, W. A. (2010). Rapid diversification of cell signaling phenotypes by modular domain recombination. *Science (New York, N.Y.)*, 328(5976), 368–372. 14

[Peles et al., 1992] Peles, E., Lamprecht, R., Ben-Levy, R., Tzahar, E., & Yarden, Y. (1992). Regulated coupling of the Neu receptor to phosphatidylinositol 3'-kinase and its release by oncogenic activation. *Journal of Biological Chemistry*, 267(17), 12266–12274. 27, 59

[Peles et al., 1991] Peles, E., Levy, R., Or, E., Ullrich, A., & Yarden, Y. (1991). Oncogenic forms of the neu/HER2 tyrosine kinase are permanently coupled to phospholipase C. *EMBO Journal*, 10(8), 2077–2086. 27, 59

[Perez-Aso et al., 2013] Perez-Aso, M., Segura, V., Montó, F., Barettino, D., Noguera, M., Milligan, G., & D'Ocon, P. (2013). The three 1-adrenoceptor subtypes show different

spatio-temporal mechanisms of internalization and ERK1/2 phosphorylation. *Biochimica et Biophysica Acta (BBA) - Molecular Cell Research*, 1833(10), 2322–2333. 12

[Plotnikov et al., 2011] Plotnikov, A., Chuderland, D., Karamansha, Y., Livnah, O., & Seger, R. (2011). Nuclear Extracellular Signal-Regulated Kinase 1 and 2 Translocation Is Mediated by Casein Kinase 2 and Accelerated by Autophosphorylation . *Molecular and Cellular Biology*, 31(17), 3515–3530. 9

[Poulikakos et al., 2010] Poulikakos, P. I., Zhang, C., Bollag, G., Shokat, K. M., & Rosen, N. (2010). RAF inhibitors transactivate RAF dimers and ERK signalling in cells with wild-type BRAF. *Nature*, 464(7287), 427–430. 6

[Printen & Sprague, 1994] Printen, J. A. & Sprague, Jr, G. F. (1994). Protein-protein interactions in the yeast pheromone response pathway: Ste5p interacts with all members of the MAP kinase cascade. *Genetics*, 138(3), 609–619. 11

[Pullikuth et al., 2005] Pullikuth, A., McKinnon, E., Schaeffer, H.-J., & Catling, A. D. (2005). The MEK1 Scaffolding Protein MP1 Regulates Cell Spreading by Integrating PAK1 and Rho Signals. *Molecular and Cellular Biology*, 25(12), 5119–5133. 14

[Rajakulendran et al., 2009] Rajakulendran, T., Sahmi, M., Lefrançois, M., Sicheri, F., & Therrien, M. (2009). A dimerization-dependent mechanism drives RAF catalytic activation. *Nature*, 461(7263), 542–545. 8, 12

[Rapp et al., 1983] Rapp, U. R., Goldsborough, M. D., Mark, G. E., Bonner, T. I., Groffen, J., Reynolds, F. H., & Stephenson, J. R. (1983). Structure and biological activity of v-raf, a unique oncogene transduced by a retrovirus. *Proceedings of the National Academy of Sciences*, 80(14), 4218–4222. 6

[Razidlo et al., 2004] Razidlo, G. L., Kortum, R. L., Haferbier, J. L., & Lewis, R. E. (2004). Phosphorylation regulates KSR1 stability, ERK activation, and cell proliferation. *The Journal of biological chemistry*, 279(46), 47808–47814. 12, 17, 60

[Reményi et al., 2006] Reményi, A., Good, M. C., & Lim, W. A. (2006). Docking interactions in protein kinase and phosphatase networks. *Current opinion in structural biology*, 16(6), 676–685. 9

[Reszka et al., 1995] Reszka, A. A., Seger, R., Diltz, C. D., Krebs, E. G., & Fischer, E. H. (1995). Association of mitogen-activated protein kinase with the microtubule cytoskeleton. *Proceedings of the National Academy of Sciences of the United States of America*, 92(19), 8881–8885. 84

[Reynolds et al., 2003] Reynolds, A. R., Tischer, C., Verveer, P. J., Rocks, O., & Bastiaens, P. I. H. (2003). EGFR activation coupled to inhibition of tyrosine phosphatases causes lateral signal propagation. *Nature Cell Biology*, 5(5), 447–453. 85

[Robbins et al., 1993] Robbins, D. J., Zhen, E., Owaki, H., Vanderbilt, C. A., Ebert, D., Geppert, T. D., & Cobb, M. H. (1993). Regulation and properties of extracellular signal-regulated protein kinases 1 and 2 in vitro. *The Journal of biological chemistry*, 268(7), 5097–5106. 9

[Roberts & Der, 2007] Roberts, P. J. & Der, C. J. (2007). Targeting the Raf-MEK-ERK mitogen-activated protein kinase cascade for the treatment of cancer. *Oncogene*, 26(22), 3291–3310. 5, 6, 7

[Rodríguez et al., 2010] Rodríguez, J., Calvo, F., González, J. M., Casar, B., Andrés, V., & Crespo, P. (2010). ERK1/2 MAP kinases promote cell cycle entry by rapid, kinase-independent disruption of retinoblastoma–lamin A complexes. *The Journal of Cell Biology*, 191(5), 967–979. 85

[Rodriguez-Viciana et al., 2006] Rodriguez-Viciana, P., Oses-Prieto, J., Burlingame, A., Fried, M., & McCormick, F. (2006). A phosphatase holoenzyme comprised of Shoc2/Sur8 and the catalytic subunit of PP1 functions as an M-Ras effector to modulate Raf activity. *Molecular cell*, 22(2), 217–230. 6

[Roskoski Jr., 2014] Roskoski Jr., R. (2014). The ErbB/HER family of protein-tyrosine kinases and cancer. *Pharmacological Research*, 79, 34–74. 27

[Rossomando et al., 1994] Rossomando, A. J., Dent, P., Sturgill, T. W., & Marshak, D. R. (1994). Mitogen-activated protein kinase kinase 1 (MKK1) is negatively regulated by threonine phosphorylation. *Molecular and Cellular Biology*, 14(3), 1594–1602. 8

[Roy et al., 2004] Roy, M., Li, Z., & Sacks, D. B. (2004). IQGAP1 Binds ERK2 and Modulates Its Activity. *Journal of Biological Chemistry*, 279(17), 17329–17337. 13

[Roy et al., 2005] Roy, M., Li, Z., & Sacks, D. B. (2005). IQGAP1 Is a Scaffold for Mitogen-Activated Protein Kinase Signaling. *Molecular and Cellular Biology*, 25(18), 7940–7952. 13

[Salazar & Höfer, 2009] Salazar, C. & Höfer, T. (2009). Multisite protein phosphorylation – from molecular mechanisms to kinetic models. *FEBS Journal*, 276(12), 3177–3198. 19

[Sancak et al., 2010] Sancak, Y., Bar-Peled, L., Zoncu, R., Markhard, A. L., Nada, S., & Sabatini, D. M. (2010). Ragulator-Rag Complex Targets mTORC1 to the Lysosomal Surface and Is Necessary for Its Activation by Amino Acids. *Cell*, 141(2), 290–303. 14

[Santos et al., 2007] Santos, S. D. M., Verveer, P. J., & Bastiaens, P. I. H. (2007). Growth factor-induced MAPK network topology shapes Erk response determining PC-12 cell fate. *Nature cell biology*, 9(3), 324–330. 6, 13, 25, 27, 59, 86

[Sasagawa et al., 2005] Sasagawa, S., Ozaki, Y.-i., Fujita, K., & Kuroda, S. (2005). Prediction and validation of the distinct dynamics of transient and sustained ERK activation. *Nature cell biology*, 7(4), 365–373. 25

[Sato et al., 2002] Sato, M., Ozawa, T., Inukai, K., Asano, T., & Umezawa, Y. (2002). Fluorescent indicators for imaging protein phosphorylation in single living cells. *Nature biotechnology*, 20(3), 287–294. 32

[Sato et al., 1999] Sato, M., Ozawa, T., Yoshida, T., & Umezawa, Y. (1999). A fluorescent indicator for tyrosine phosphorylation-based insulin signaling pathways. *Analytical chemistry*, 71(18), 3948–3954. 32

[Schaeffer et al., 1998] Schaeffer, H. J., Catling, A. D., Eblen, S. T., Collier, L. S., Krauss, A., & Weber, M. J. (1998). MP1: A MEK Binding Partner That Enhances Enzymatic Activation of the MAP Kinase Cascade. *Science*, 281(5383), 1668–1671. 14

[Schoeberl et al., 2002] Schoeberl, B., Eichler-Jonsson, C., Gilles, E. D., & Müller, G. (2002). Computational modeling of the dynamics of the MAP kinase cascade activated by surface and internalized EGF receptors. *Nature Biotechnology*, 20(4), 370–375. 25

[Schubbert et al., 2007] Schubbert, S., Bollag, G., & Shannon, K. (2007). Deregulated Ras signaling in developmental disorders: new tricks for an old dog. *Current Opinion in Genetics & Development*, 17(1), 15–22. 5

[Semenov et al., 2013] Semenov, S. N., Markvoort, A. J., Gevers, W. B. L., Piruska, A., de Greef, T. F. A., & Huck, W. T. S. (2013). Ultrasensitivity by molecular titration in spatially propagating enzymatic reactions. *Biophysical journal*, 105(4), 1057–1066. 23

[Serber & Ferrell, 2007] Serber, Z. & Ferrell, J. E. (2007). Tuning Bulk Electrostatics to Regulate Protein Function. *Cell*, 128(3), 441–444. 20

[Shalin et al., 2006] Shalin, S. C., Hernandez, C. M., Dougherty, M. K., Morrison, D. K., & Sweatt, J. D. (2006). Kinase Suppressor of Ras1 Compartmentalizes Hippocampal Signal Transduction and Subserves Synaptic Plasticity and Memory Formation. *Neuron*, 50(5), 765–779. 84

[Shaner et al., 2007] Shaner, N. C., Patterson, G. H., & Davidson, M. W. (2007). Advances in fluorescent protein technology. *Journal of Cell Science*, 120(24), 4247–4260. 28

[Shimomura et al., 1962] Shimomura, O., Johnson, F. H., & Saiga, Y. (1962). Extraction, Purification and Properties of Aequorin, a Bioluminescent Protein from the Luminous Hydromedusan, Aequorea. *Journal of Cellular and Comparative Physiology*, 59(3), 223–239. 28

[Shin et al., 2009] Shin, S.-Y., Rath, O., Choo, S.-M., Fee, F., McFerran, B., Kolch, W., & Cho, K.-H. (2009). Positive- and negative-feedback regulations coordinate the dynamic behavior of the Ras-Raf-MEK-ERK signal transduction pathway. *Journal of Cell Science*, 122(3), 425–435. 27

[Sibilski et al., 2013] Sibilski, C., Mueller, T., Kollipara, L., Zahedi, R. P., Rapp, U. R., Rudel, T., & Baljuls, A. (2013). Tyr728 in the kinase domain of the murine kinase suppressor of RAS 1 regulates binding and activation of the mitogen-activated protein kinase kinase. *The Journal of biological chemistry*, 288(49), 35237–35252. 12, 60

[Simon et al., 1993] Simon, M. A., Dodson, G. S., & Rubin, G. M. (1993). An SH3-SH2-SH3 protein is required for p21ras1 activation and binds to sevenless and Sos proteins in vitro. *Cell*, 73(1), 169–177. 6

[Slack-Davis et al., 2003] Slack-Davis, J. K., Eblen, S. T., Zecevic, M., Boerner, S. A., Tarcsafalvi, A., Diaz, H. B., Marshall, M. S., Weber, M. J., Parsons, J. T., & Catling, A. D. (2003). PAK1 phosphorylation of MEK1 regulates fibronectin-stimulated MAPK activation. *The Journal of cell biology*, 162(2), 281–291. 8

[Sliwkowski et al., 1994] Sliwkowski, M. X., Schaefer, G., Akita, R. W., Lofgren, J. A., Fitzpatrick, V. D., Nuijens, A., Fendly, B. M., Cerione, R. A., Vandlen, R. L., & Carraway, K L, r. (1994). Coexpression of erbB2 and erbB3 proteins reconstitutes a high affinity receptor for heregulin. *The Journal of biological chemistry*, 269(20), 14661–14665. 27

[Smith et al., 2008] Smith, S. D., Jaffer, Z. M., Chernoff, J., & Ridley, A. J. (2008). PAK1-mediated activation of ERK1/2 regulates lamellipodial dynamics. *Journal of cell science*, 121(Pt 22), 3729–3736. 85

[Steglich et al., 2013] Steglich, B., Sazer, S., & Ekwall, K. (2013). Transcriptional regulation at the yeast nuclear envelope. *Nucleus*, 4(5), 379–389. 85

[Stevenson et al., 1992] Stevenson, B. J., Rhodes, N., Errede, B., & Sprague, G. F. (1992). Constitutive mutants of the protein kinase STE11 activate the yeast pheromone response pathway in the absence of the G protein. *Genes & Development*, 6(7), 1293–1304. 49, 83

[Strickfaden et al., 2007] Strickfaden, S. C., Winters, M. J., Ben-Ari, G., Lamson, R. E., Tyers, M., & Pryciak, P. M. (2007). A mechanism for cell-cycle regulation of MAP kinase signaling in a yeast differentiation pathway. *Cell*, 128(3), 519–531. 16

[Subach et al., 2009] Subach, F. V., Subach, O. M., Gundorov, I. S., Morozova, K. S., Piatkevich, K. D., Cuervo, A. M., & Verkhusha, V. V. (2009). Monomeric fluorescent timers that change color from blue to red report on cellular trafficking. *Nature chemical biology*, 5(2), 118–126. 28

[Sulzmaier et al., 2012] Sulzmaier, F. J., Valmiki, M. K. G., Nelson, D. A., Caliva, M. J., Geerts, D., Matter, M. L., White, E. P., & Ramos, J. W. (2012). PEA-15 potentiates H-Ras-mediated epithelial cell transformation through phospholipase D. *Oncogene*, 31(30), 3547–3560. 13

[Sun et al., 2014] Sun, J., Yi, M., Yang, L., Wei, W., Ding, Y., & Jia, Y. (2014). Enhancement of Tunability of MAPK Cascade Due to Coexistence of Processive and Distributive Phosphorylation Mechanisms. *Biophysical Journal*, 106(5), 1215–1226. 23, 25, 26, 82

[Sundaram & Han, 1995] Sundaram, M. & Han, M. (1995). The C. elegans ksr-1 gene encodes a novel Raf-related kinase involved in Ras-mediated signal transduction. *Cell*, 83(6), 889–901. 11

[Takahashi & Pryciak, 2008] Takahashi, S. & Pryciak, P. M. (2008). Membrane Localization of Scaffold Proteins Promotes Graded Signaling in the Yeast MAP Kinase Cascade. *Current Biology*, 18(16), 1184–1191. 20

[Takeda et al., 2003] Takeda, H., Kawasaki, A., Takahashi, M., Yamada, A., & Koike, T. (2003). Matrix-assisted laser desorption/ionization time-of-flight mass spectrometry of phosphorylated compounds using a novel phosphate capture molecule. *Rapid communications in mass spectrometry: RCM*, 17(18), 2075–2081. 33

[Takiyama et al., 2009] Takiyama, K., Kinoshita, E., Kinoshita-Kikuta, E., Fujioka, Y., Kubo, Y., & Koike, T. (2009). A Phos-tag-based fluorescence resonance energy transfer system for the analysis of the dephosphorylation of phosphopeptides. *Analytical biochemistry*, 388(2), 235–241. 33

[Tanoue et al., 2000] Tanoue, T., Adachi, M., Moriguchi, T., & Nishida, E. (2000). A conserved docking motif in MAP kinases common to substrates, activators and regulators. *Nature cell biology*, 2(2), 110–116. 8, 9

[Tavassoli et al., 1989] Tavassoli, M., Quirke, P., Farzaneh, F., Lock, N. J., Mayne, L. V., & Kirkham, N. (1989). c-erbB-2/c-erbA co-amplification indicative of lymph node metastasis, and c-myc amplification of high tumour grade, in human breast carcinoma. *British journal of cancer*, 60(4), 505–510. 27

[Teis et al., 2006] Teis, D., Taub, N., Kurzbauer, R., Hilber, D., Araujo, M. E. d., Erlacher, M., Offterdinger, M., Villunger, A., Geley, S., Bohn, G., Klein, C., Hess, M. W., & Huber, L. A. (2006). p14–MP1-MEK1 signaling regulates endosomal traffic and cellular proliferation during tissue homeostasis. *The Journal of Cell Biology*, 175(6), 861–868. 14

[Teis et al., 2002] Teis, D., Wunderlich, W., & Huber, L. A. (2002). Localization of the MP1-MAPK Scaffold Complex to Endosomes Is Mediated by p14 and Required for Signal Transduction. *Developmental Cell*, 3(6), 803–814. 14

[Terry et al., 1995] Terry, B. R., Matthews, E. K., & Haseloff, J. (1995). Molecular Characterization of Recombinant Green Fluorescent Protein by Fluorescence Correlation Microscopy. *Biochemical and Biophysical Research Communications*, 217(1), 21–27. 29

[Terskikh et al., 2000] Terskikh, A., Fradkov, A., Ermakova, G., Zaraisky, A., Tan, P., Kajava, A. V., Zhao, X., Lukyanov, S., Matz, M., Kim, S., Weissman, I., & Siebert, P. (2000). "Fluorescent Timer": Protein That Changes Color with Time. *Science*, 290(5496), 1585–1588. 28

[Therrien et al., 1995] Therrien, M., Chang, H. C., Solomon, N. M., Karim, F. D., Wassarman, D. A., & Rubin, G. M. (1995). KSR, a novel protein kinase required for RAS signal transduction. *Cell*, 83(6), 879–888. 11, 12

[Thomson & Gunawardena, 2009] Thomson, M. & Gunawardena, J. (2009). Unlimited multistability in multisite phosphorylation systems. *Nature*, 460(7252), 274–277. 21

[Thottassery et al., 2004] Thottassery, J. V., Sun, Y., Westbrook, L., Rentz, S. S., Manuvakhova, M., Qu, Z., Samuel, S., Upshaw, R., Cunningham, A., & Kern, F. G. (2004). Prolonged extracellular signal-regulated kinase 1/2 activation during fibroblast growth factor 1- or heregulin beta1-induced antiestrogen-resistant growth of breast cancer cells is resistant to mitogen-activated protein/extracellular regulated kinase kinase inhibitors. *Cancer research*, 64(13), 4637–4647. 17, 27, 59, 61

[Torii et al., 2004] Torii, S., Kusakabe, M., Yamamoto, T., Maekawa, M., & Nishida, E. (2004). Sef Is a Spatial Regulator for Ras/MAP Kinase Signaling. *Developmental Cell*, 7(1), 33–44. 10, 13

[Traverse et al., 1994] Traverse, S., Seedorf, K., Paterson, H., Marshall, C. J., Cohen, P., & Ullrich, A. (1994). EGF triggers neuronal differentiation of PC12 cells that overexpress the EGF receptor. *Current biology: CB*, 4(8), 694–701. 6

[Tsang et al., 2002] Tsang, M., Friesel, R., Kudoh, T., & Dawid, I. B. (2002). Identification of Sef, a novel modulator of FGF signalling. *Nature Cell Biology*, 4(2), 165–169. 13

[Tsuboi et al., 2010] Tsuboi, T., Kitaguchi, T., Karasawa, S., Fukuda, M., & Miyawaki, A. (2010). Age-dependent Preferential Dense-Core Vesicle Exocytosis in Neuroendocrine Cells Revealed by Newly Developed Monomeric Fluorescent Timer Protein. *Molecular Biology of the Cell*, 21(1), 87–94. 28

[van Drogen et al., 2001] van Drogen, F., Stucke, V. M., Jorritsma, G., & Peter, M. (2001). MAP kinase dynamics in response to pheromones in budding yeast. *Nature cell biology*, 3(12), 1051–1059. 16, 54

[Verkhusha & Lukyanov, 2004] Verkhusha, V. V. & Lukyanov, K. A. (2004). The molecular properties and applications of Anthozoa fluorescent proteins and chromoproteins. *Nature biotechnology*, 22(3), 289–296. 28

[Verveer et al., 2000] Verveer, P. J., Squire, A., & Bastiaens, P. I. H. (2000). Global Analysis of Fluorescence Lifetime Imaging Microscopy Data. *Biophysical Journal*, 78(4), 2127–2137. 31

[Wada et al., 1990] Wada, T., Qian, X. L., & Greene, M. I. (1990). Intermolecular association of the p185neu protein and EGF receptor modulates EGF receptor function. *Cell*, 61(7), 1339–1347. 27

[Walther et al., 2011] Walther, K. A., Papke, B., Sinn, M. B., Michel, K., & Kinkhabwala, A. (2011). Precise measurement of protein interacting fractions with fluorescence lifetime imaging microscopy. *Molecular bioSystems*, 7(2), 322–336. 96

[Waterman et al., 1998] Waterman, H., Sabanai, I., Geiger, B., & Yarden, Y. (1998). Alternative Intracellular Routing of ErbB Receptors May Determine Signaling Potency. *Journal of Biological Chemistry*, 273(22), 13819–13827. 27, 59, 86

[Waters et al., 2004] Waters, C., Pyne, S., & Pyne, N. J. (2004). The role of G-protein coupled receptors and associated proteins in receptor tyrosine kinase signal transduction. *Seminars in cell & developmental biology*, 15(3), 309–323. 6

[Weber et al., 2001] Weber, C. K., Slupsky, J. R., Kalmes, H. A., & Rapp, U. R. (2001). Active Ras induces heterodimerization of cRaf and BRaf. *Cancer research*, 61(9), 3595–3598. 8

[Westheimer, 1987] Westheimer, F. H. (1987). Why nature chose phosphates. *Science*, 235(4793), 1173–1178. 19

[White et al., 2012] White, C. D., Erdemir, H. H., & Sacks, D. B. (2012). IQGAP1 and its binding proteins control diverse biological functions. *Cellular Signalling*, 24(4), 826–834. 13

[White et al., 2011] White, C. D., Li, Z., Dillon, D. A., & Sacks, D. B. (2011). IQGAP1 Protein Binds Human Epidermal Growth Factor Receptor 2 (HER2) and Modulates Trastuzumab Resistance. *Journal of Biological Chemistry*, 286(34), 29734–29747. 13

[Whitehurst et al., 2004] Whitehurst, A. W., Robinson, F. L., Moore, M. S., & Cobb, M. H. (2004). The Death Effector Domain Protein PEA-15 Prevents Nuclear Entry of ERK2 by Inhibiting Required Interactions. *Journal of Biological Chemistry*, 279(13), 12840–12847. 13

[Wiegert & Bading, 2011] Wiegert, J. S. & Bading, H. (2011). Activity-dependent calcium signaling and ERK-MAP kinases in neurons: A link to structural plasticity of the nucleus and gene transcription regulation. *Cell Calcium*, 49(5), 296–305. 85

[Wiget et al., 2004] Wiget, P., Shimada, Y., Butty, A.-C., Bi, E., & Peter, M. (2004). Site-specific regulation of the GEF Cdc24p by the scaffold protein Far1p during yeast mating. *The EMBO journal*, 23(5), 1063–1074. 16

[Wilsbacher et al., 2006] Wilsbacher, J. L., Juang, Y.-C., Khokhlatchev, A. V., Gallagher, E., Binns, D., Goldsmith, E. J., & Cobb, M. H. (2006). Characterization of mitogen-activated protein kinase (MAPK) dimers. *Biochemistry*, 45(44), 13175–13182. 10

[Winters & Pryciak, 2005] Winters, M. J. & Pryciak, P. M. (2005). Interaction with the SH3 domain protein Bem1 regulates signaling by the Saccharomyces cerevisiae p21-activated kinase Ste20. *Molecular and cellular biology*, 25(6), 2177–2190. 16

[Witzel et al., 2012] Witzel, F., Maddison, L., & Blüthgen, N. (2012). How scaffolds shape MAPK signaling: what we know and opportunities for systems approaches. *Frontiers in physiology*, 3, 475. 11

[Wolf & Seger, 2002] Wolf, I. & Seger, R. (2002). The mitogen-activated protein kinase signaling cascade: from bench to bedside. *The Israel Medical Association journal: IMAJ*, 4(8), 641–647. 6

[Wosikowski et al., 1993] Wosikowski, K., Küng, W., Hasmann, M., Löser, R., & Eppenberger, U. (1993). Inhibition of growth-factor-activated proliferation by anti-estrogens and effects on early gene expression of MCF-7 cells. *International journal of cancer. Journal international du cancer*, 53(2), 290–297. 17, 27, 59

[Wouters & Bastiaens, 1999] Wouters, F. S. & Bastiaens, P. I. (1999). Fluorescence lifetime imaging of receptor tyrosine kinase activity in cells. *Current biology: CB*, 9(19), 1127–1130. 41

[Xing et al., 1997] Xing, H., Kornfeld, K., & Muslin, A. J. (1997). The protein kinase KSR interacts with 14-3-3 protein and Raf. *Current biology: CB*, 7(5), 294–300. 12

[Xiong et al., 2003] Xiong, S., Zhao, Q., Rong, Z., Huang, G., Huang, Y., Chen, P., Zhang, S., Liu, L., & Chang, Z. (2003). hSef Inhibits PC-12 Cell Differentiation by Interfering with Ras-Mitogen-activated Protein Kinase MAPK Signaling. *Journal of Biological Chemistry*, 278(50), 50273–50282. 13

[Yang et al., 2006] Yang, C., Liu, Y., Lemmon, M. A., & Kazanietz, M. G. (2006). Essential Role for Rac in Heregulin ?1 Mitogenic Signaling: a Mechanism That Involves Epidermal Growth Factor Receptor and Is Independent of ErbB4. *Molecular and Cellular Biology*, 26(3), 831–842. 59

[Yang et al., 2003] Yang, R.-B., Ng, C. K. D., Wasserman, S. M., Kömüves, L. G., Gerritsen, M. E., & Topper, J. N. (2003). A Novel Interleukin-17 Receptor-like Protein Identified in Human Umbilical Vein Endothelial Cells Antagonizes Basic Fibroblast Growth Factor-induced Signaling. *Journal of Biological Chemistry*, 278(35), 33232–33238. 13

[Yarden & Schlessinger, 1987] Yarden, Y. & Schlessinger, J. (1987). Epidermal growth factor induces rapid, reversible aggregation of the purified epidermal growth factor receptor. *Biochemistry*, 26(5), 1443–1451. 27

[Yazicioglu et al., 2007] Yazicioglu, M. N., Goad, D. L., Ranganathan, A., Whitehurst, A. W., Goldsmith, E. J., & Cobb, M. H. (2007). Mutations in ERK2 Binding Sites Affect Nuclear Entry. *Journal of Biological Chemistry*, 282(39), 28759–28767. 9

[Yeung et al., 2000] Yeung, K., Janosch, P., McFerran, B., Rose, D. W., Mischak, H., Sedivy, J. M., & Kolch, W. (2000). Mechanism of Suppression of the Raf/MEK/Extracellular Signal-Regulated Kinase Pathway by the Raf Kinase Inhibitor Protein. *Molecular and Cellular Biology*, 20(9), 3079–3085. 13

[Yeung et al., 1999] Yeung, K., Seitz, T., Li, S., Janosch, P., McFerran, B., Kaiser, C., Fee, F., Katsanakis, K. D., Rose, D. W., Mischak, H., Sedivy, J. M., & Kolch, W. (1999). Suppression of Raf-1 kinase activity and MAP kinase signalling by RKIP. *Nature*, 401(6749), 173–177. 13, 25

[Yoon & Seger, 2006] Yoon, S. & Seger, R. (2006). The extracellular signal-regulated kinase: multiple substrates regulate diverse cellular functions. *Growth factors (Chur, Switzerland)*, 24(1), 21–44. 10, 84

[York et al., 1998] York, R. D., Yao, H., Dillon, T., Ellig, C. L., Eckert, S. P., McCleskey, E. W., & Stork, P. J. S. (1998). Rap1 mediates sustained MAP kinase activation induced by nerve growth factor. *Nature*, 392(6676), 622–626. 25

[Yu et al., 2008] Yu, L., Qi, M., Sheff, M. A., & Elion, E. A. (2008). Counteractive control of polarized morphogenesis during mating by mitogen-activated protein kinase Fus3 and G1 cyclin-dependent kinase. *Molecular biology of the cell*, 19(4), 1739–1752. 83

[Yudushkin et al., 2007] Yudushkin, I. A., Schleifenbaum, A., Kinkhabwala, A., Neel, B. G., Schultz, C., & Bastiaens, P. I. H. (2007). Live-cell imaging of enzyme-substrate interaction reveals spatial regulation of PTP1b. *Science (New York, N.Y.)*, 315(5808), 115–119. 32

[Zang et al., 2008] Zang, M., Gong, J., Luo, L., Zhou, J., Xiang, X., Huang, W., Huang, Q., Luo, X., Olbrot, M., Peng, Y., Chen, C., & Luo, Z. (2008). Characterization of Ser338 phosphorylation for Raf-1 activation. *The Journal of biological chemistry*, 283(46), 31429–31437. 8

[Zhang et al., 2005] Zhang, Y., Wolf-Yadlin, A., Ross, P. L., Pappin, D. J., Rush, J., Lauffenburger, D. A., & White, F. M. (2005). Time-resolved mass spectrometry of tyrosine phosphorylation sites in the epidermal growth factor receptor signaling network reveals dynamic modules. *Molecular & cellular proteomics: MCP*, 4(9), 1240–1250. 45

[Zheng & Guan, 1994] Zheng, C. F. & Guan, K. L. (1994). Activation of MEK family kinases requires phosphorylation of two conserved Ser/Thr residues. *The EMBO journal*, 13(5), 1123–1131. 8, 16

[Zhou et al., 2002] Zhou, M., Horita, D. A., Waugh, D. S., Byrd, R. A., & Morrison, D. K. (2002). Solution structure and functional analysis of the cysteine-rich C1 domain of kinase suppressor of Ras (KSR). *Journal of molecular biology*, 315(3), 435–446. 12